THE SAFE STORAGE STUDY OF AUTOCATALYTIC REACTIVE CHEMICALS

A Dissertation

by

LIJUN LIU

Submitted to the Office of Graduate Studies of
Texas A&M University
in partial fulfillment of the requirements for the degree of

DOCTOR OF PHILOSOPHY

August 2009

Major Subject: Chemical Engineering

THE SAFE STORAGE STUDY OF AUTOCATALYTIC REACTIVE CHEMICALS

A Dissertation

by

LIJUN LIU

Submitted to the Office of Graduate Studies of
Texas A&M University
in partial fulfillment of the requirements for the degree of

DOCTOR OF PHILOSOPHY

Approved by:

Chair of Committee,	M. Sam Mannan
Committee Members,	Kenneth R. Hall
	Rayford Anthony
	Debjyoti Banerjee
Head of Department,	Michael Pishko

August 2009

Major Subject: Chemical Engineering

ABSTRACT

The Safe Storage Study of Autocatalytic Reactive Chemicals. (August 2009)

Lijun Liu, B.S., Tianjin University;

M.S., Tianjin University

Chair of Advisory Committee: Dr. M. Sam Mannan

In the U.S. Chemical Safety and Hazard Investigation Board (CSB) report, Improving Reactive Hazard Management, there are 37 out of 167 accidents, which occurred in a storage tank or a storage area. This fact demonstrates that thermal runaway problems in chemical storage processes have not been give enough attention.

Hydroxylamine Nitrate (HAN) is an important member of the hydroxylamine compound family and its diluted aqueous solution is widely used in the nuclear industry for equipment decontamination. It is also used as a solid or aqueous propellant. Due to its instability and autocatalytic behavior, it has been involved in several incidents at the Hanford and Savannah River Sites (SRS). Much research has been conducted on HAN in different areas, such as combustion mechanism, decomposition mechanism, and runaway behavior. However, the autocatalytic behavior of HAN at runaway stage has not been fully addressed due to its highly exothermic and rapid decomposition behavior.

This work focuses on extracting its autocatalytic kinetics mechanism and studying its critical behavior from adiabatic calorimetry measurements. The lumped autocatalytic kinetics model, the associated model parameters and HAN critical

condition are determined for the first time. The contamination effect of iron ions and nitric acid on diluted hydroxylamine nitrate solution is also studied.

This work also identified the safe storage conditions for a small quantity HAN diluted solution with thermal explosion theory. Computational Fluid Dynamics (CFD) was used to further study the influence of natural convection and system scale on the critical behavior for a large quantity of chemical and thus proposed the practical storage guidelines for industrial practice.

To my wife, Jin

my son, Hanying

my parents and parents-in-law

and my other family members

ACKNOWLEDGEMENTS

I would like to express my sincere appreciation to my advisor, Dr. M. Sam Mannan, for his support, encouragement, and guidance throughout my graduate study. Over the past years, his insights on reactivity hazard management and chemical process safety motivated and inspired me to finish this research project.

I would like to thank Dr. Kenneth R. Hall, Dr Rayford Anthony, and Dr. Debjyoti Banerjee for their dedication to serving as my committee members.

I would like to express my sincere gratitude to Dr. Yuyan Guo, Dr. William J. Rogers, and Dr. Chunyang Wei for their insightful discussion and great contribution to this project. I also want to thank Dr. Chunyang Wei and Ms. Chuanji Zhang for discussion and troubleshooting of APTAC. I also feel grateful to Dr. Yingchun Zhang and Dr. Yanjun Wang for their mentoring at the beginning of this project and encouragement throughout my graduate study.

I also want to express my gratitude to all the staff at the Mary Kay O'Connor Process Safety Center and the Chemical Engineering Department staff for their help to make this research project reach this final stage.

Last, but not least, I am deeply grateful to my wife, Jin, my parents, parents-in-law, and my son, Hanying, for their love, understanding and help through the years.

TABLE OF CONTENTS

Page

LIST OF FIGURES

Page

Page

LIST OF TABLES

1. INTRODUCTION

Chemical reactions are the cornerstone of modern chemical, biochemical and petroleum chemical industries. Many products used daily are manufactured via chemical reactions by using all kinds of chemicals. Most of these chemicals are stable and can be safely used in the normal storage and handling conditions. However some chemicals can undergo uncontrolled reactions within a slight deviation from the normal conditions to release a large amount of energy and incur a catastrophic consequence. In 2002, the US Chemical Safety and Hazard Investigation Board (CSB) published an investigation report on 167 serious incidents from 1980 to 2001 involving uncontrolled chemical reactions. These incidents caused 108 deaths as well as significant property and environmental loss. CSB recommends government agencies and industries should improve their practice on reactive chemicals hazard management [1].

Figure 1.1 illustrates the statistics of runaway reaction incidents investigated by CSB. Thermal runaway causes almost 35% incidents and is the second leading cause. This indicates that thermal runway hazard control still needs to be improved to ensure safe production in chemical industries.

This dissertation follows the style of Industrial & Engineering Chemistry Research.

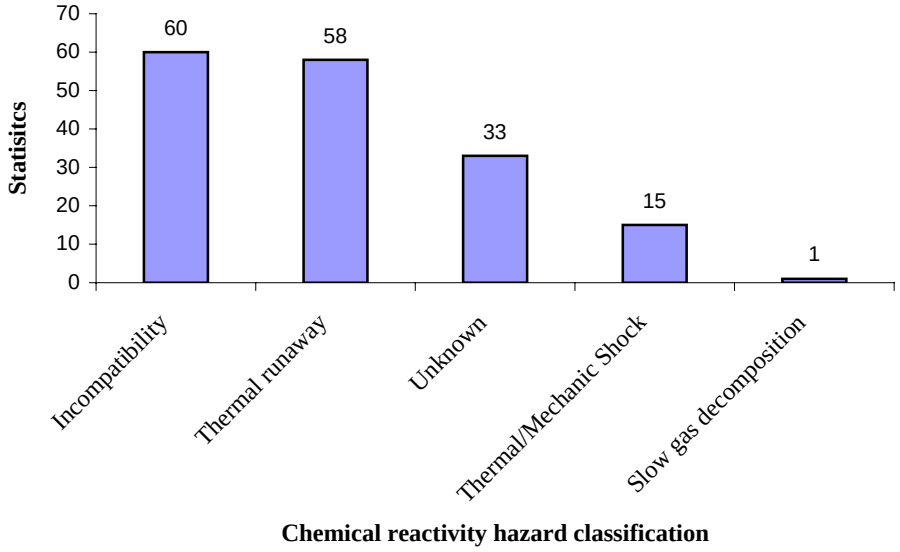

Figure 1.1 Runaway reaction classification due to reactive hazards

The definition of uncontrolled chemical reaction by CSB is the reactions with significant increases in temperature, pressure and/or gas evolution. Because of the self-regulatory characteristics of endothermic and reversible reactions, exothermal and irreversible reaction is the principle source of uncontrolled reactions. Although this fact has been accepted by academia and industry for years, the potential thermal runaway hazards for exothermal, irreversible, and autocatalytic reactions still tend to be neglected by the industrial practices.

Several explosion incidents involving autocatalytic chemicals happened recently in the storage process, such as hydroxylamine nitrate (HAN) explosion at Hanford and Savannah River Sites (SRS) and Methyl Ethyl Ketone Peroxide (MEKPO) explosions in China, Taiwan, and Japan [1, 2]. In current chemical storage practices, reactive chemicals

are normally stored in proper conditions and they seem to be safe. However a reactive chemical storage vessel is a special batch reactor. When unanticipated situations or conditions happen in the storage area or vicinity, this “reactor” may introduce severe hazards to its surrounding equipment and personnel. The explosion of HAN at Hanford was thoroughly investigated by the Department of Energy (DOE). DOE concluded that the leading cause was HAN and nitric acid solution was not drained in time and the solution concentration increased about 25% due to water evaporation. Eventually the explosion occurred at ambient temperature and pressure four years later after the solution was prepared. DOE also concluded most accidents related with HAN had some common issues, including accidental concentration increase, acid addition, and metal ions contamination. The higher the concentration of HAN, nitric acid, and metal ions, the higher the possibility the autocatalytic decomposition will be initiated. Overall these accidents demonstrated the reactive hazards of autocatalytic chemicals has not been fully understood and given enough attention during the storage operation.

Runaway reactions related with reactive chemicals are often initiated by several factors, including apparent activation energy reduction, energy addition, reaction pathway change, and heat removal rate reduction. Any of these factors or their combination may affect the system behavior and result in undesired consequence. Therefore, the current approach in preventing chemical runaway reactions includes reaction rate control, cooling capacity enhancement, and decontamination.

To develop effective reactive hazards control strategies, the accurate decomposition kinetics must be determined at the first step. Although the detailed

chemical kinetics is very useful and desired, uncertainties and cost involved in its development is also very high. It is only possible for very limited cases. Traditionally, overall reaction/decomposition kinetics of reactive chemical can be obtained by using thermal analysis techniques, including differential scanning calorimetry (DSC) and adiabatic calorimetry etc. The overall reaction kinetics can be derived from temperature and pressure profiles. The obtained reaction kinetics can be used in the critical behavior analysis to seek safe storage and handling conditions. Thermal analysis techniques are still widely used today and provided conservative and valuable information for current reactive hazards control with relatively low cost.

Hydroxylamine nitrate or hydroxylammonium nitrate (HAN) is the salt of hydroxylamine and nitric acid. It is an energetic material with the chemical formula $NH_2OH \bullet HNO_3$. It is normally used in aqueous solution, which is colorless, odorless, homogenous, toxic and corrosive. In pure form, it is a hygroscopic solid. Diluted aqueous HAN solution is mainly used as the plutonium reductant in nuclear industry. It also has some application in rocket propellant in either solid form, where it is a propellant oxidizer, or aqueous form, where it functions as monopropellant. Furthermore, it is also a reagent for preparing various industrial specialty and pharmaceutical chemicals.

Due to its instability, HAN has been involved in several incidents at Hanford and Savannah River Sites (SRS). The incidents investigation report reveals that introduction of heat, acids, and unanticipated concentration are the root causes of past HAN explosion incidents [3]. Mary Kay O'Connor Process Safety Center (MKOPSC) of TAMU

and other research institutions have conducted extensive research on its thermal stability, decomposition mechanism and the effect of metal ion catalysis by using various techniques at different conditions [4-6]. Significant amount of knowledge and data of HAN were accumulated, which can be used to improve HAN processing safety.

Previous studies of HAN decomposition kinetics either used oversimplified assumptions or were obtained for highly concentrated HAN solutions or for its solid. For example, Zhang and Schoppelrei independently obtained HAN decomposition kinetic parameters by assuming the decomposition reaction is first order [4, 5]. Lee et al. obtained the decomposition kinetic parameter of HAN at very high temperatures and concentrations [6]. All these work had their limitations and did not provide insightful information for practical storage operation and transportation. This work uses a traditional thermal analysis technique, adiabatic calorimetry, to study the autocatalytic decomposition kinetics of hydroxylamine nitrate.

One critical issue in storage of HAN is contamination of iron ions by leaching from the storage vessel. Most commercial storage and transportation vessels are made with stainless steel. Nitric acid, HNO_3, will be dissociated from HAN and exacerbate the iron ion leaching from the steel vessel into the solution. As concluded by DOE, the higher the concentration of iron ions, the higher the instability of HAN solution. However the influence of iron ions on the diluted HAN solution has not been quantitatively studied. This work uses adiabatic calorimeter to systematically study their influences.

In the industrial practice, reactive chemicals are often stored in bulk quantities, which causes more severe problem than storage process of small quantity chemical. Volume to surface area ratio can significantly affect energy balance of storage system. Accumulated excess energy may slowly increase system temperature over time. Consequently, chemical reactivity hazard increase with material quantity and non-hazardous materials in small quantity may become hazardous when its quantity becomes larger. The storage and handling conditions derived from small-scale system, which normally is non-convective or pure heat conduction system, can not be simply scaled up and directly applied to industrial practices. The influence of system size on the cooling capacity must be carefully examined. Although this issue is well known, current research has not given enough attention to the system size issue.

Chemical reactivity hazard evaluation procedure, including the widely used thermal analysis techniques, is briefly reviewed in Section 2. Classical theories used to study critical behavior of reactive chemical are reviewed in Section 3. Thermal decomposition behavior and kinetics of diluted HAN solution are studied and presented in Section 4. An improved Semenov Theory is used to study critical behavior of small quantity diluted HAN solution. This result is presented in Section 5 and can be used to provide guidance for small quantity reactive chemical storage and handling. In Section 6, Computational Fluid Dynamics (CFD) is used to conduct critical behavior analysis for large quantity diluted HAN solution. The system size issue is carefully examined.

The objective of this work includes: a) determination of autocatalytic decomposition kinetics of diluted HAN solution, b) determination of the influence of

iron ions and nitric acid on thermal stability of diluted HAN solution, c) critical behavior analysis for small quantity diluted HAN solution, d) critical behavior analysis for large quantity diluted HAN solution and system size issue discussion.

2. REACTIVE HAZARDS EVALUATION PROCEDURE

Reactive hazards arise from the reactions associated with the rapid exothermic and/or gas generation processes. Rapid exothermic reactions can quickly raise the system temperature and cause the whole system to boil violently. It can lead to mechanical explosion, such as the boiling liquid expanding vapor explosion (BLEVE), which is possibly followed by combustion or explosion of the combustible contents. If a reaction releases a large amount of gases in a short period, a mechanical or chemical explosion may occur.

Experimental methods are always the most reliable and accurate method to conduct reactivity hazard evaluation. However it is clearly not realistic or safe to conduct full size tests for unknown or new compounds. First, such a test can not be conducted in the early stage of a new compound because of their availability. Secondly, vigorous exotherm or gas evolution hazard may overwhelm an available protection system. Therefore, various small-scale tests, theoretical, and numerical techniques have been proposed to provide data and estimation for the likelihood and consequence of runaway reactions. Although there is no standard evaluation procedure, the commonly accepted procedure and techniques are briefly reviewed in this Section. The typical testing procedure includes following steps:

- Reactivity information collection and theoretical calculation
- Reactivity hazard screening tests
- Reaction rate and kinetics parameter measurements

- Thermal runaway hazard evaluation

2.1 Reactivity information collection and theoretical calculation

2.1.1 Reactivity information collection

Although available reactivity information can never replace reactivity hazard testing, reactivity hazard assessment always benefits from the available literature from many aspects, such as safety, time and cost saving. One widely used information source would be the material safety data sheet (MSDS). There are also other excellent resources and handbooks compiled to provide guidance on reactivity hazard assessment, such as Lees' Loss Prevention in the Process Industries and Bretherick's Handbook of Reactive Chemical Hazards [7, 8].

2.1.2 Thermodynamic calculation

Heat of reaction is the enthalpies difference between products and reactants at constant pressure and a definite temperature. Heat of reaction determination is always the first step of reaction hazard identification. There are a variety of methods for measuring or estimating heat of reactions, including calorimeters, literature resources, and thermodynamic estimation techniques.

Adiabatic temperature increase, ΔT_{ad}， and maximum adiabatic temperature，T_{max}, are two important indicators for reactivity hazard evaluation. They can be calculated by using the heat of reaction and the specific heat for the reaction mixture with equations 2.1 and 2.2.

$$\Delta T_{ad} = \Delta H / (mC_p) \tag{2.1}$$

$$T_{\max} = T_0 + \Delta T_{ad} \tag{2.2}$$

where m is reactant mass, C_p is heat capacity of reactant, T_0 is initial temperature, and ΔH is heat of reaction. If maximum adiabatic temperature is above reactants or products boiling point or decomposition temperature of any individual reactant, product or the mixture, appropriate safeguards, such as pressure relief valves, have to be installed to mitigate the potential overpressure hazard or prevent uncontrolled thermal runaway reactions. The disadvantages of this approach are mainly the uncertainties involved in the determination of the decomposition temperature, enthalpy of formation, and specific heat for the reacting mixture. For example, the decomposition temperature normally is not a definite temperature because it highly depends on the measurement apparatus sensitivity.

Heat of reaction data for many standard reactions, such as nitration, sulphonation, and hydrogenation are available in literature [9]. Whenever heat of reaction data is not available in the literature, they can be calculated by using their enthalpies of formation [10]. In addition, some other semi-empirical or theoretical methods can also be used to estimate exothermicity for chemical reactions, such as average bond energy summation method [11], molecular group contribution method [12, 13], and quantum chemistry [14].

The average bond energy summation method relies on knowledge of molecular structures of the involved chemicals and average bond energy. Although it can not provide very accurate result, it is very useful for preliminary evaluation and screening.

The Benson method of group additivity has several improvements over the average bond energy summation method, including consideration of rings and isotopic

effects and so on. When applying this method to the chemicals with elements, C, H, N, and O, the uncertainty is normally between 9 and 13 kJ/mol.

The most widely used program for the preliminary screening of reactivity hazard is ASTM Computer Program for Chemical Thermodynamic and Energy (CHETAH) [15]. CHETAH includes the most extensive database of Benson groups. However this program has several limitations. First, all calculated thermodynamic data is only for gas species. This drawback may limit its applicable area because most organic reactions are carried out in condense phase. Second, it does not include some organic functional groups.

Quantum chemistry method theoretically can describe the behavior of all chemical system. In reality, only the simplest chemical system can be studied in pure quantum-mechanical terms and different level approximations must be made to solve real problems. The optimum molecular structures of reactants, possible intermediates, and possible products can be obtained by using the appropriate level of theory. Then, frequency calculations can be conducted on these molecular structures to determine their thermochemical properties.

2.1.3 Chemical dynamics calculation

Arrhenius's law is a simple and fairly accurate empirical formula and is widely used to describe temperature dependence behavior of reaction rate. Its rate constant is shown as below.

$$k = Ae^{-E_a / RT} \tag{2.3}$$

where A is the pre-exponential factor, R is the gas constant, E_a is the activation energy, and T is the absolute temperature. Arrhenius's law is one of the milestones of modern physical chemistry and is still widely used in today's reaction kinetics study. Collision theory and transition state theory are proposed to calculate the rate constant.

2.1.3.1 Collision theory

Collision theory originated from the kinetic theory of gases. Original collision theory proposed that reaction only occurs between collided reactant particles. And only those effective collisions exceeding activation energy can make the reaction happen. Reaction rate can be determined by multiplying total number of collision and reaction probability, which is a function of energy. For example, the rate of reaction for a bimolecular reaction is given by

$$r = Z_{AB} pf \tag{2.4}$$

where Z_{AB} is the collision frequency, p is the steric factor describing the collision orientation, f is the fraction of effective collisions. With kinetic theory and Maxwell Boltzmann distribution, the rate of a bimolecular reaction for ideal gases can be represented as follows.

$$r = p\sigma_{AB}^2 \sqrt{\frac{8\pi k_B T}{\mu_{AB}}} e^{-E_a/RT} C_A C_B \tag{2.5}$$

where σ_{AB} is mean molecular diameter, k_B is Boltzmann constant, μ_{AB} is reduced mass, C_A and C_B are concentration for species A and B, respectively. Therefore, concentration and temperature are the two important factors that determine the reaction rate. The collision theory can also be extended to unimolecular and trimolecular reactions.

2.1.3.2 Transition state theory

Transition state theory was a significant advancement over collision theory on predicting the preexponential factor for Arrhenius's law. Transition state theory aims to identify the energy barrier that must be overcome before a reaction could happen. The barrier lays on the potential energy surface and separates reactants and products. This barrier is corresponding to a molecular configuration, activated complex, which is in dynamic equilibrium with reactant molecules. With the aid of statistical mechanics, the probability that the molecule stays in certain states is proportional to its partition function, which is shown in equation (2.6).

$$\sum_i g_i e^{-\frac{E_i}{kT}} = q \tag{2.6}$$

where g_i is statistical weight, E_i is energy of a particular state, and q is the partition function per unit volume. The equilibrium constant for any arbitrary reaction is represented as below by using the thermodynamic equation, $\Delta G = -RTlnK_P$, with Gibbs free energy change described by partition functions.

$$K_p = (N_A V)^{(a+b+\ldots-c-d\ldots)} \left[\frac{q_C^c \bullet q_D^d \bullet \ldots}{q_A^a \bullet q_B^b \bullet \ldots} \right] e^{-N_A \Delta U_0 / RT} \tag{2.7}$$

where N_A is the Avogadro constant and V is the system volume. The term, $N_A \Delta U_0$, is standard increase of system internal energy per mole at absolute zero temperature. After determination of partition function, the equilibrium constant can be calculated with equation (2.7). Although total partition function includes translational, rotational, vibrational, and electron energy terms, only the first three partition functions are used in

kinetic application. With conventional transition state theory, general rate constant of an elementary process can be expressed as follows.

$$K_p = (N_A V)^{(a+b+\ldots-1)} \left(\frac{RT}{N_A h} \right) \frac{q_{\pm}}{q_A^a \bullet q_B^b \bullet \ldots} e^{-N_A \Delta U_0 / RT} \qquad (2.8)$$

where *h* is Planck constant and $q_{\pm}$ is partition function of the activated complex. The rate constant can be determined once the partition function of the activated complex is determined. Theoretically, the partition function can be determined if an accurate potential-energy surface, which normally is hard to get, is available. An alternative is to estimate the molecular structure and vibrational frequencies of the activated complex on the basis of a similar stable molecule. Therefore, it is more realistic to make estimation for rate constant by using mere order-of-magnitude values of partition functions.

2.2 Reactivity hazard screening test

Several small-scale screening tests are available to provide preliminary results and information on thermal stability, heat of reaction, gas evolution and so on. Those techniques have several advantages, such as quick screening, wide temperature measurement range, and small sample requirement etc.

2.2.1 Differential scanning calorimetry and differential thermal analysis

Both Differential Thermal Analysis (DTA) and Differential Scanning Calorimetry (DSC) are concerned with measurement of energy changes in materials. With DTA, temperature difference between sample and reference is obtained as a function of time or temperature. Whereas, DSC curve describes heat flux versus temperature or time. In order to reduce the influence of sample properties on the

integrated area under DTA curve, thermocouples are rarely placed in the sample. Modern DSC normally places the thermocouple under the sample furnace. DTA instruments are still valuable, particularly at higher temperatures (>1000°C), or in aggressive environments, where true heat-flux DSC instruments may not be able to operate.

Differential scanning calorimetry (DSC) is a widely used thermoanalytical technique. DSC not only can be used to study phase transition, but also provide thermal stability information and reaction kinetics. It also can be used to easily determine the exothermicity and significant decomposition temperature range for a reactive chemical.

A modern DSC apparatus normally used a small quantity of sample (1-20mg). The sample normally is placed in a metal capsule and heated at a constant rate (1-10K min^{-1}) in the temperature range from $–20^oC$ to $+500^oC$. There are two types of DSC apparatuses available. The power-compensation DSC uses independent furnaces to match the temperature of the sample and reference by varying furnace energy input. The energy input difference provides information of enthalpy or heat capacity of sample relative to the reference. The heat-flux DSC has only one furnace, where the sample and reference are connected together with a low-resistance metal disc. The temperature difference between sample and reference indicates enthalpy or heat capacity changes. Both sketches of these two types of DSC are shown in Figure 2.1. Although most modern DSC instruments are of the heat-flux design, power-compensation DSC can give equivalent results to heat-flux designs in most practical cases.

Typical DSC curve for an exothermic reaction is illustrated in Figure 2.2. There are three dash lines shown in the figure. The cross section with lower temperature represents the onset temperature for the sample. Normally detected onset temperature is used to determine reaction kinetics and serve as a stability indicator. The exothermicity or heat of reaction can be determined by integrating the area below heating curve.

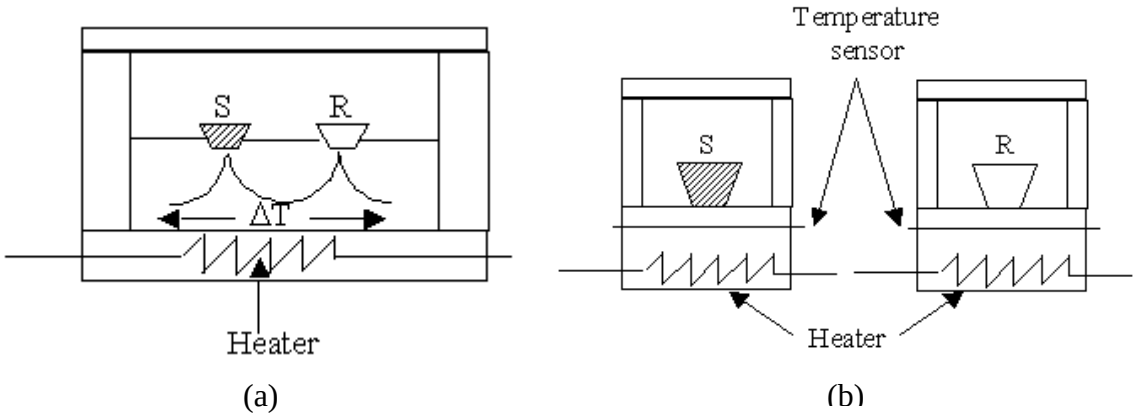

Figure 2.1 Sketch of DSC (a) heat-flux (b) power-compensation

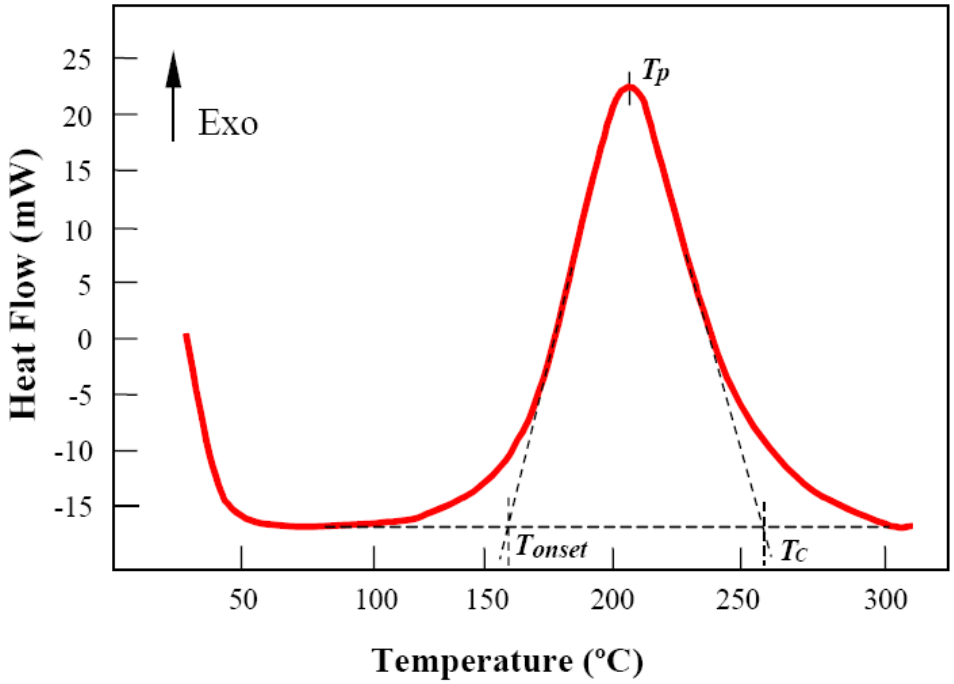

Figure 2.2 Exothermal reaction DSC curve

Traditional DSC can not provide pressure measurement and their applicable area is limited. Recently, some advanced DSC was released to provide more information about the kinetics and gas evolution for reaction chemicals, such as the SENSYS evo DSC [16]. Its pressure measurement and controllable range is up to 500 bars at 600 °C.

2.2.2 Reactive System Screening Tool (RSST)

The Reactive System Screening Tool (RSST) manufactured by Fauske & Associates is another commonly used reactivity hazard screening tool and illustrated in Figure 2.3 [17]. RSST uses a 10 ml glass cell as the reaction vessel and a 350 ml stainless steel containment. One significant feature of RSST is its low thermal inertia, 1.04, that it can provide quasi-adiabatic data. Magnetic stirring can be used to enhance the mixing

effect. Because the original RSST is operated at open cell mode, heat loss due to solvent evaporation may affect the result accuracy. However it does provide pressure vs. temperature, temperature vs. time, pressure vs. time, and Arrhenius plots with a relative low cost. It normally serves as a fast screening tool for reactivity hazard assessment.

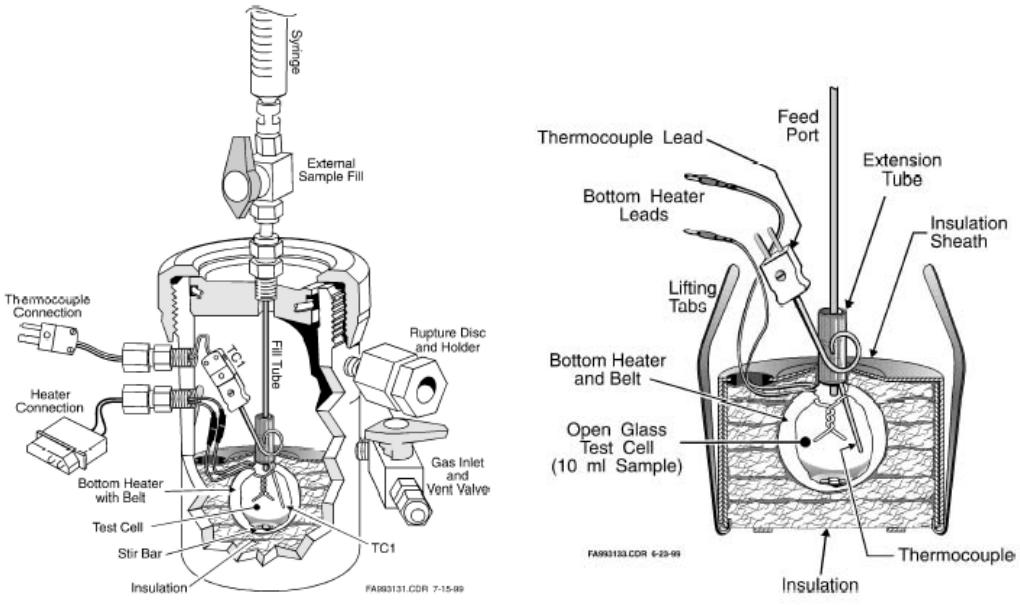

Figure 2.3 Schematic drawing of reaction vessel and containment of RSST

2.2.3 Thermogravimetric Analysis (TGA)

Thermogravimetry (TG) measures mass changing while the sample is subjected to a controlled heating or cooling. The data is recorded as a function of time or temperature. It normally includes thermobalance, furnace, temperature control system, and containment. Its typical operating temperature is up to 2400 ^{o}C, with heating rate up

to 100 ^{o}C/min, and sample mass is up to 100 g. Operation of thermogravimetry requires an inert atmosphere to ensure the data quality. Because thermogravimetry gives absolute changes in sample weight, calculated extent of reaction is not affected by heating rate used. It is another screening tool widely used to test thermal stability and conduct kinetic studies for reactive chemicals [18].

2.3 Reaction rates and kinetic parameters determination

Reaction kinetics and thermodynamics of chemical reaction are essential information to characterize chemical reactivity hazards. This information plays a crucial role on scaling-up, determination of reactor constructing materials, feeding concentration and residence time determination etc. The essential information for determining safe operating conditions on commercial reactor includes following data:

- heat of reaction;
- heat generation rate;
- physical properties of reactant mixture, such as density, heat capacity etc;
- reaction kinetic model;
- impurities and contaminants study;
- effects of mis-charging;
- decomposition conditions, such as temperature range, contaminant concentration etc;
- amount and rate of gas generation

Because most chemical reaction processes are associated with heating or cooling effects, calorimetry is a unique technique to obtain both reaction kinetics and

thermodynamics information simultaneously. Since heat flow rate is proportional to the conversion rate, calorimetry normally uses differential kinetic analysis method to get kinetic parameters and thermodynamic information. Several types of calorimetry, such as isothermal calorimetry and adiabatic calorimetry can be used to achieve this objective.

Isothermal calorimetry is operated at constant temperature and is the easiest in application because of absence of heat accumulation. Therefore, system properties, such as heat capacity, density, and viscosity, and reactor inert parts do not need to be considered as a function of temperature. Isothermal calorimeter can be categorized into heat-flow, power-compensation, heat-balance, and Peltier ones on the basis of their measurement and control principles. Isothermal calorimeter generates process power output versus time, which allows determination of required cooling capacity for a given condition or vice versa. The data can also be used to examine whether there is any accumulation of dangerous reagents or reaction intermediates, which may violently release their stored energy in a later stage and cause catastrophic consequences. Isothermal calorimeter is also the most widely used apparatus to determine the cooling capacity for a chemical manufacturing process.

Adiabatic calorimetry is another calorimetry technique that is widely used to determine reaction kinetics, thermodynamics, and pressurization information. Typical adiabatic calorimeter, such as accelerating rate calorimetry (ARC), has a detection limit of 0.02 K/min. This effective sweep rate allows much broader exothermic reaction testing range. Adiabatic calorimeter also provides gas evolution information, which can also be used to validate reaction kinetics obtained from thermal analysis.

2.4 Thermal runaway hazard evaluation

Adiabatic calorimetry is not only able to provide kinetic information, but also is the most important experimental tool to conduct chemical thermal safety analysis. Adiabatic calorimetry can allow the reaction to safely proceed at thermal runaway stage, which is normally characterized by high temperature, high pressure, and extremely high heating and pressurization rates. The information obtained in runaway stage is very useful for emergency relief system design. Because the research is focused on thermal runaway hazard evaluation of reactive chemicals in storage practice, adiabatic calorimeter is the primary experimental tool used in this work. Fundamental principles of adiabatic calorimeter and the one used in this research are briefly summarized as follow.

2.4.1 Fundamental principles of adiabatic calorimeter

Adiabatic condition is applied to the reactor of calorimetry to prevent any heat flow from the reaction system to its surrounding environment. In the reality, all adiabatic calorimeters are operated in quasi-adiabatic mode, where ambient temperature is controlled to follow and match that of reactive samples. Normally the heat loss is quite small due to the very small temperature difference and small heat transfer coefficient of surrounding inert gases. As a consequence, released energy can be almost completely accumulated in the system and drive temperature increase and decomposition. With Arrhenius's law, energy balance of the adiabatic reactor is represented as follows.

$$\rho C_p \frac{dT}{dt} = \Delta H A \exp(-\frac{E_a}{RT}) f(c) \qquad (2.9)$$

where *f(c)* is an appropriate reaction model for the sample. With this equation, adiabatic temperature increase and adiabatic induction time can be estimated. It is generally accepted that this adiabatic induction time and maximum adiabatic temperature can be extrapolated to other temperatures and give conservative estimations of storage time and temperature.

At any temperature, *T*, or time, *t*, reactant conversion is approximately proportional to temperature changing.

$$\alpha = \frac{T - T_0}{\Delta T_{ad}} \tag{2.10}$$

where ΔT_{ad} is the adiabatic temperature increase, $T_f - T_0$, and α is the reactant conversion. With α equal to $(C_0\text{-}C)/C_0$, reaction order, preexponential factor, and activation energy could be determined with equation (2.9) and temperature versus time data or self-heating rate versus time data.

2.4.2 Automatic Pressure Tracking Adiabatic Calorimeter (APTAC)

Accelerating Rate Calorimeter (ARC) was originally developed in Dow Chemical and then commercialized by Columbia Scientific Industries (CSI). Because original ARC uses thick wall vessel, vessel wall absorbs most of the energy released by decomposition reaction and it normally has a large thermal inertia, $\phi = 1 + M_b C_{vb} / MC_v$, where M_b and C_{vb} are reactor mass and heat capacity, M_b and C_{vb} are sample mass and heat capacity. This makes it very different from an industrial reactor, which normally has a small thermal inertia, close to 1. In addition, original ARC does not have pressure

compensation capability so reaction vessel can be broken due to fast pressure increase and can not be used to study highly gasified chemicals.

Later on, several advanced calorimeters, such as Automatic Pressure Tracking Adiabatic Calorimeter (APTAC), PHI-TEC II, and Venting Size Package (VSP), adopted pressure compensation method of DIERS (the Design Institute for Emergency Relief Systems) technology to overcome the limitation of high pressure and fast pressurization rate in the original ARC. Their advantages are listed as follows.

- Use thin wall reaction vessel to generate low thermal inertia data
- Have very high heat generation rate tracking capability
- Have fast pressurization tracking capacity

APTAC is used in the present research. APTAC can also add reagents to the reaction vessel during the experiment to simulate a semi-batch or continuous semi-batch process. This feature endows the reactivity hazard test more flexibility and the capability to simulate the behavior of some real reaction process. APTAC has several operation modes, such as heat-wait-search, isoaging, heat ramp, and isothermal modes. Its temperature measurement ranges is up to 500^{o}C and pressure tracking range from vacuum to 2000 Pisa. It can detect exotherm with heat generation rates from 0.04 to 400 °C/min. Heat-Wait-Search (HWS) operation mode was proved to be the most suitable mode to study thermal runaway hazard of reactive chemicals and this mode is used throughout the experimental work of the present research [19]. The typical heat-wait-search mode temperature changing profile is illustrated in Figure 2.4.

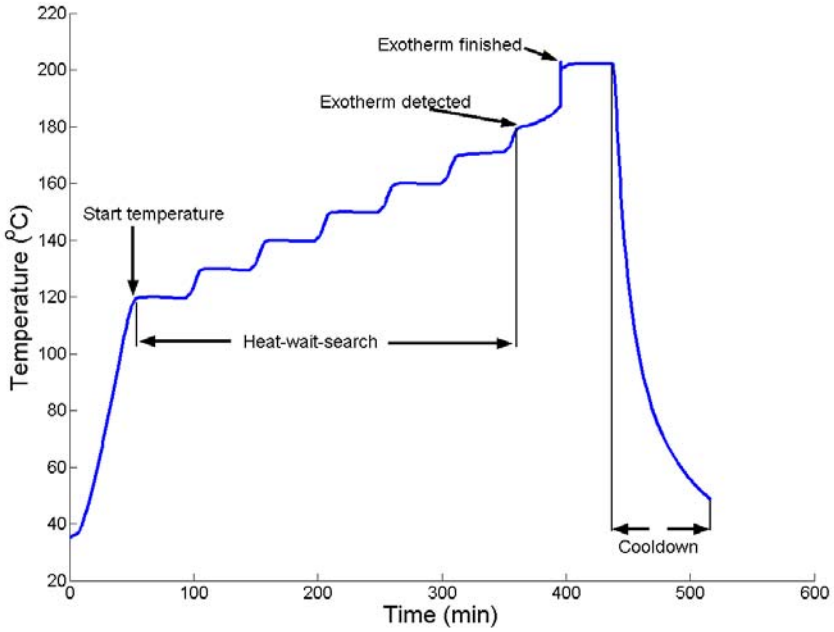

Figure 2.4 Illustration of heat-wait-search mode

3. CRITICAL BEHAVIOR ANALYSIS OF REACTIVE CHEMICALS

3.1 Introduction

Because every exothermic reaction has potential fire or explosion hazard, thermal runaway hazard must be paid particular attention. Thermal runaway represents rapid energy buildup due to exothermic reactions. Thermo kinetic research reveals that thermodynamic data, kinetic parameters and physical properties are key parameters to assess thermal runaway or thermal explosion hazards of reactive chemicals [20]. The key parameters are summarized in Table 3.1.

Thermal runaway or thermal explosion is generally characterized by self-heating before larger amount of explosion energy is released. Once energy removal rate is less than self-heating rate, accumulated energy will exponentially accelerate the reaction. Thermal runaway can happen even at low temperatures. Although its occurrence probability is less than that at high temperatures, special attention should be given to this particular danger of low temperature thermal explosions because they are normally neglected. Thermal explosion theory is very useful for development of safe operating conditions for reactive chemicals in storage, manufacture, and transportation practices.

Primary goal of thermal explosion theory is to identify the parameter condition where the system exhibits thermal runaway. Near the critical magnitude of several process parameters, such as temperature and heat transfer coefficient, a small perturbation may significantly change system status. To adhere to the original work of Semenov, the term “explosion” in thermal explosion theory means reaction kinetics and

not the gas dynamics. Furthermore the explosion regime is defined as the rapid process of converting reactants into final products.

Table 3.1 The key parameters for reactive chemicals hazards assessment

Thermodynamic data	Heat of reaction
	Adiabatic temperature increase
	Specific quantity of gas generated
	Maximum pressure in a closed vessel
Kinetic parameters	Reaction rate
	Rate of heat production
	Rate of pressure increase in closed vessel
	Adiabatic time to maximum rate
	Apparent activation energy
	Initial temperature of detectable exothermic reaction
Physical properties	Heat capacity
	Thermal conductivity

3.2 Classic thermal explosion theory

The theory of thermal explosion begins with work of Le Chatelier and van't Hoff in the 19th century. Then this theory was further developed by numerous researchers. Several milestones of thermal explosion theory are briefly introduced as follows.

3.2.1 Semenov Theory

The foundation of thermal explosion theory is built upon the original work of Semenov and collaborators [21]. Several fundamental assumptions of this original work are summarized as follows.

- Uniform temperature distribution in the reactant volume;
- A single temperature-dependent zero-order reaction;
- All process parameters remain constant.

Energy balance of reactant system can be described by the following equation with the above assumptions.

$$\rho C_p \frac{dT}{dt} = QA\rho \exp(-\frac{E_a}{RT}) - \frac{hS}{V}(T - T_S) \qquad (3.1)$$

where T: the reacting system temperature,

T_S: the environmental temperature,

t: time,

ρ: reacting system density,

Cp: heat capacity of the reacting system,

Q: heat of reaction,

A: pre-exponential factor,

E_a: reaction activation energy,

h: heat transfer coefficient,

S: heat transfer area,

R: gas constant,

V: reacting system volume.

Mathematical analysis on the heat conservation equation used by Semenov laid the foundation of thermal explosion theory. Temperature-dependence diagrams of heat generation, $QAexp(-E_a/RT)$, and heat loss, $hS(T-T_s)/V$, gives the definition of subcritical and supercritical regimes and is often called a Semenov diagram as illustrated in Figure 3.1, where heat loss is represented by a series of straight lines and heat generation is denoted by the curve. In Figure 1, lines 1, 2 and 3 illustrate the heat loss, $hS(T-T_s)/V$, for different surround temperatures and their intercepts on the temperature axis represent different surround temperatures and the slope of the lines is hS/V.

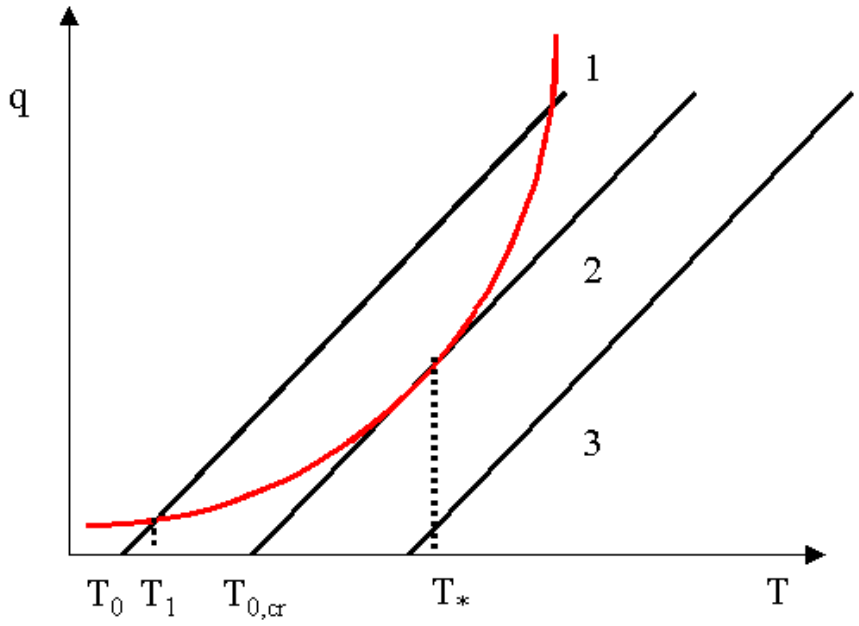

Figure 3.1 Semenov diagram

In Figure 3.1, the critical point of thermal explosion is defined as the tangency between the heat generation curve and heat loss straight line, which also defines the critical temperature T*. And $T_{0,cr}$ defines the critical surrounding temperature. When the heat generation curve has two intersections with the heat loss curve, line 1 with surrounding temperature T_0, the reactant system is in the subcritical regime and the reactant temperature always remain around temperature T_1. When they do not have any intersection, the reacting system enters the supercritical regime and will be exponentially self-heated. This self-heating eventually leads to thermal explosion or runaway. System criticality can be altered by changing some process variables, such as surrounding temperature or the heat transfer coefficient, as well as reactant concentration. However the influence of concentration is not included in this least sophisticated model and will be discussed later in this work. The influences of a process parameter variation on explosion limits are demonstrated in Figure 3.2 and Figure 3.3. As shown in Figure 3.2, an increase of surrounding temperature will make the system become supercritical. Figure 3.3 shows that the decrease of heat transfer coefficient will also enlarge the thermal runaway region.

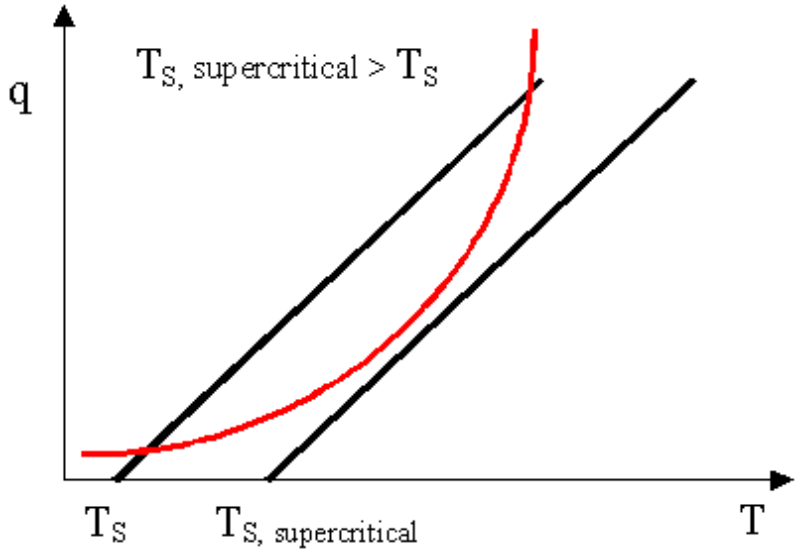

Figure 3.2 The effect of ambient temperature changes on the critical conditions for a thermal explosion

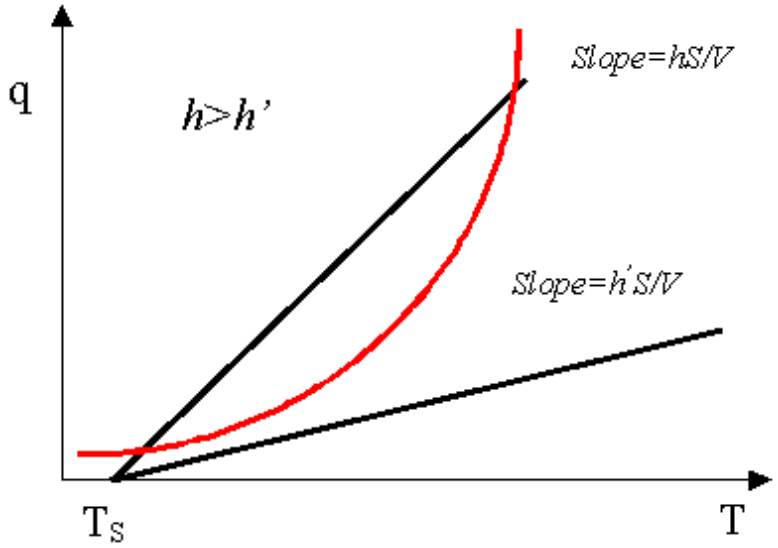

Figure 3.3 The effect of the heat transfer coefficient reduction on the critical conditions for a thermal explosion

The Semenov Theory provides a straightforward method for calculation of the critical temperature by equating the rates of energy generation and energy removal as well as their derivatives with respect to temperature T at the critical temperature T*.

$$\frac{Q\rho V}{hS} A \exp(-\frac{E_a}{RT_*}) = T_* - T_S \tag{3.2}$$

$$T_* - T_S = \frac{RT_*^2}{E_a} \tag{3.3}$$

Only one root of equation (3.3) is feasible and as follows, the other root is not physically possible.

$$T_* = \frac{E_a}{2R}(1 - \sqrt{1 - \frac{4RT_S}{E_a}}) \tag{3.4}$$

Because the term RT_S normally is far less than E_a for explosives and propellants, equation (3.4) can be further simplified with a Taylor series expansion to give the following approximate solution for the critical temperature.

$$T_* = T_S + \frac{RT_S^2}{E_a} \tag{3.5}$$

With equation (3.5), another approximation could be made and derived as follows.

$$\frac{1}{T_*} = \frac{1}{T_S}(1 + \frac{RT_S}{E_a})^{-1} \approx \frac{1}{T_S}(1 - \frac{RT_S}{E_a} + \frac{R^2T_S^2}{E_a^2} - \frac{R^3T_S^3}{E_a^3} + ...) \tag{3.6}$$

Substituting equation (3.5) and first two terms of (3.6) into equation (3.2) gives the following equation.

$$\frac{Q\rho VA}{hS}\frac{E_a}{RT_S^2}\exp(-\frac{E_a}{RT_S})=\frac{1}{e} \tag{3.7}$$

Equation (3.7) defines the critical condition of thermal explosion for the Semenov problem. Its left-hand side includes all principal process parameters that determine the reacting system criticality and normally is defined as Semenov parameter, *Se*, in recognition of Semenov's great contribution to thermal explosion theory development. The right-hand side, *1/e*, is the critical Semenov value.

$$Se=\frac{Q\rho VA}{hS}\frac{E_a}{RT_S^2}\exp(-\frac{E_a}{RT_S}) \tag{3.8}$$

And the time it takes to reach the critical temperature T^* can be obtained by integrating equation (3.1) from T_S to T^*. However an analytical expression is not possible without using some approximation, such as the Frank-Kamenetskii approximation or quadratic approximation.

3.2.2 Frank-Kamenetskii theory

Semenov's theory is valid as long as no temperature gradients exists inside the reactant mixture, which is possible when heat transfer at the interface is dominant or the sample size is fairly small. But in other circumstances, the heat of reaction normally generates temperature gradient in the reacting system. Frank-Kamenetskii theory was proposed to deal with this situation.

With Semenov's assumptions 2, 3 and heat conduction, governing energy balance equation gives following result.

$$-\lambda\frac{d^2T}{dx^2}=\rho QA\exp(-\frac{E_a}{RT}) \tag{3.9}$$

where λ represents thermal conductivity and x represents the reacting system dimensions. With the boundary condition of

$$-\lambda \left.\frac{dT}{dx}\right|_{x=1} = h(T - T_S) \tag{3.10}$$

and several dimensionless quantities are defined as follows.

$$T^* = T/T_S, \quad x^* = x/r, \quad \theta = E_a/RT_S, \quad \phi = (T - T_S)\frac{E_a}{RT_S^2}$$

where r is the dimension of the reaction vessel and ϕ is a small dimensionless temperature difference measured from ambient temperature.

$$T^* = 1 + \frac{\phi}{\theta} \tag{3.11}$$

In Frank-Kamenetskii theory, Frank-Kamenetskii approximation was made and widely used in its follow up research to get an analytical solution. The approximation, $\exp(-\frac{\theta}{T^*}) = \exp\left[-\theta(1+\frac{\phi}{\theta})^{-1}\right] \approx \exp(-\theta)\exp(\phi)$, is valid for small ϕ (T ≈ T_S) and the reaction has a very large activation energy. The dimensionless variables transform equations (3.9) and (3.10) to the following equations.

$$-\frac{d^2\phi}{dx^{*2}} = (\frac{\theta\rho A r^2 \exp(-\theta)}{\lambda T_S})\exp(\phi) \tag{3.12}$$

$$-\left.\frac{d\phi}{dx^*}\right|_{x^*=1} = Bi\phi|_{x^*=1} \tag{3.13}$$

$\frac{\theta\rho Ar^2 \exp(-\theta)}{\lambda T_S}$ is defined as the Frank-Kamenetskii constant, δ, which is a measure of the reactivity of chemicals, the dimension of the reacting system, and the effect of surrounding temperature. Bi is the Biot number and its magnitude determines the main resistance to heat transfer. However analytical solutions could be obtained only for symmetric shapes, such as a sphere, an infinitely long cylinder and infinite slab, which are defined by a single coordinate and belongs to “class A geometries”. The dimensionless temperature profiles for an infinite slab with different Frank-Kamenetskii constants and Bi equal to infinity are illustrated in Figure 3.4. The critical values of Frank-Kamenetskii constant for three major types of vessel are summarized in Table 3.2 [22]. Therefore, the critical volume for reactive storage vessel can be estimated with the critical Frank-Kamenetskii constant and this is extremely useful for storage practices of highly explosive chemicals.

Table 3.2Critical values of Frank-Kamenetskii constant for three main types of vessels

Shape	Energy equation	Critical Frank-Kamenetskii constant	Critical dimensionless temperature	Characteristic dimension
Infinite slab	$-\frac{d^2\phi}{dx^{*2}} = \delta \exp(\phi)$	0.88	1.12	Half-width of slab
Infinite cylinder	$-\frac{1}{r^*}\frac{d}{dr^*}\left(r^*\frac{d\phi}{dr^*}\right) = \delta \exp(\phi)$	2.00	1.39	Cylinder radius
Sphere	$-\frac{1}{r^{*2}}\frac{d}{dr^*}\left(r^{*2}\frac{d\phi}{dr^*}\right) = \delta \exp(\phi)$	3.32	1.6	Sphere radius

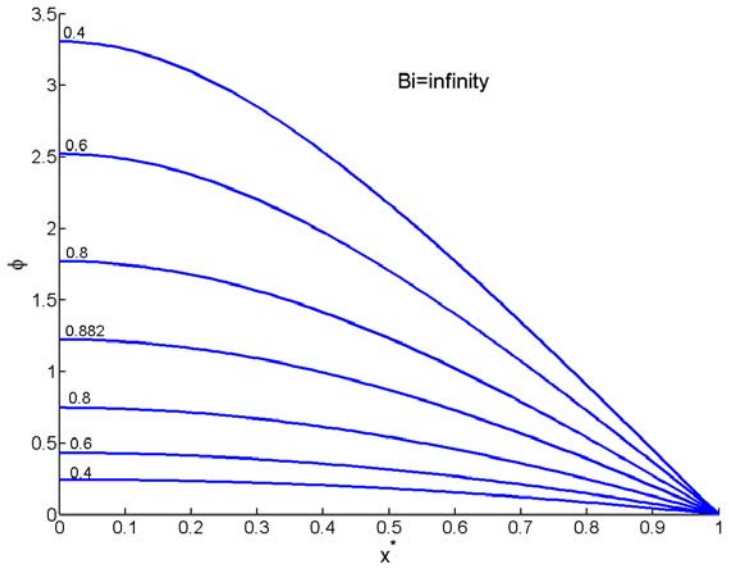

Figure 3.4 Dimensionless temperature profiles for infinite slab

Similar to the Semenov diagram, thermal runaway events under Frank-Kamenetskii conditions can be illustrated by plotting maximum dimensionless temperature versus Frank-Kamenetskii constants as shown in Figure 3.5.

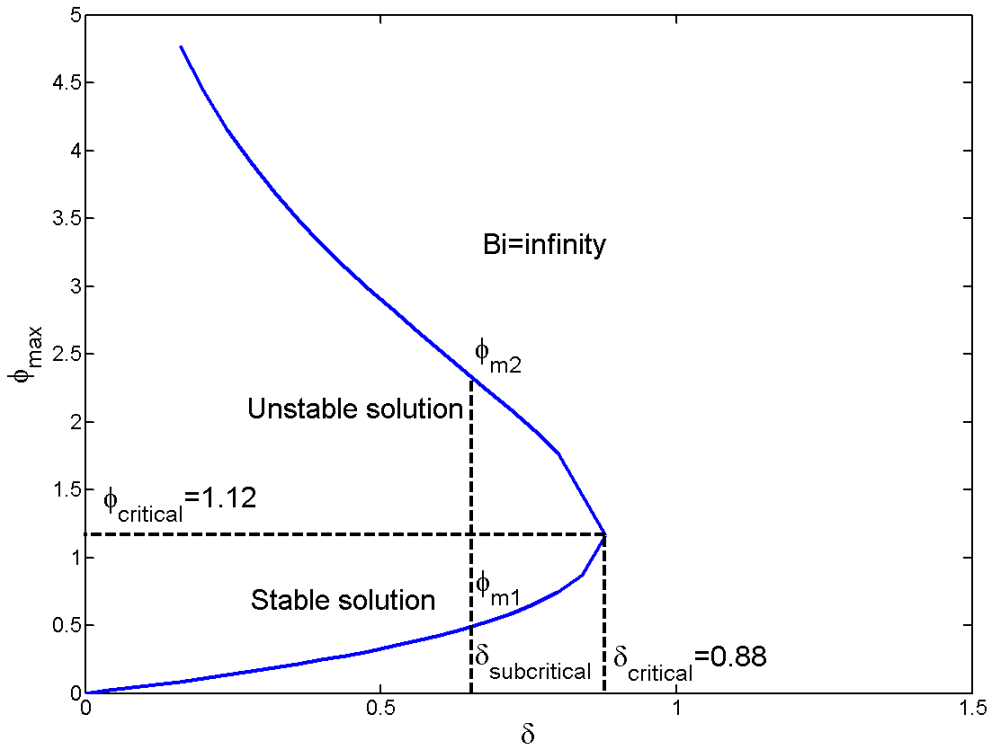

Figure 3.5 Maximum dimensionless temperature versus Frank-Kamenetskii number

As illustrated in Figure 3.5, there are three possible behaviors for a reactive chemical subjected to Frank-Kamenetskii conditions. The system is subcritical when its Frank-Kamenetskii constant is less than the critical value, $\delta_{critical}$. The system will be

heated up and the maximum dimensionless temperature inside reactive chemical due to self-heat is the corresponding ϕ_{m1} unless extra energy is provided to the system by heating to ϕ_{m2}, which will make thermal runaway occur.

When the system Frank-Kamenetskii constant is larger than the critical value, $\delta_{critical}$, system does not have a stable status and its temperature continues to increase. In the last case, the system is at a critical status with Frank-Kamenetskii constant equal to critical value, $\delta_{critical}$. The system will be heated to $\phi_{critical}$ and then undergo rapid self-heating.

3.3 Limitations of Semenov and Frank-Kamenetskii theories

Semenov and Frank-Kamenetskii theories are the foundation of the thermal explosion theory. However their basic assumptions impair their accuracy and applicable scope.

First of all, Semenov Theory assumes no reactant consumption. This assumption impairs their capability of describing real circumstances that reactants are always continually consumed until completely used up. The system with reactant consumption always shows a unique steady state where the reactant conversion is one and the system temperature, after passing through a maximum value, is equal to that of surrounding [23]. The system temperature will no longer reach an infinite value. so it is not possible to detect the supercritical behavior with temperature stability criteria. Instead, sensitivity approach, such as geometric sensitivity and normalized sensitivity, was proposed to distinguish subcritical and supercritical behavior [23-25].

Another significant limitation is that the heat transfer in Semenov Theory is only Newtonian cooling type, while several heat transfer modes exist in real situations. Frank-Kamenetskii theory made some improvement over Semenov Theory by considering the temperature gradient inside the reacting system. But this theory did not consider convection or buoyancy force that occurs in fluids. Both of these two fundamental theories encounter some difficulties for fluid systems, especially for a large quantity fluid, although they could give comparably satisfactory results for small systems [26, 27]. To get reliable result for a real situation, CFD simulation is needed to study the heat transfer phenomena for fluid systems.

3.4 Current thermal explosion study progress

3.4.1 Sensitivity approach for small-scale system

Bilous and Amundson proposed to use a parametric sensitivity concept, which measures the system response output for a small change of external parameters, instead of temperature stability to describe the behavior of tubular reactor, which is well-known to be sensitive to small inlet parameters variation [26]. The comparison between the governing equations of explosion theory and those of classical homogeneous tubular reactors indicates that parametric sensitivity concept is also applicable for the improvement of thermal explosion theory. Therefore several parametric sensitivity definitions were proposed to study the critical condition of thermal explosion with reactant consumption considered.

Bilous et al. defined sensitivity as the first order derivative of the temperature with respect to its initial value. Gray et al. adopted this approach for thermal explosion

theory [28]. However this approach requires a fixed sensitivity value to distinguish subcritical and supercritical behavior. Several other researchs also proposed some similar intuitive definitions based on the geometric characteristics of the temperature profile [24].

Several researchers claimed that it would be more convenient to develop an intrinsic parametric sensitivity definition. For example Lacey defined the sensitivity as the derivative of the maximum temperature value with respect to the Semenov number *Se*. The value of maximum sensitivity, the critical Semenov number, was used to distinguish subcritical and supercritical regions [25]. Morbidelli and Varma used the normalized sensitivity concept to include any independent process parameters and demonstrated this definition is more rigorous and can be applied to thermal explosion and chemical reactors [29].

Rice et al. defined the criticality or sensitivity as the inflection before the maximum in temperature-time trajectories [30], which is widely accepted by most researchers [31]. Recently Shouman and El-Sayed published a series of papers on the discussion of thermal explosion with reactant consumption from inflection point viewpoint [31-36]. In the work of Shouman and El-Sayed, the criticality or sensitivity was defined by the inflection point on the temperature-time and temperature-concentration planes. With consideration of reactant consumption, the critical condition not only is a function of temperature, but also a function of reactant concentrations. So the rigorous critical condition should be defined on the temperature-concentration plane. Shouman

and El-Sayed also proved that the critical condition defined on temperature-concentration plane includes the critical condition defined in previous works [25, 29].

In the work of Shouman and El-Sayed, the inflection point was determined by solving ($d^2\theta / dZ^2 = 0$) and ($d^3\theta / dZ^3 = 0$), where θ and Z are defined as dimensionless temperature and reactant concentration, respectively. The possible behaviors of ($d^2\theta / dZ^2 = 0$) and ($d^3\theta / dZ^3 = 0$) for n[th] order reaction on temperature-concentration plane are illustrated in Figure 3.6. As shown in Figure 3.6, system with two inflection points is supercritical and system without any inflection point is subcritical. The system with only one inflection point is at critical condition.

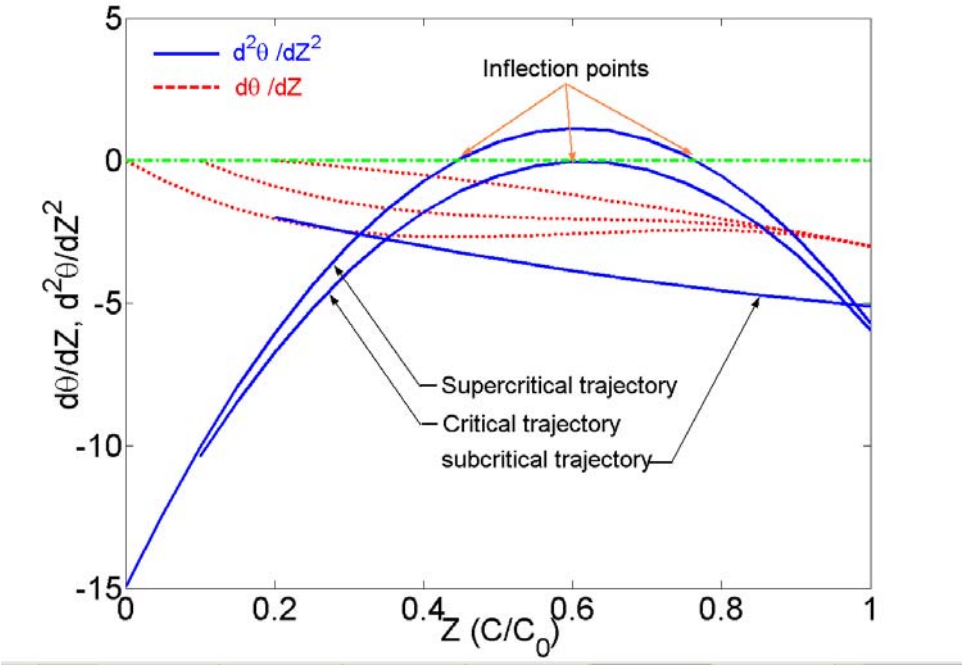

Figure 3.6 Mathematical behavior of n[th] order reaction on temperature-concentration plane

However a sufficient condition of inflection point existence is where the second derivative of the curve changes sign and the curve tangent exists [37]. With this rigorous definition, in order to get true inflection point, higher order derivatives need to be checked when the third order derivative is equal to zero. Therefore setting the third derivative to zero may omit some solutions. In this present work, the rigorous definition of inflection point is used to study the critical behavior of HAN.

3.4.2 Application of CFD into thermal explosion

Most research mainly focuses on experimental test on reactive chemicals and numerical regression of experimental data, which are mainly obtained from small scale experimental systems. Therefore, the neglect of convection and buoyancy will not significantly affect the correlation and analysis result accuracy. However in the practical fluid storage vessels, mass and heat transfer caused by convection can not be neglected for the spatial segregation of temperature and concentration, which may have significant influence on critical behavior of reactive chemicals.

CFD simulation technology has been widely used in polymerization reactors, combustors, and engines studies for many years [38-41]. Those studies prompted the understanding on the behavior and stability issues inside all these reactors and their design, control etc. Furthermore CFD is also capable to assist in the simulation and design of multiphase microreactors [42]. Although CFD has been widely used in industries and research institutes, applying CFD to thermal explosion phenomena is still at its very beginning stages.

Unlike the decomposition kinetics, which remains the same regardless of the storage quantity, heat and mass transfer mechanism is significantly affected by the system scale. Recently Sheu et al. conducted numerical analysis on the hot spot distribution for reactive chemical whose reaction mechanism follows zero order reaction [43]. Campbell et al. compared the experimental temperature distribution and numerical analysis results with natural convection considered [44]. Both the work of Sheu et al. and Campbell et al. used Boussinesq approximation to represent the buoyancy force. Although Boussinesq approximation has been widely used to describe the natural convective flow in many cases and given faster convergence and reasonable results, it is not applicable for the reacting flow problem [45].

In the work of Sheu et al., a modified Rayleigh number was used to characterize the natural convection developed inside a cylinder storage tank. However this modified Rayleigh number is related to the apparent activation energy and is not equivalent to the commonly used Rayleigh number. And the application of their results to other chemicals is not straightforward or convenient. Besides, they did not consider an important fact that most storage vessels are installed in air. The fluid inside the tank will be cooled by the surrounding fluid, which typically is air. The heat transfer resistance for such a storage tank includes fluid-film resistance, vessel-wall resistance, and the air-film resistance. The air-film resistance normally is the dominant term among the three and the heat transfer coefficient of air typically is in the range of 10-100 $W/m^2/K$ [46]. And the ratio of volume to surface area also impacts the system energy balance, which subsequently affects the system temperature. So the study of Sheu et al. may not sufficiently describe

the real phenomena. This present work revisits this problem by taking into account air-film thermal resistance.

Traditional analytical and numerical methods are not capable to solve those partial differential equations (PDE) for a large quantity of fluid. CFD simulation utilizes Finite Volume Method (FVM) or Finite Element Method (FEM) to solve the Navier-Stokes equation for a fluid system. This method is beyond the scope of this work and its detail could be referenced from software vendor websites as well as CFD textbooks. In the present work, this sophiscated solver engine combining with traditional thermal explosion theory is used to study the critical behavior for a large quantities of a HAN aqueous solution. The present work focuses on storage critical conditions determination for a large quantity HAN aqueous solution and aim to improve HAN related process safety as well as other reactive chemicals.

4. HYDROXYLAMINE NITRATE THERMAL DECOMPOSITION STUDY

4.1 Introduction

Hydroxylamine nitrate is an onium salt, whose specific feature is its dynamic equilibrium status between initial salt-forming compounds and the salt. Hydroxylamine nitrate is commercially available as a clear and colorless aqueous solution. It has been used as a reductant in nuclear industry and also considered for use as a liquid propellant or oxidizer for hybrid rockets. Its main advantages are high energy density and environmental friendliness.

Poor thermal stability and contamination issue of this compound have caused several incidents in the past [3]. Mary Kay O'Connor Process Safety Center (MKOPSC) and other research institutions and groups have conducted extensive research on its thermal stability, decomposition mechanism, and the effect of metal ion catalysis by using various techniques under different conditions [5, 6, 47-51]. These works have accumulated significant amount of knowledge and data on HAN that can be used to improve HAN processing safety. However more information is needed to ensure safe HAN storage and processing.

Previous research attempted to correlate the self-catalytic kinetic parameters with n^{th} order reactions even though the self-catalytic behavior of HAN had been confirmed by adiabatic decomposition tests and modeling. So the work reported here aims to explore HAN autocatalytic parameters using adiabatic calorimetry data. Several

researchers proposed to explore the decomposition reaction network of reactive chemicals by measuring concentration of reactants, intermediates and products during the reaction with analytical instruments, such as IR spectroscopy, GC, and HPLC [5, 6, 49, 51]. The drawback of this approach is the concentrations of decomposition intermediates, such as HNO and HNO_2, still cannot be accurately determined. The obtained reaction pathway and associated kinetic parameters are not easy to apply to the thermal runaway/explosion stages study because problem independent variables increase dramatically and it is beyond the capability of current numerical methods. Although the decomposition process of HAN consists of many consecutive and competitive reaction steps, the work reported here proves that the observed thermal behavior could still be modeled well with a single overall reaction.

Past research and industrial practices have demonstrated the kinetic parameters obtained from adiabatic calorimeters are reliable, conservative, and widely accepted for practical application [48, 52, 53]. HAN adiabatic decomposition experiments were conducted to estimate its autocatalytic reaction kinetic. The contamination effect of nitric acid and iron ions are also investigated in this work. This work could be used to provide guidance on determining safety margins for storage and manufacture conditions.

4.2 Experimental setup and method

4.2.1 Reagents

Hydroxylamine nitrate (24 mass%, Aldrich catalog number 438235) aqueous solution was used in this work. Nitric acid (68 mass%, EMD catalog number NX0409-2) was used to study the contamination effect of nitric acid and the coexistence effect of

nitric acid and iron ions. Ferrous Sulfate (1 mol/L, Fisher catalog number S74262-1) and Ferric Nitrate (1 mol/L, Fisher catalog number S74200-1) were used to determine the effect of contamination by iron ions and coexistence of nitric acid and iron ions. All of these chemicals were used without further purification or analysis.

4.2.2 Automatic Pressure Tracking Adiabatic Calorimeter (APTAC)

Adiabatic calorimeter is the most important apparatus to obtained reaction kinetics and conduct thermal hazard evaluation for a reactive chemical in safety analysis. Automatic Pressure Tracking Adiabatic Calorimeter (APTAC) is the most advanced apparatus in this area. APTAC calorimeter can be operated in a variety of test modes, such as Heat-Wait-Search, and isothermal mode with temperatures up to 500°C and pressures ranging from vacuum to 2,000 Pisa. It can detect the exotherm with heat generation rates from 0.04 to 400°C/min. It can also produce low thermal inertia data with the DIERS pressure compensation technique, in which the pressure outside the sample cell is controlled to match the pressure inside the sample cell. APTAC and its Heat-Wait-Search (HWS) were used to perform thermal decomposition studies on HAN. Glass sample cells and Teflon coated thermocouples were used to reduce the catalytic and contamination effect of thermocouple metals. The detailed introduction about APTAC equipment and its HWS mode are described in the references [48, 53].

Although the specific heat of a reacting system changes with the solution composition and temperature during the decomposition process, the specific heat of diluted HAN solution was assumed to be constant (4.3 kJ/kg/K) in the analysis for the similarity of diluted aqueous HAN solution to water [5, 48].

4.2.3 Kinetics analysis method

The classic kinetics analysis method for adiabatic calorimeter was developed by Townsend et al [54]. The general principles of kinetic analysis method of Townsend et al. are energy conservation equation under adiabatic condition. And one important assumption of this method is that reactant concentration at any temperature or time is approximately proportional to reactant temperature. This method can be summarized by following equations.

$$C = \frac{T_f - T}{\Delta T_{ad}} C_0 \tag{4.1}$$

$$\frac{dC}{dt} = -\frac{C_0}{\Delta T_{ad}} \frac{dT}{dt} \tag{4.2}$$

$$\frac{dC}{dt} = Ae^{-\frac{E_a}{RT}} f(c) \tag{4.3}$$

With an appropriate overall reaction, heating rate or temperature can be correlated with temperature measurement in adiabatic tests by using equation (4.2) and (4.3). Then the reaction order, apparent activation energy, and preexponential factor can be determined with equations (4.1-4.3). For example, the self-heating rate of a n^{th} order reaction is related to onset temperature as follows.

$$\ln\left(\left.\frac{dT}{dt}\right|_0\right) = \ln\left(\Delta T_{ad} C_0^{n-1} A\right) - \frac{E_a}{R}\frac{1}{T_0} \tag{4.4}$$

With equation (4.4), all kinetic parameters can be obtained from adiabatic calorimeter measurements. Other important reactivity hazard indicators, such as time to

maximum rate, can also be estimated with this method. This method is widely accepted and used in current adiabatic calorimeter analysis and thermal safety analysis area.

However the applicability of this method is highly affected by thermal inertia, applicable model for reactive chemical, and instrument accuracy and sensitivity. This method is not able to describe the decomposition behavior of certain reactive chemical with complicated reaction networks, such as hydroxylamine nitrate with an autocatalytic reaction [4, 47].

Because self-heating data actually is obtained from temperature data by numerical differential method, it may not be able to accurately describe the self-heating behavior due to numerical error. Therefore, direct temperature prediction using an appropriate reaction model may give better result. It is also able to eliminate numerical error induced by numerical differentiation. Wilcock et al. proposed and applied this approach to methanol/Acetic anhydride system, which also undergoes autocatalysis reaction [55]. This method obtains very good results and has proved to be an effective kinetic analysis method for adiabatic calorimeter measurements. This approach will be adopted in this present work.

4.3 Experimental results

4.3.1 HAN decomposition behavior study

The APTAC HWS mode was utilized to determine the decomposition behavior of HAN. The pressure and temperature profiles of HAN decomposition of two identical tests using about 6 gram HAN under the HWS mode of the APTAC are shown in Figure 4.1 and Figure 4.2.

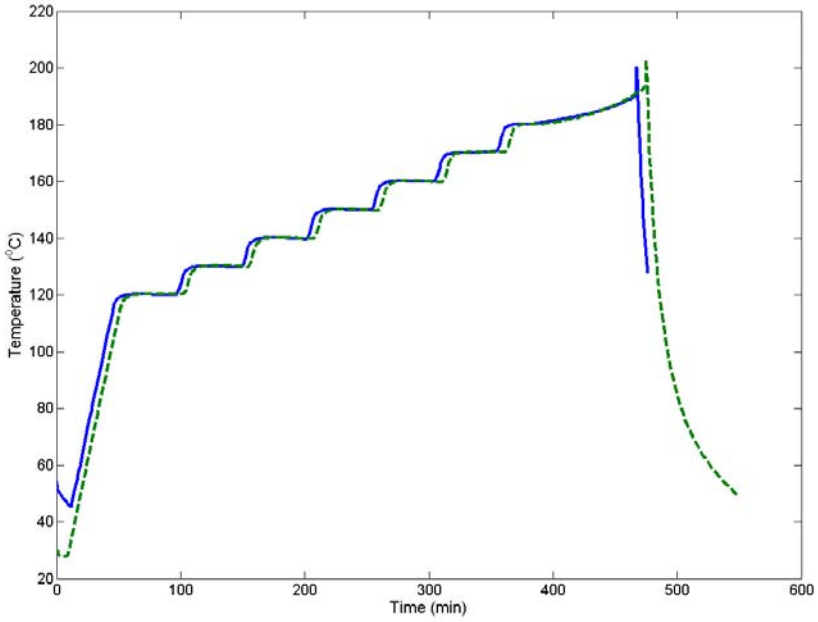

Figure 4.1Temperature evolution profile of HAN decomposition at HWS mode

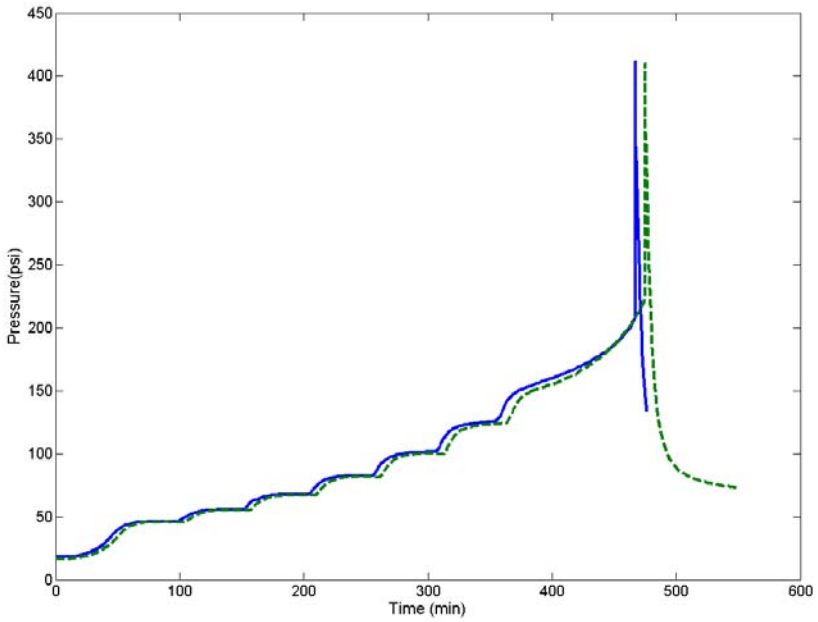

Figure 4.2 Pressure evolution profile of HAN decomposition at HWS mode

As shown in Figure 4.1, the reactant in the reaction vessel will first be heated to the start temperature, such as 120^{o}C, with the heating rate of 2^{o}C/min. Then the reactant will be stabilized for about 15 minutes. Afterwards, APTAC goes to search mode to see whether there is an exothermal phenomena. If not, the reactant will be heated to the next target temperature, 130^{o}C, which is 10^{o}C higher than the previous target temperature. This procedure will be reproduced until thermal runaway is detected and the APTAC then enters the adiabatic operation mode.

With the assistance of heating rate and pressurization rate profiles, which are shown in Figure 4.3, the onset temperature (T_0) and maximum temperature (T_{max}) etc. can be determined and summarized in Table 4.1. As shown in Figure 4.3, the initial heating rate continues to increase to the preset value, 2^{o}C/min. Then the heating rate maintains at 2^{o}C/min until reaching preset start temperature, 120^{o}C. Meantime, the system is slowly pressurized due to steam and possible evaporated nitric acid pressure. After reaching 120^{o}C, APTAC enters wait-search mode and tries to maintain the temperature at 120^{o}C. Because hydroxylamine nitrate does not have significant decomposition at this stage yet, system temperature and pressure does not change very much. So both heating rate and pressurization rate decrease until wait-search mode is terminated and enter next heat stage. This procedure is repeated until an exotherm is detected. Heat of reaction of HAN decomposition measured by APTAC is about 118 ± 20 kJ/mol.

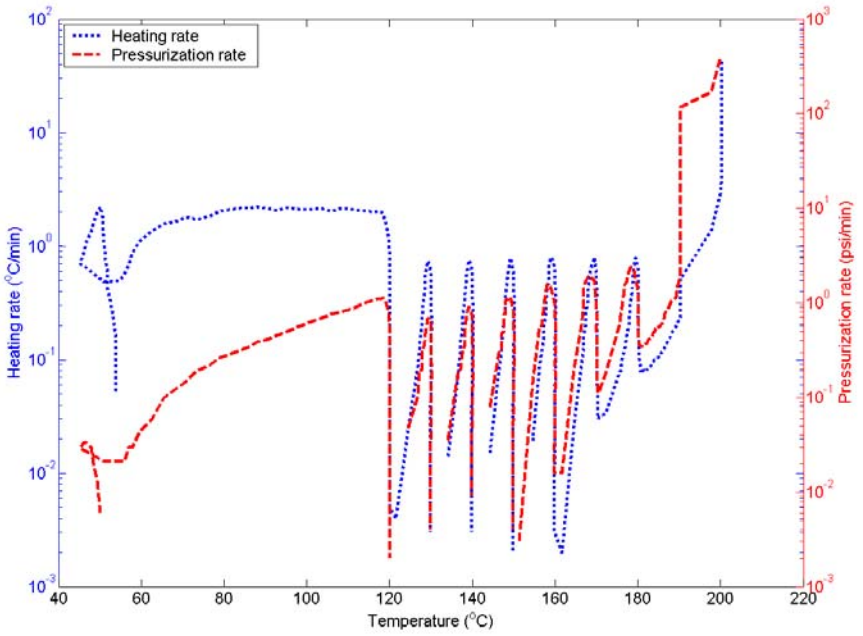

Figure 4.3 Heating rate and pressurization rate of HAN decomposition process

Table 4.1 APTAC Heat-Wait-Search results of HAN thermal decomposition

	T_0 (°C)	T_{max} (°C)	P_{max} (psi)	dT/dt_0 (°C/min)	dT/dt_{max} (°C/min)	dP/dt_{max} (psi/min)	Phi factor (ϕ)	$\Delta H_{r\times n}$ (kJ/mol)
Glass cell	181.6±2.0	201.6±1.8	410.6±1.0	0.08±0.004	33.1±13.2	429.6±43.2	2.80	118±20

The system pressure-temperature profile is illustrated in Figure 4.4. After the runaway reaction, the system pressure cannot return to the original pressure. This indicates that there are non-condensable gases generated in this system, probably including nitrogen and nitrogen oxide. This phenomenon demonstrates that HAN could

release large amount of gases at thermal runaway stage and has severe explosion hazard. The pressure profile of the system passes the saturated steam profile around 180^{o}C. This may indicate the occurrence of significant exothermal phenomena and some heat loss due to solvent evaporation.

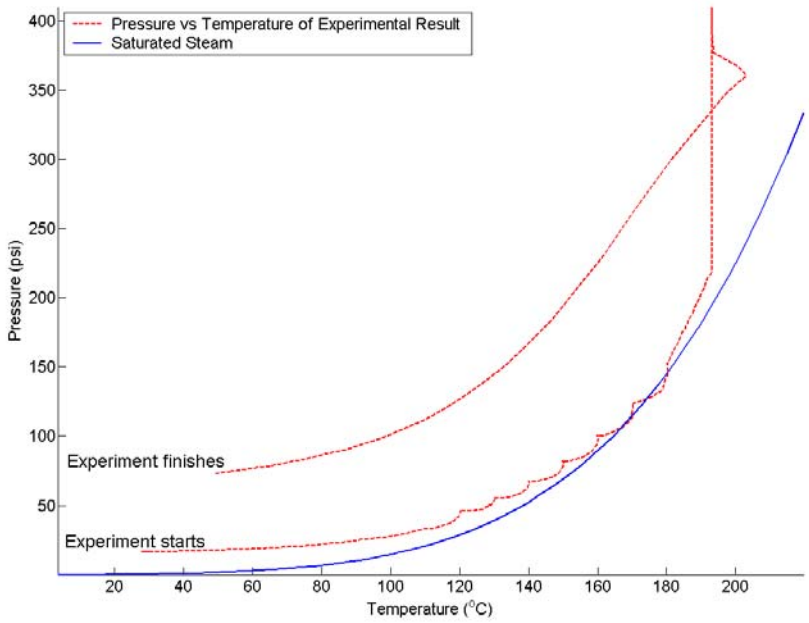

Figure 4.4 Experimental pressure changing profile with temperature

Because the final gas phase pressure is not very high as illustrated in Figure 4.4, idea gas law can be used to roughly estimate the amount of gases generated in the decomposition process of hydroxylamine nitrate. The moles of non-condensable gases is estimated as follows.

$$\Delta n = \frac{\Delta PV}{RT} \tag{4.5}$$

where ΔP=3.85e5 Pa, V=100ml, and T=50^{o}C. Gas generation of HAN in current experimental conditions is 0.95 mol-gases/mol-HAN. In the work of Wei, 4.2 g HAN was used to conduct similar adiabatic decomposition test with APTAC [56]. With her result, gas generation of HAN in similar experimental conditions is 0.98 mol-gases/mol-HAN. Therefore, both tests give consistent results about gas generation capability of HAN in adiabatic condition. Although decomposition reaction stoichimometry is significantly affected by experimental conditions, non-condensable gas generation profile under adiabatic condition is an important indicator to evaluate an explosion hazard for reactive chemicals because adiabatic condition normally represents the worst-case scenario. The overall decomposition mechanism of HAN proposed in the past is summarized in Table 4.2. Only the mechanism proposed by Schoppelrei et al is able to explain observed gas release capability of hydroxylamine nitrate [51]. However this mechanism is different from all other proposed mechanism. Further research is needed to propose appropriate mechanism under adiabatic condition.

Table 4.2 Overall decomposition mechanisms of HAN

Researcher	Overall decomposition mechanism	Condition
Wei [56]	$3NH_3OH \bullet NO_3 \rightarrow N_2O + N_2 + 2HNO_3 + 5H_2O$ $4NH_3OH \bullet NO_3 \rightarrow 3N_2O + 2HNO_3 + 7H_2O$	Adiabatic 24 mass% HAN
Amariei et al. [49]	$6NH_3OH \bullet NO_3 \rightarrow 2NO + 3N_2 + 4HNO_3 + 10H_2O$ $6NH_3OH \bullet NO_3 \rightarrow 2N_2O + 2N_2 + 4HNO_3 + 10H_2O$	200°C 80 mass% HAN
Oxley et al. [57]	$3NH_3OH \bullet NO_3 \rightarrow N_2O + N_2 + 2HNO_3 + 5H_2O$ $4NH_3OH \bullet NO_3 \rightarrow 3N_2O + 2HNO_3 + 7H_2O$	140°C 24 mass% HAN
DOE [3]	$5NH_3OH \bullet NO_3 \rightarrow 3N_2 + 4HNO_3 + 8H_2O$ $4NH_3OH \bullet NO_3 \rightarrow 3N_2O + 2HNO_3 + 7H_2O$	N/A
Sugikawa et al. [58]	$3NH_3OH \bullet NO_3 \rightarrow N_2O + N_2 + 2HNO_3 + 5H_2O$	N/A
Schoppelrei et al. [51]	$4NH_3OH \bullet NO_3 \rightarrow 3.2N_2O + 0.4O_2 + 1.6HNO_3 + 7.2H_2O$	Adiabatic 0.2M, 0.1M 463K-523K

Although evaporated nitric acid may also contribute to pressure increases in this process, Amariei et al. conducted HAN decomposition test in a dynamic reactor at 200°C and their results show the major gas products are NO, NO_2, and N_2O [49]. Because gas phase cannot be analyzed with current APTAC configuration, current gas products were not subjected to any analysis. Overall further work needs to be conducted to determine decomposition stoichimometry for hydroxylamine nitrate.

4.3.2 The effect of nitric acid on the HAN decomposition behavior

Nitric acid plays a very important role in the application and manufacture of HAN. For example, nitric acid is used in the manufacturing process of HAN from hydroxylamine sulfate or hydrochloride by an electrolysis method, which uses cation and anion exchange resins and a double decomposition reaction. However the appearance of nitric acid does accelerate the decomposition process of HAN [3]. Therefore, it is necessary to understand the decomposition behavior of HAN mixed with nitric acid. The temperature changing profiles of HAN/nitric acid solution are shown in Figure 4.5, where the phi factor, ϕ, is about 3.3.

Figure 4.6 illustrates that the onset temperature of HAN under adiabatic condition significantly decreases with increasing nitric acid concentration. The onset temperatures were significantly decreased from 171^{o}C to 147^{o}C by increasing nitric acid concentrations from 0 mol/L to 1.38 mol/L. Current work did not further increase nitric acid concentration to avoid changing thermal inertia. The result reported here is also compared with other available literature. Although the results are not completely same for different apparatus used, they have the same trend and comparable magnitude.

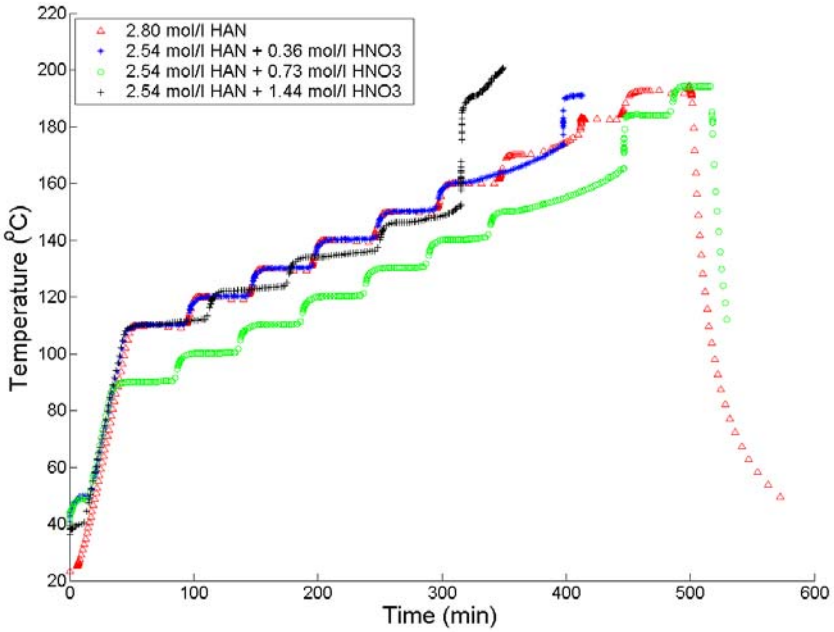

Figure 4.5 Temperature profiles of HAN contaminated by nitric acid

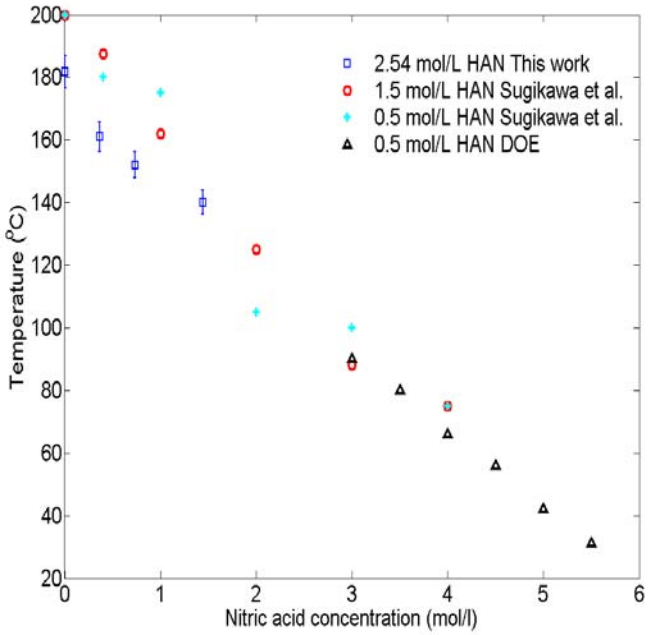

Figure 4.6 Influence of nitric acid on the onset temperature of HAN

In the decomposition process of HAN, HAN will first dissociate to nitric acid and hydroxylamine. Thereafter, hydroxylamine can be oxidized by nitric acid and nitrous acid. The oxidation mechanism of hydroxylamine by nitric acid and nitrous acid is as follows [59, 60].

$$HAN + H_2O \rightarrow NH_2OH + HNO_3 + H_2O \quad (4.6)$$

$$NH_2OH + 2HNO_3 \rightarrow 3HNO_2 + H_2O \quad (4.7)$$

$$NH_2OH + HNO_2 \rightarrow N_2O + 2H_2O \quad (4.8)$$

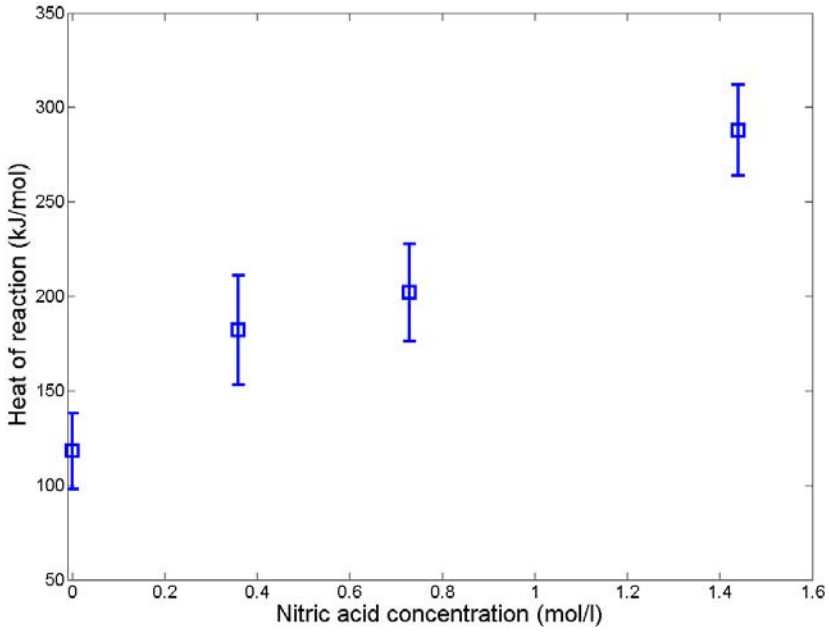

Figure 4.7 Effect of nitric acid concentration on heat of reaction

With increasing concentrations of nitric acid, oxidation process will accelerate and heat release rate will increase. Therefore, the onset temperature will decrease with the increase of nitric acid concentration. However the increase of nitric acid concentration may exacerbate the leaching of iron from practical stainless steel storage vessels. The coexistence effect of nitric acid and iron ions is studied in Section 4.3.4.

Figure 4.7 illustrates that heat of reaction increases with nitric acid concentration, which indicates the reaction pathway changes with addition of nitric acid. Addition of nitric acid may affect the disassociation equilibrium of HAN and the following oxidation pathway. Liquid phase analysis is needed in the future to study the function of nitric acid. Furthermore, gas generation amount per mole HAN with contaminant, nitric acid, is 1.08 mol-gases/mol-HAN, which is higher than that of pure HAN. This indicates the mixture of HAN and nitric acid has more severe explosion hazard than HAN solution does in two aspects. One is poorer thermal stability and the other is higher gas generation capability.

4.3.3 Effect of iron ions on the HAN decomposition behavior

Because hydroxylamine nitrate is an onium salt, it will disassociate to nitric acid and hydroxylamine in water solution. Both nitric acid and hydroxylamine stay at ionization status. Hydroxylamine can easily react with transition metals for its chemical structure. Both nitrogen and oxygen atom of hydroxylamine can donate their electron lone pairs to transition metals. This feature not only provides oxidization or reductive capability, which endow hydroxylamine nitrate many applications in nuclear and rocket

industries, but also impairs hydroxylamine nitrate thermal stability and compatibility with contaminants.

On the other hand, most storage vessels are made with stainless steel, which will leach iron ions into hydroxylamine nitrate solution at acid environment. Ferric ion probably is the most common contaminant for hydroxylamine nitrate. Therefore, it is necessary to study the influence of iron ions on the thermal stability of hydroxylamine nitrate for safe storage, transportation, and handling.

Ferric nitrate and ferrous nitrate are added into hydroxylamine nitrate solution, respectively, and then heat-wait-search mode is used to examine the influence of Fe^{2+} and Fe^{3+}. Temperature and pressure changing profiles for hydroxylamine nitrate contaminated with iron ions are similar to Figure 4.1 and Figure 4.2 and not going to be shown here.

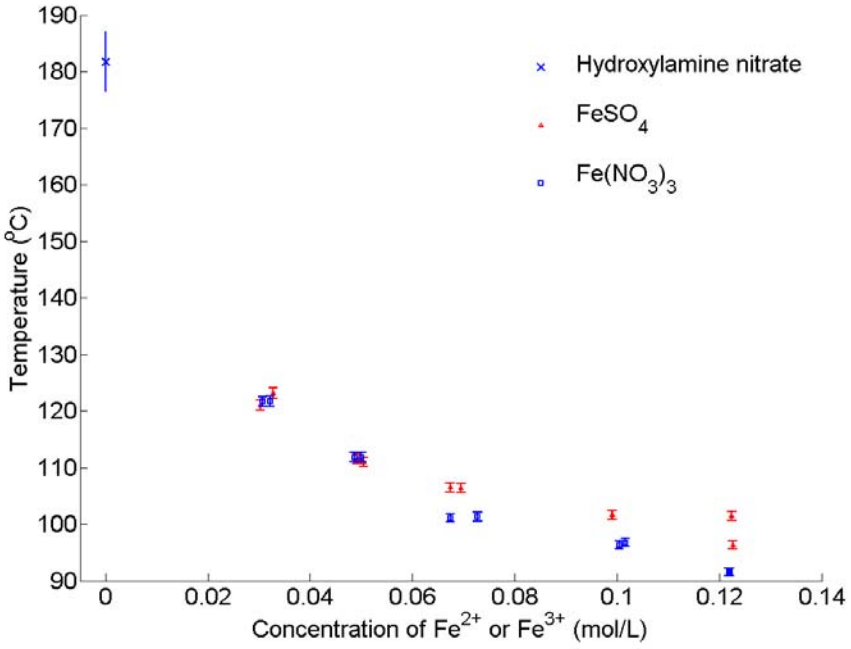

Figure 4.8 Effect of iron ions on the onset temperature of HAN decomposition

As illustrated in Figure 4.8, onset temperature of hydroxylamine nitrate contaminated by iron ions is significantly lower than that of pure hydroxylamine nitrate. The iron-catalyzed hydroxylamine nitrate decomposition reaction mechanism is as follows [3].

$$2NH_3OH^+ + 4Fe^{3+} \rightarrow 4Fe^{2+} + N_2O + H_2O + 6H^+ \quad (4.9)$$

$$2Fe^{2+} + HNO_3 + 2H^+ \rightarrow 2Fe^{3+} + HNO_2 + H_2O \quad (4.10)$$

As shown in Figure 4.8, ferrous ion and ferric ion do not have any significantly different influence on the onset temperature-decreasing trend and magnitude and this fact is consistent with iron-catalyzed hydroxylamine nitrate decomposition mechanism,

which indicates both ions only participate in the reaction loop consisted of reaction (4.9) and (4.10).

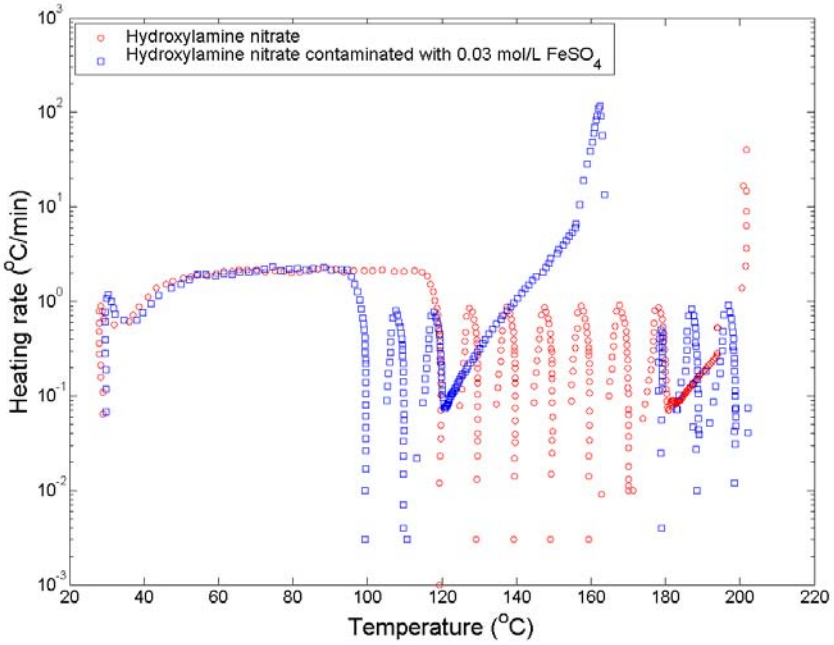

Figure 4.9 Heating rate profile for HAN and contaminated HAN decomposition

Figure 4.9 illustrated the influence of iron contamination on self-heating rate and decrease of onset temperature of HAN decomposition process. Not only onset temperature of contaminated hydroxylamine nitrate is much lower than that of pure hydroxylamine nitrate, but also maximum self-heating rate of contaminated HAN is much bigger than that of pure hydroxylamine nitrate. As shown in Figure 4.10, pressurization rate of contaminated hydroxylamine nitrate is also higher than that of pure

HAN. Overall, iron contaminant not only decreases thermal stability but also increases explosion hazard of hydroxylamine nitrate. Therefore, iron concentration must be strictly controlled to ensure safe application of hydroxylamine nitrate.

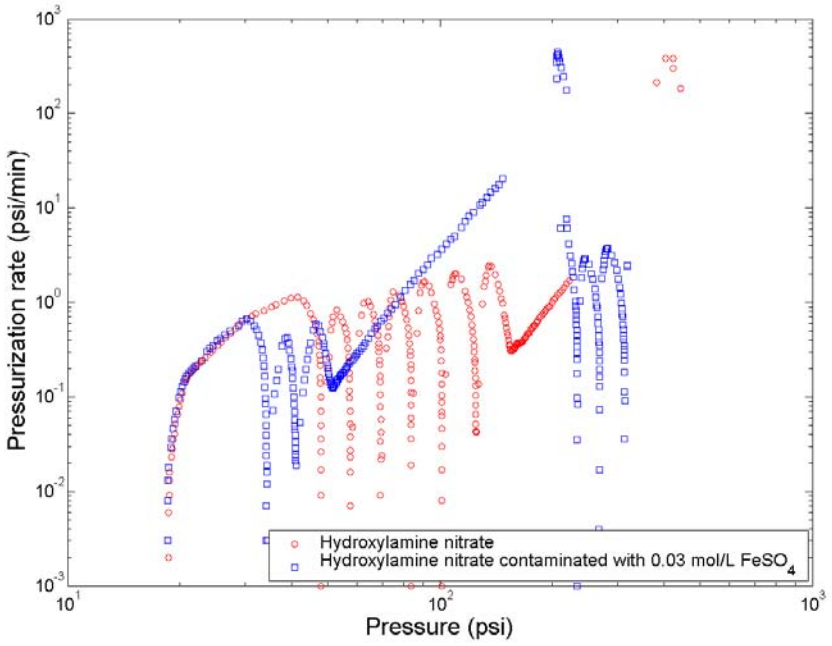

Figure 4.10 Pressurization rate profile for HAN and contaminated HAN decomposition

Figure 4.11 is used to compare the cool down pressure after the decomposition. It indicates the quantity of generated non-condensable gases remain the same regardless of the presence and quantity of iron ions. Therefore, hydroxylamine nitrate decomposition reaction pathway does not change under contamination of iron ions. Heat of reaction for contaminated hydroxylamine nitrate is 113±8 kJ/mol, which is almost the same

magnitude to that of pure hydroxylamine nitrate. It further confirms decomposition pathway of hydroxylamine nitrate is not affected by the presence of iron ions. Liquid and gas phase composition analysis may need to be conducted to further investigate the function of iron ions.

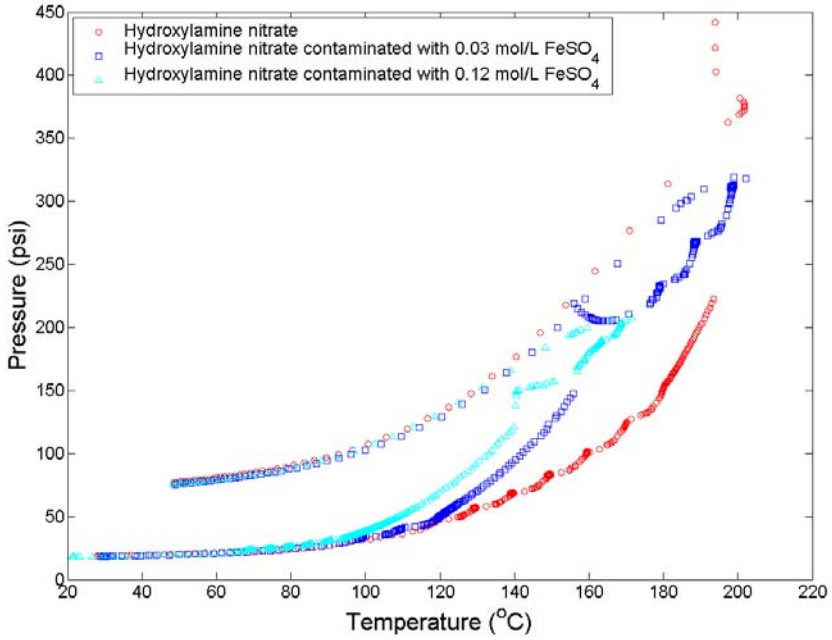

Figure 4.11 Pressure versus temperature profile for contaminated HAN and pure HAN solution

4.3.4 Coexistence effect of iron ion and nitric acid

Because most storage vessels are made with stainless steel, it is very common that iron ions are present in stored hydroxylamine nitrate solution because of the dissociated nitric acid. As reported by Sugikawa et al., a stainless steel reactor vessel

does leach iron ion into the sample solution during thermal analysis and iron ion concentration is as high as 0.14 g-Fe/L [58]. Furthermore, hydroxylamine nitrate and nitric acid solution is always prepared before the start of Plutonium Uranium Extraction (PUREX) process. This solution normally is stored in a stainless steel vessel. Therefore, the influence of coexistence of iron ion, nitric acid, and hydroxylamine nitrate on the mixture thermal stability must be examined to avoid similar accident occurring at DOE Hanford site [3].

Figure 4.12 illustrates influence of coexistent iron ion and nitric acid on thermal stability of HAN and shows that onset temperature of hydroxylamine nitrate decomposition further decrease with nitric acid concentration increase.

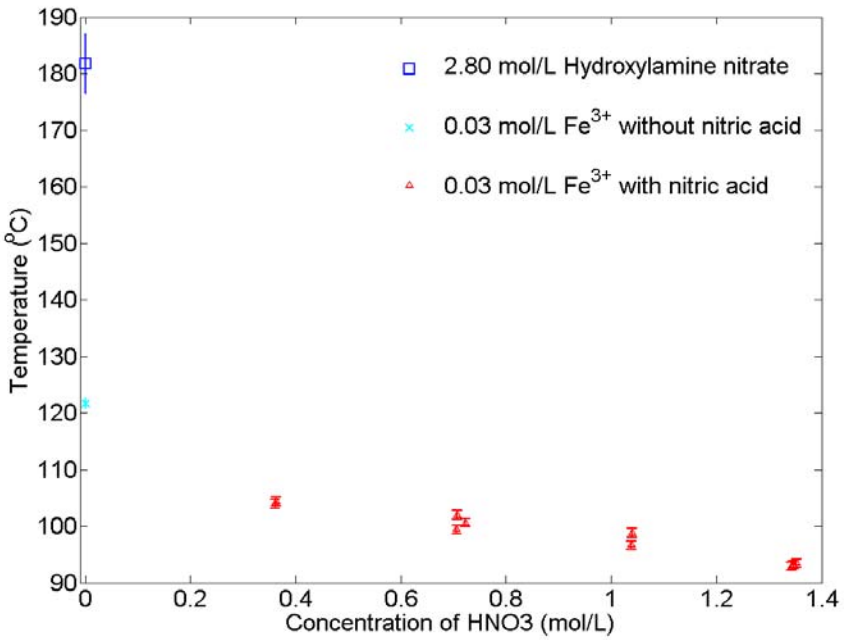

Figure 4.12 Influence of coexistent iron ion and nitric acid on thermal stability of HAN

4.3.5 Autocatalytic reaction model and its parameter determination

4.3.5.1 Hydroxylamine nitrate decomposition kinetics

The first step of HAN decomposition process is generally agreed to be the disassociation of HAN to hydroxylamine and nitric acid. This dissociation step has been confirmed to be very fast when the temperature is above 450K [5, 6] and that subsequent HAN decomposition becomes the hydroxylamine oxidation by nitric acid and nitrous acid at current experimental conditions. Therefore nitrous acid actually functions as the catalyst in this process. Although several works proposed that hyponitrous acid, HNO, could generate and oxidize hydroxylamine [59, 60], it was neglected in this work because of its extreme instability and limited information obtained from an adiabatic calorimeter. Among several lumped autocatalytic models developed to describe autocatalytic reaction behavior [55, 61, 62], the model developed at the Technical University of Berlin was adopted here for its better regression and prediction capabilities compared to the other models [55]. With this model the conversion rate can be expressed as follows.

$$\frac{d\alpha}{dt} = AC_0^{n-1}\exp(-\frac{E_a}{RT})(1-\alpha)^n(1+p\alpha^m) \tag{4.11}$$

where p and m are the parameters used to describe the catalytic effect of HNO_2.

Most of the data points recorded by APTAC are in the heat/wait/search stage. Only data points following detection of an appreciable exothermic reaction rate are kept to clearly show the HAN self-heating behavior and displayed in Figure 4.13. The result of experiment 1 was used to regress the five kinetic parameters. Several other experimental results were used to validate the model and its parameters. Both regression and prediction results for these experiments are also shown in Figure 4.13. With the

Matlab® ODE solver and optimization toolbox, the autocatalytic reaction model, equation (4.11) was used to regress the five parameters used in this model, which are summarized in Table 4.3. As shown in Figure 4.13, the prediction quality is fairly good and demonstrates that this model can accurately describe the decomposition behavior of HAN obtained with adiabatic calorimeter, APTAC.

Table 4.3 Nominal decomposition model parameters of hydroxylamine nitrate

Frequency factor	Activation energy (kJ/mol)	n	p	m
7.0e5 ± 2.3e3	82 ± 0.4	0.55 ± 0.06	165.2 ± 22.4	3.3 ± 0.21

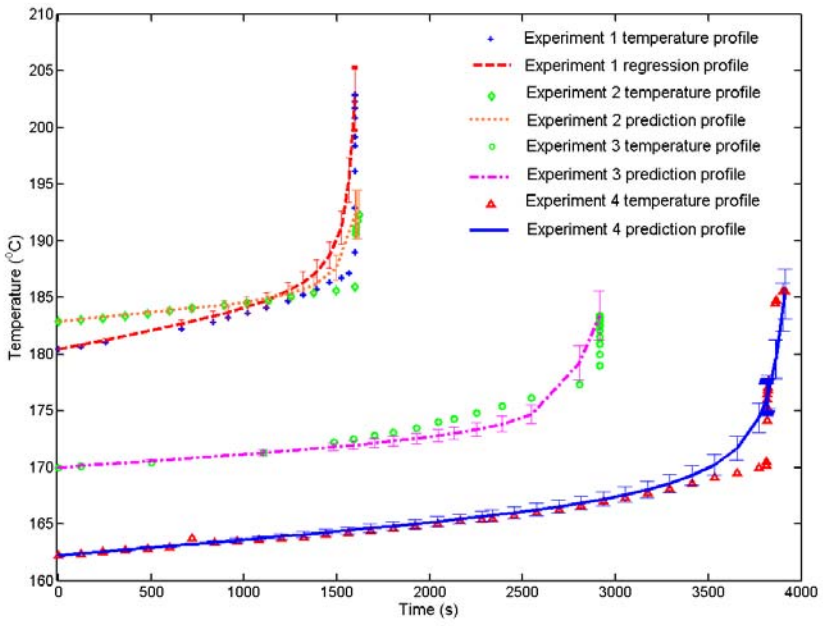

Figure 4.13 Self-heating curves of HAN and their regression/prediction results

Pembridge and Stedman reported that the activation energy for oxidation of hydroxylamine (HA) by nitric acid and by nitrous acid are 107 kJ/mol and 65 kJ/mol, respectively [63]. In addition, Shaw and Williams concluded that the activation energy of HAN decomposition is between 61 and 71 kJ/mol [64]. Furthermore, Schoppelrei used a lumped first order reaction to simulate the decomposition of HAN under similar conditions. Also they proposed that the apparent activation energy of HAN decomposition depends on the aqueous solution concentration. They reported that the activation energies for 0.92-1.52 M and 1.58-1.74 M HAN are 129 and 66 kJ/mol, respectively [5]. However Lee reported much smaller activation energies for the apparent elementary reactions of the HAN decomposition process for highly concentrated HAN solutions and solid HAN [6]. Comparison between result of this work and past research results is summarized in Table 4.4.

Table 4.4Comparison of apparent activation energy of present work and past research work

Activation Energy(kJ/mol)	Hydroxylamine oxidation by nitric acid	Hydroxylamine oxidation by nitrous acid	HAN decomposition
This present work	N/A	N/A	82 ± 0.4
Shaw et al.	N/A	N/A	$61 < E_a < 71$
Pembridge et al.	107	65	N/A
Schoppelrei et al.	N/A	N/A	129 ±29(0.92-1.52M) 66 ±8(1.58-1.74M)

The apparent activation energy reported in this work has the same magnitude as those for diluted HAN solution. The obtained apparent activation energy lies between the activation energies of oxidation of HA by nitric acid and by nitrous acid. This indicates that the self-heating stage of HAN may consist of oxidation of HA by nitric acid and nitrous acid.

4.3.5.2 Iron-catalyzed hydroxylamine nitrate decomposition kinetics

As discussed in Section 4.3.3, presence of iron ions does not change decomposition pathway of hydroxylamine nitrate. Reaction model (4.11) can also be used to simulate the temperature changing profile of contaminated hydroxylamine nitrate by iron ions. Both regression and prediction results for iron-catalyzed hydroxylamine nitrate decomposition are shown in Figure 4.14 and all parameters are summarized in Table 4.5.

Table 4.5 Nominal decomposition model parameters of iron contaminated hydroxylamine nitrate

Frequency factor	Activation energy (kJ/mol)	n	p	m
7.0e5 ± 1.0e3	62 ± 0.2	0.54 ± 0.02	164.7 ± 10.2	3.3 ± 0.1

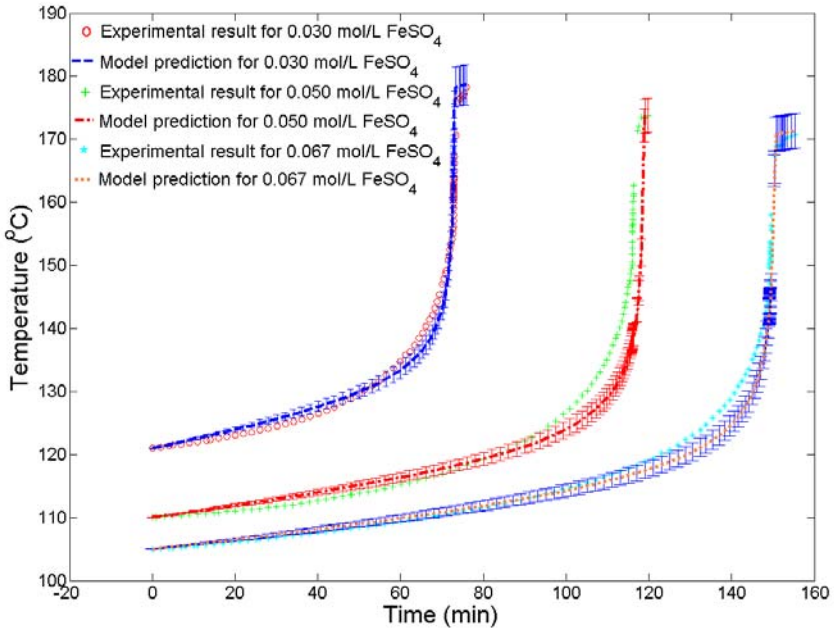

Figure 4.14 Self-heating curves of contaminated HAN by iron ion and their regression/prediction results

Comparison between Table 4.3 and Table 4.5 shows that most kinetic parameters except activation energy do not change much. Iron presence reduces activation energy of hydroxylamine nitrate decomposition about 18 kJ/mol. Therefore, appreciable exothermic decomposition of contaminated hydroxylamine nitrate occurs at much lower temperature than that of pure hydroxylamine nitrate as illustrated in Figure 4.8.

4.4 Conclusions

Hydroxylamine nitrate thermal decomposition was studied with heat-wait-search mode of Automatic Pressure Tracking Adiabatic Calorimeter (APTAC). Onset temperature and heat of reaction of hydroxylamine nitrate decomposition under adiabatic

condition are obtained. It is worth noting that the amount of generated non-condensable gas during hydroxylamine nitrate decomposition cannot be explained by most current proposed mechanisms. Further research is needed to discover hydroxylamine nitrate gas generation capability under adiabatic condition. This information is very important in pressure relief design because adiabatic decomposition represents worst-case scenario.

Influence of most common contaminants, including iron ions and nitric acid, on thermal stability of hydroxylamine nitrate are carefully examined. Pressurization profile and heat of reaction indicate iron ion may not change HAN decomposition pathway, it only reduces the decomposition activation energy. This fact is further confirmed by regressing temperature changing profile by using the same decomposition model as hydroxylamine nitrate. Iron ions contamination also increases energy and gas releasing rate during adiabatic decomposition of hydroxylamine nitrate. Therefore, iron ion concentration must be strictly controlled in storage and production process. Hydroxylamine nitrate directly stored in a stainless steel vessel must be inspected periodically to monitor the concentration of iron ions.

Influence of nitric acid on thermal stability and gas generation of hydroxylamine nitrate is also studied with APTAC by varying its concentration. Both heat of reaction and gas generation amount of hydroxylamine nitrate contaminated by nitric acid are higher than those of pure hydroxylamine nitrate. Potential causes include decomposition pathway changing and contribution of nitric acid decomposition. Further research is needed to determine the effect of nitric acid to provide guidance for industrial practices, such as hydroxylamine nitrate/nitric acid mixing and hydroxylamine nitrate production

with nitric acid. Coexistence of nitric acid and iron ion further reduce thermal stability of hydroxylamine nitrate. Nitric acid and hydroxylamine nitrate mixture cannot be stored in long term and storage temperature must be carefully controlled.

Autocatalytic kinetic model and associated parameters for hydroxylamine nitrate adiabatic decomposition is determined for the first time. This model and its parameters can accurately predict temperature-changing profile of hydroxylamine nitrate and contaminated hydroxylamine nitrate by iron ions under adiabatic condition. This model could be used to provide guidance on operation procedure development and so on. Furthermore, critical behavior of hydroxylamine nitrate can also be analyzed with this model and will be further discussed in Section 5 and Section 6.

5. HYDROXYLAMINE NITRATE CRITICAL BEHAVIOR ANALYSIS OF SMALL-SCALE BATCH SYSTEM

5.1 Introduction

Storage process typically is a batch process and its behavior is very similar to that of batch reactors used in the chemical industries. It is worth noting that batch processes may be very dangerous as reported by Barton et al.[24]. About 45% accidents reported to UK's Health and Safety Executive (HSE) between 1986 and 1990 are related to batch or semi-batch processes. By using the incidents data of U.S. Chemical Safety and Hazard Investigation Board (CSB) report, Improving Reactive Hazard Management, those incidents can be further classified according to the involved equipments and its statistics is illustrated in Figure 5.1, where there are 37 out of 167 accidents occurred in storage tank or storage area. Because CSB did not specify the operation mode of reported incidents, this statistics does not include other batch processes, which occurred in process tank, reactor, and separation equipment etc. However batch reactors or processing is widely used in the chemical industry, it is believed that about 50% percent of runaway incidents occurred in batch processing processes, including batch reactors and storage tanks.

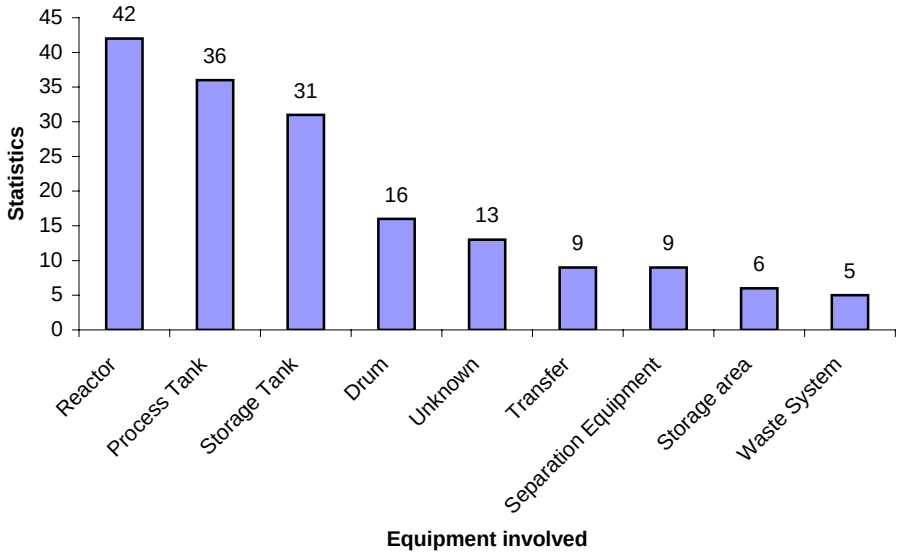

Figure 5.1 Runaway reaction classification according to involved equipment

One of the recent biggest batch process explosion occurred in a hydroxylamine batch reactor at Concept Science Inc. There were five fatalities and fourteen injuries in this explosion. Therefore the safety of storage tanks, batch reactors, and other batch processing must be improved to avoid similar tragedies. Furthermore CSB also postulated that many small-scale equipments are typically "over-designed' and used for multipurposes. So critical behavior analysis for small-scale batch systems is urgently needed to prevent thermal runaway incidents.

5.2 HAN critical behavior analysis

Following the determination of a HAN autocatalytic reaction model, the critical behavior of HAN was studied with this validated model. Traditional Semenov Theory remains the basis of sensitivity analysis for small-scale batch system over the decades [24,

[31-36]. Shouman et al. recently made the most significant improvement for Semenov Theory [31] by proposing that critical point should be defined on a temperature-concentration plane by using the inflection point concept. Therefore Semenov Theory combined with inflection point concept is used to determine the critical behavior for small quantities of hydroxylamine nitrate.

5.2.1 Mathematical formulation and derivation

The fundamental principles of the Semenov Theory are energy conservation and mass conservation, which are represented as follows for the autocatalytic reaction discussed in this work for small-scale system.

$$\rho V C_V \frac{dT}{dt} = QVAC_0^n (1-x)^n (1+px^m) e^{-\frac{E_a}{RT}} - hs(T - T_S) \tag{5.1}$$

$$\frac{dC}{dt} = -Ae^{-\frac{E_a}{RT}} C_0^n (1-x)^n (1+px^m) \tag{5.2}$$

With dimensionless variables $\theta = RT/E_a$, $\theta_s = RT_s/E_a$, $x = (C_0 - C)/C_0$, $B = QC_0R/(\rho C_V E)$, $\psi = (QVAC_0^n R)/(hsE_a)$, and $\tau = (QRAC_0^n t)/(\rho C_V E_a)$, equation (5.1) and (5.2) can be written in dimensionless form as follows:

$$\frac{d\theta}{d\tau} = (1-x)^n (1+px^m) e^{-1/\theta} - \frac{\theta - \theta_s}{\psi} \tag{5.3}$$

$$\frac{d\alpha}{d\tau} = \frac{(1-x)^n (1+px^m) e^{-1/\theta}}{B} \tag{5.4}$$

Equations (5.3) and (5.4) were combined as equation (5.5) to study the critical behavior on the temperature-concentration plane.

$$\frac{d\theta}{d\alpha} = B\left[1 - \frac{(\theta - \theta_s)/\psi}{(1-x)^n(1+px^m)e^{-1/\theta}}\right] \tag{5.5}$$

To determine a meaningful inflection point, appropriate parameters for the thermal explosion model must be chosen. So far the undetermined model parameters are the overall heat transfer coefficient, h, and the vessel dimension radius (a spherical vessel was used in this work). To obtain a conservative estimate, the overall heat transfer coefficient, h, of 15~75 W/m^2/K [65], was used, and the vessel radius was 0.05 m.

Because the critical region is determined by inflection points as shown in the previous work [31], the critical behavior analysis is equivalent to the determination of the inflection points. The inflection points on the temperature-concentration plane are determined by selecting the roots of the second order derivative $d^2\theta/d\alpha^2 = 0$ and checking whether the first non-zero higher order derivative has an odd order. The second derivative on the temperature-concentration plane is written as follows.

$$\frac{d^2\theta}{d\alpha^2} = B\left[\begin{array}{l} -\dfrac{n(\theta-\theta_s)}{\psi(1-\alpha)^{n+1}(1+p\alpha^m)e^{-1/\theta}(1-\alpha)} + \dfrac{mp(\theta-\theta_s)\alpha^{m-1}}{\psi(1-\alpha)^n(1+p\alpha^m)^2e^{-1/\theta}} + \\ \dfrac{\theta-\theta^2-\theta_s}{\psi(1-\alpha)^n(1+p\alpha^m)\theta^2e^{-1/\theta}}\dfrac{d\theta}{d\alpha} \end{array}\right] \tag{5.6}$$

5.2.2 Critical point determination

The roots of the second order derivative $d^2\theta/d\alpha^2 = 0$ and the first order derivative $d\theta/d\alpha = 0$ for surrounding temperature, 25^{o}C, were superimposed on the temperature-concentration plane as illustrated in Figure 5.2, where there are two roots for the first and second order derivatives, respectively. Solid lines and dash lines represent the two roots for the first and the second order derivates, respectively, in Figure 5.2. Because the third order derivatives for both roots of the second order derivative $d^2\theta/d\alpha^2 = 0$ are nonzero, both of these two roots are inflection points on the temperature-concentration plane. The temperature changing profiles with different initial reactant temperature were also superimposed on the temperature-concentration plane as in Figure 5.3 to study the system critical behavior. The system enters the non-return status when its temperature profile has an intersection with or is above the large root trajectory of inflection points. So the root with large value of inflection point defines the critical behavior for diluted HAN solution, and the temperature-concentration plane is separated to subcritical, critical, and supercritical regions by the root trajectory of the inflection point with large value. The root of extreme temperature with small value defines a stable status for the system, which is determined by the surrounding temperature. The system temperature eventually develops to this stable status if it is in the subcritical region.

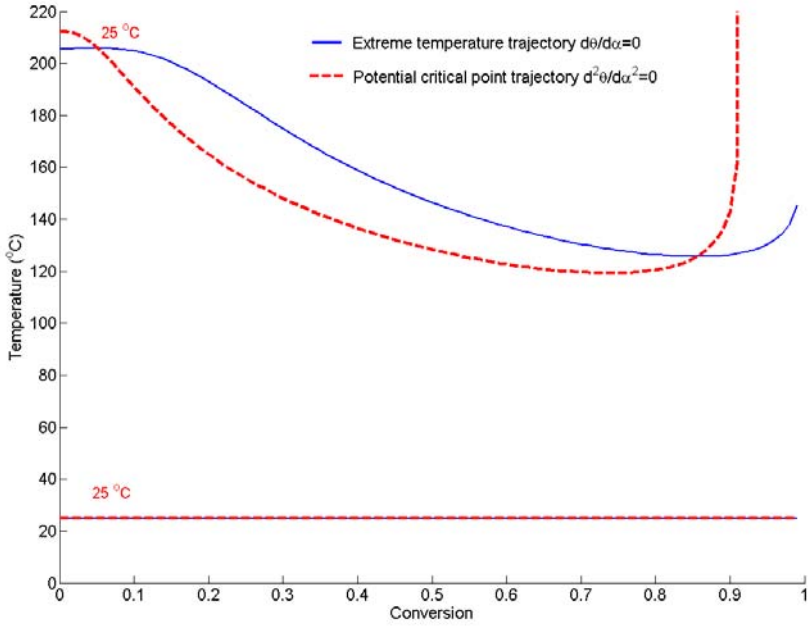

Figure 5.2 Roots of extreme temperature and inflection points on temperature-concentration plane

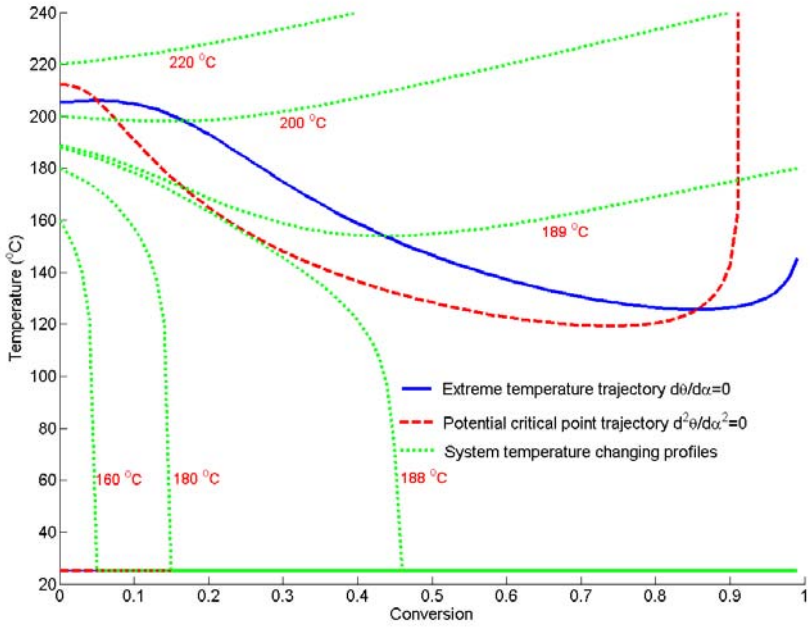

Figure 5.3 Critical behavior demonstrations on temperature-concentration plane

5.2.3 Lowest storage temperature for small quantity hydroxylamine nitrate

Because storage environment temperature always varies in practice, influence of temperature variation on critical behavior should be examined to give a complete picture about the safety margin.

Influence of surrounding temperature was analyzed and shown in Figure 5.4. To clearly show the result, the roots with large value of the second order derivative $d^2\theta/d\alpha^2 = 0$ and the first order derivative $d\theta/d\alpha = 0$ for the 45°C and 65°C cases are not shown in Figure 5.4, because they exhibit similar behavior to those of 25°C. As in Figure 5.4, the two roots for the second order derivative $d^2\theta/d\alpha^2 = 0$ have an intersection, which defines the lowest critical temperature, for the high temperature cases. For high temperature cases larger or equal to 90°C as shown in Figure 5.4, the subcritical region is the part below the large root trajectory of the inflection point. The other regimes are the critical or supercritical regions, where the system temperature will continuously increase until the reactant is completely consumed. This fact demonstrates that the feasible storage regime becomes smaller with the increase of surrounding temperature. Furthermore, connecting these intersections and extending to zero conversion obtained an estimate of 187°C for the critical temperature of fresh diluted HAN solution. This prediction result is consistent with the adiabatic test results as well as result of other researchers [5]. On the other hand, the critical temperature lower boundary, which is also illustrated in Figure 5.4, also defines the highest feasible storage temperature for diluted hydroxylamine nitrate solution.

As illustrated in Figure 5.4, the critical trajectory is a function of temperature and concentration, and it could enter the low temperature regime for the non-zero conversion system. The critical temperature is higher when the reactant is fresh, where the catalytic intermediates or products have not accumulated significantly in the solution, but becomes smaller with the continuation of reaction and the accumulation of catalysts. This fact confirms that thermal explosion/runaway reactions can occur at low temperature. However, this important behavior attribute of autocatalytic reactions may not be known or identified.

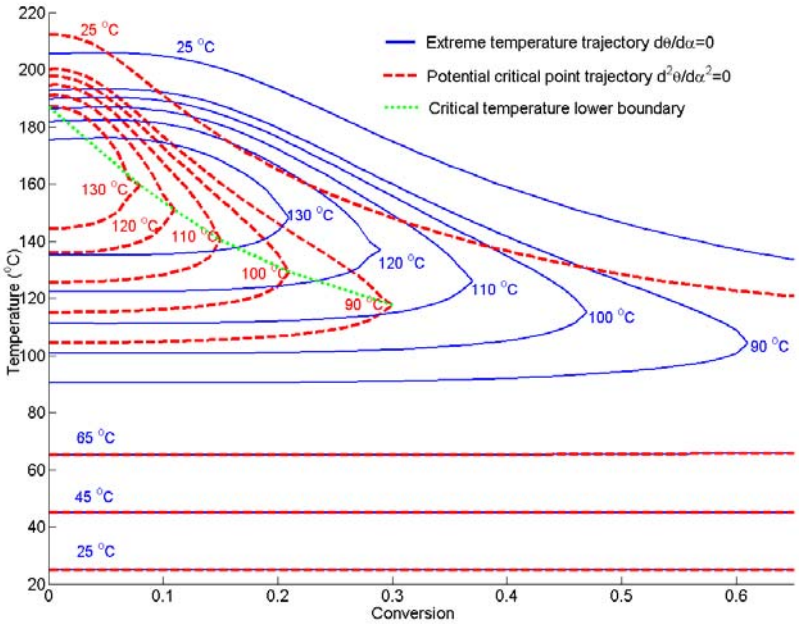

Figure 5.4 Different surrounding temperature influences on critical behavior development

5.2.4 Sensitivity analysis of heat transfer coefficient

So far all analysis has been conducted with an overall heat transfer coefficient 15 $W/m^2/K$. Figure 5.5 shows the influence of the overall heat transfer coefficient on the temperature changing profile with surrounding temperature of 25^oC and initial reactant temperature of 200^oC. Figure 5.5 demonstrates effective heat transfer can significantly reduce the thermal runaway hazard of HAN. However for certain operations, such as storage, the heat transfer condition is comparably harder to improve. An easier and cost-effective solution may be to maintain the reactive chemical surrounding temperature well below its critical temperature.

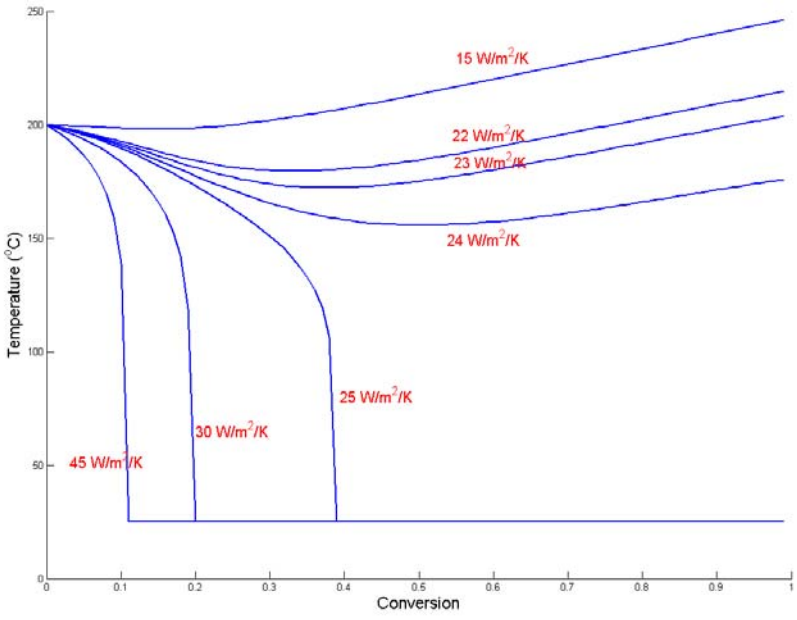

Figure 5.5 The influence of overall heat transfer coefficient on temperature-concentration plane

5.3 Conclusions

Critical behavior of hydroxylamine nitrate is analyzed by using the improved Semenov Theory and most rigorous definition for critical point. The highest feasible storage temperature for diluted hydroxylamine nitrate solution is identified through critical behavior analysis. This methodology can also be applied to other concentration hydroxylamine nitrate. The highest feasible storage temperature for fresh hydroxylamine nitrate also coincides with its onset temperature, which is consistent with adiabatic calorimeter test results.

Because the thermal runaway reaction may occur at low temperatures for autocatalytic chemical systems due to generation and accumulation of catalytic intermediates, autocatalytic reactive chemicals must be inspected periodically to insure that catalytic intermediate accumulation is sufficiently below critical conditions within the low temperature region.

6. HYDROXYLAMINE NITRATE CRITICAL BEHAVIOR ANALYSIS FOR LARGE-SCALE SYSTEM

6.1 Introduction

Critical behavior of small quantity diluted hydroxylamine nitrate solution has been analyzed with the Semenov Theory and the inflection point concept. Because heat transfer model used by traditional thermal explosion theory, including Semenov and Frank-Kamenetskii theories, is fairly simple, it is only applicable to solid or small quantity fluid systems. Most of following research aims to consider reactant consumption and analyze critical behavior for more complex reaction mechanism. Very few works have been conducted to improve heat transfer model used in traditional thermal explosion theory until recently. However chemicals are normally stored in bulk quantity and many chemicals are liquid in ambient conditions. Heat and mass transfer mechanism in bulk liquid system is much more complicated than those of small-scale system. Conduction, diffusion, and convection should be considered simultaneously to describe bulk system behaviors.

Convection modes involved in fluid flow can be divided into two types according to fluid motion driving forces. If an external device drives fluid flow, such as fan or agitator, the pressure difference drives the flow and this type of flow is called forced convection. On the other hand, fluid flow driven by density difference is called natural convection or free convection. The density difference is normally generated by temperature or concentration gradient in gravity force field. Free convection is more

likely to occur in storage practices and there is growing interest in thermal safety area to address its influence on critical behavior of reactive chemicals [43, 44, 66-70].

6.1.1 Rayleigh-Benard convection

Rayleigh-Benard convection is also called thermal convection and normally describes heat transfer through fluid flow. When the fluid is heated from the bottom, liquid at the bottom tends to expand and produce a downward density gradient because of its positive thermal expansion coefficient. However, convective motion only occurs when density gradient is high enough to overcome its opposite processes, including viscous damping and thermal diffusion.

6.1.2 Boussinesq approximation

Boussinesq approximation is widely used in buoyancy-driven flow problem given that temperature variation is very small. It normally gives faster convergence than setting up a temperature-dependent density. If temperature variation is very small, density variation can also be neglected in the governing equations except in the buoyancy term of the momentum equation, which is as follows.

$$(\rho - \rho_0)g \approx -\rho_0 \beta (T - T_0)g \tag{6.1}$$

where β is the thermal expansion coefficient. Equation (6.1) is obtained by using Boussinesq approximation, $\rho = \rho_0(1 - \beta \Delta T)$, to replace ρ in the buoyancy term. It is valid as long as $\beta \Delta T << 1$. However, Boussinesq approximation can not used in cases when chemical reaction involved, such as combustion and reacting flow problem [45].

6.2 Theory and calculation method

6.2.1 CFD governing equations

The HAN storage vessel and its surrounding air are studied in this work and they are two concentric cylinders. Considering the symmetry of the problem, only half of the cylinders are adopted as the computational domain. The storage tank is a vertical cylinder and the ratio of height to radius is one, which is same as that used by Sheu et al. [43].

The governing equation for the conservation of HAN can be written as Eq. (6.2), where average diffusivity is used to reduce the problem complexity.

$$\frac{\partial(\rho x)}{\partial t} + \nabla \bullet (\rho \vec{u} x - D_A \nabla \rho x) = \rho A e^{-\frac{E_a}{RT}} C_0^{n-1} (1-x)^n (1+px^m) \tag{6.2}$$

Because low flow is encountered in natural convection, viscous heating will be extremely small and thus can be neglected. Eq. (6.3) represents the energy conservation equation in the HAN storage vessel

$$\frac{\partial(\rho C_v T)}{\partial t} + \nabla \bullet (\rho C_P \vec{u} T) = \nabla \bullet (\lambda \nabla T) + S_f \tag{6.3}$$

The energy source term, S_f, is due to the decomposition reaction of HAN and described by Eq. (6.4).

$$S_f = A e^{-\frac{E_a}{RT}} C_0^n (1-x)^n (1+px^m) \bullet \Delta H \tag{6.4}$$

The Navier-Stokes equation describing the momentum conservation in the HAN storage vessel is represented by using Eq. (6.5).

$$\frac{\partial(\rho \vec{u})}{\partial t} + \nabla \bullet (\rho \vec{u}\vec{u}) = -\nabla p + \nabla \bullet \vec{\tau} + \rho \vec{g} \tag{6.5}$$

The continuity equation in the HAN storage vessel is written as Eq. (6.6).

$$\frac{\partial \rho}{\partial t} + \nabla \bullet (\rho \vec{u}) = 0 \tag{6.6}$$

Due to difficulties encountered by the Boussinesq approximation in reacting flow problem, temperature-dependent density is used in the present analysis to describe the buoyancy force. Pressure increasing effects and molar density change are neglected to adhere to the original thermal explosion definition of Semenov [71], even though HAN decomposition generates gases, including N_2 or nitrogen oxide, and other liquid products, such as nitric acid [6, 49]. The energy, mass, and momentum conservation equations are also solved for the surrounding fluid, air. The equations are similar to those of HAN except that there are no source terms.

The initial concentration of HAN is assumed to be uniform in the HAN zone and the initial fluid temperature and velocities are assumed to be zero in both HAN and air zones. Heat transfer inside the vessel wall is not considered in this work to simplify the calculations by assuming vessel wall thickness is zero. It is assumed that no-slip condition, zero mass and momentum flux applies at the storage tank wall, and the coupled thermal transfer condition applies on the storage vessel walls. The temperature on the outer surface of air cylinder is assumed to be fixed at 298*K*. The initial reactant temperature is set to be 460*K*, which is a subcritical temperature for a small quantity of diluted HAN solution[72], to examine whether the heat transfer enhancement induced by natural convection can significantly reduce thermal runaway hazard. Initial conditions and boundary conditions are summarized as follows..

$$t = 0: \vec{u} = 0,\ T_f = 460K,\ T_a = 298K, \text{ and } C = C_0$$

$$r = 0: \frac{\partial \vec{u}}{\partial r} = 0,\ \frac{\partial T}{\partial r} = 0, \text{ and } \frac{\partial C}{\partial r} = 0$$

$$r = R,\ H = 0,\ H = R: \vec{u} = 0 \text{ and } \frac{\partial C}{\partial r} = 0$$

$$r = 3R: T_a = 298K$$

$$H = -3R,\ H = 4R: T_a = 298K \tag{6.7}$$

6.2.2 Transport process dimensionless analysis

Both temperature and concentration gradients can induce natural convection. The thermal Grashof number (*Gr*) and the Prandtl number (*Pr*) are used to characterize natural convection induced by a temperature gradient. The diffusional Grashof number (Gr_w) and the Schmidt number (*Sc*) are used to characterize natural convection induced by concentration inhomogeneities[73]. Their definitions are summarized as follows.

$$Gr = \frac{g\beta(D/2)^3 \Delta T}{\nu^2} \tag{6.8}$$

$$Gr_w = \frac{g\gamma(D/2)^3 \Delta w}{\nu^2} \tag{6.9}$$

$$\mathrm{Pr} = \nu/\alpha = C_p \mu / k \tag{6.10}$$

$$Sc = \nu / D_A = \mu/(\rho D_A) \tag{6.11}$$

The dominant transport process in the HAN storage tank is determined by comparing these dimensionless variables.

6.2.3 Calculation method

The governing equations for continuity, momentum, energy, and species conservation are solved by ANSYS Fluent 6.3.26. The standard k-ε model is employed

as the turbulent model for turbulent flow with consideration of full buoyancy effect. The Reynolds-averaged Navier-Stokes equations are solved in conjunction with mass and heat transfer equations for turbulent kinetics energy and dissipation rate. The standard wall function is used in the present analysis. An unsteady segregated solver is used with a second order upwind scheme for convective terms in the mass, momentum, energy, species, and turbulence equations. For pressure discretization, the PRESTO scheme is employed and the PISO-algorithm is used for pressure-velocity coupling discretization.

The mesh for a storage tank and surrounding air are created with a tetrahedral cell of Gambit 2.3.16. The details of the computational domain and the system coordinates are shown in Figure 6.1. The radius and height of HAN storage tank are both 1 m. The height and the radius of surrounding air are 7 m and 4 m, respectively. The origin of coordinate is at the center of the bottom surface of the tank.

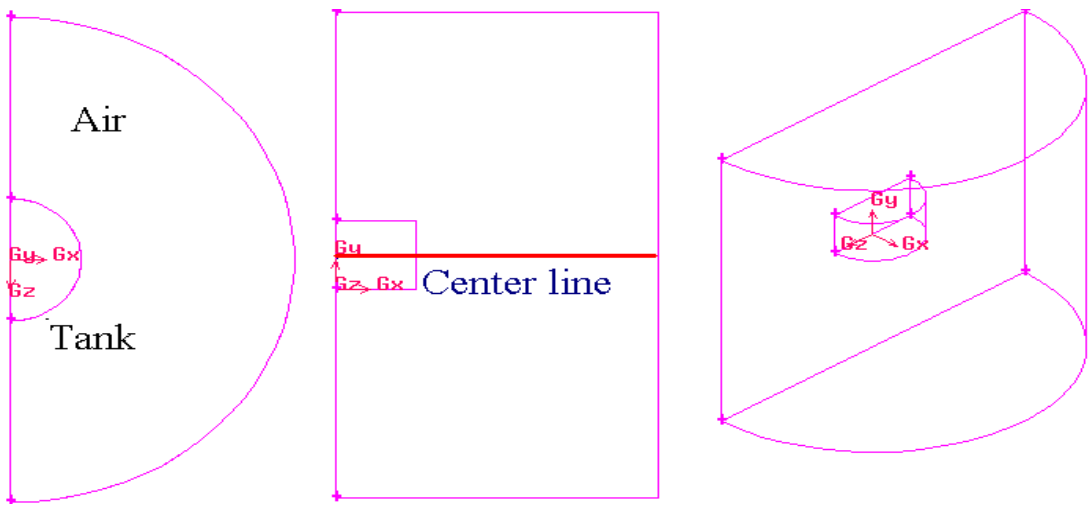

(a) Top view **(b) Side view** **(c) 3D view**

Figure 6.1 Computational domain for the storage tank

The reaction kinetics used in the present analysis was obtained from 24% mass HAN solution, the physical properties of which, such as density and heat conductivity, are very similar to those of water[74]. Furthermore, the physical properties of HAN solution at high temperatures are difficult to measure due to its vigorous reactivity. Therefore, the physical properties of water were used in the simulation to replace the corresponding properties of diluted HAN solution. The ideal gas density is used to simulate the transport phenomena of surrounding air. Other air properties, such as heat capacity and conductivity, are assumed to be constant throughout the simulation because the temperature variation is very small in the air zone.

A grid independence study was conducted using five different interval sizes for the tank and four different interval sizes for air. The velocity magnitudes at different times are calculated and compared to choose the appropriate mesh interval size. Figure 6.2 illustrates the velocity magnitude of HAN solution and air for different mesh interval sizes at 0.5 second along the center line illustrated in Figure 6.1, at y = 0.5 m. As illustrated in Figure 6.2, when the tank and air mesh interval size is around 0.04 and 0.3, the average difference of velocity magnitude is within 10%. Thus, 0.04 and 0.3 are chosen as the tank and air mesh interval size, respectively.

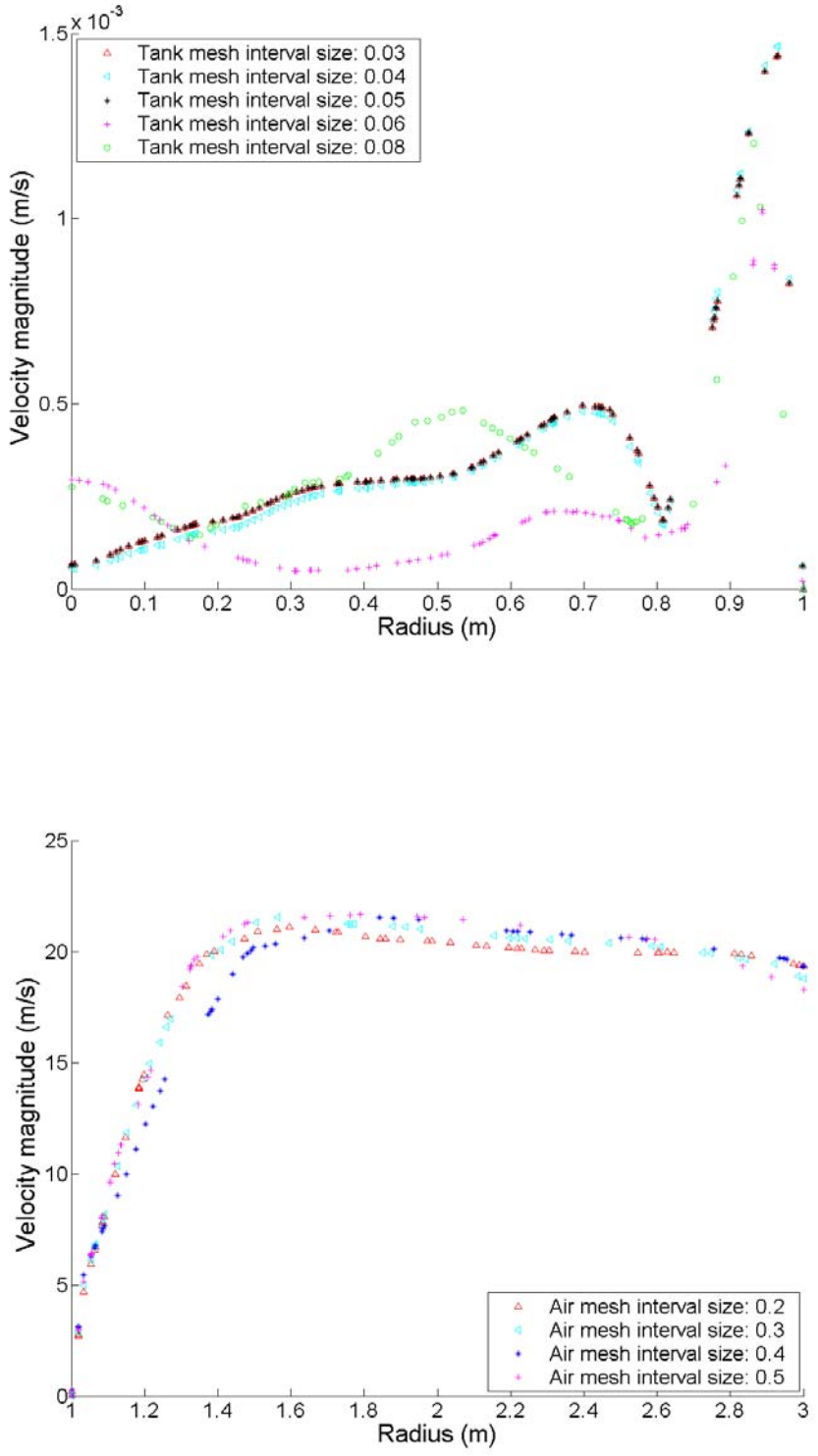

Figure 6.2 Tank and air grid independence test illustration

6.3 Results and discussions

6.3.1 Temperature distribution and fluid flow in air zone

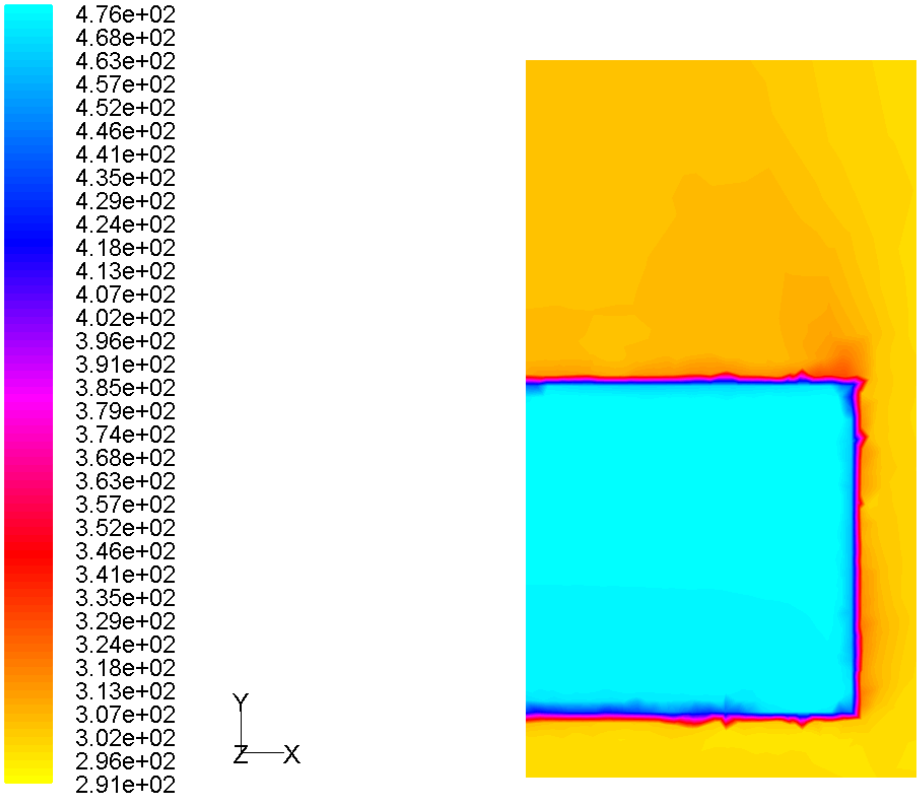

Figure 6.3 Side view of air and tank fluid temperature

First of all, side view of temperature distributions in storage tank and air zone are illustrated in Figure 6.3. Even though thermal radiation becomes important in current setup, its effect is not included in current simulation for divergence problem. Furthermore, major objectives of this work are to study heat transfer enhancement induced by natural convection and obtain reasonable heat transfer coefficient for storage

tank installed in air. In addition, heat radiation in normal storage practices is too small to affect storage behavior. Overall, neglect of heat radiation will not affect the accuracy of the current work.

Although the temperature of most air still maintains around 25^{o}C as illustrated in Figure 6.3, the temperature of air near the tank is much higher than 25^{o}C. The major cause of this phenomenon is due to small heat conductivity of air and heat transfer in theair zone is fairly slow. Therefore, previous boundary conditions setup of Sheu et al. and Vyn [43, 69], where they set tank boundary temperature to a constant value on all tank surfaces, is not an appropriate setup and can not describe the real situation. In addition, they did not specify what fluid is used to cool the tank. Subsequently, they did not consider heat transfer resistance in that fluid. Due to the above two limitations, they significantly overestimate cooling capacity for reactant system and probably obtain overoptimistic conclusion.

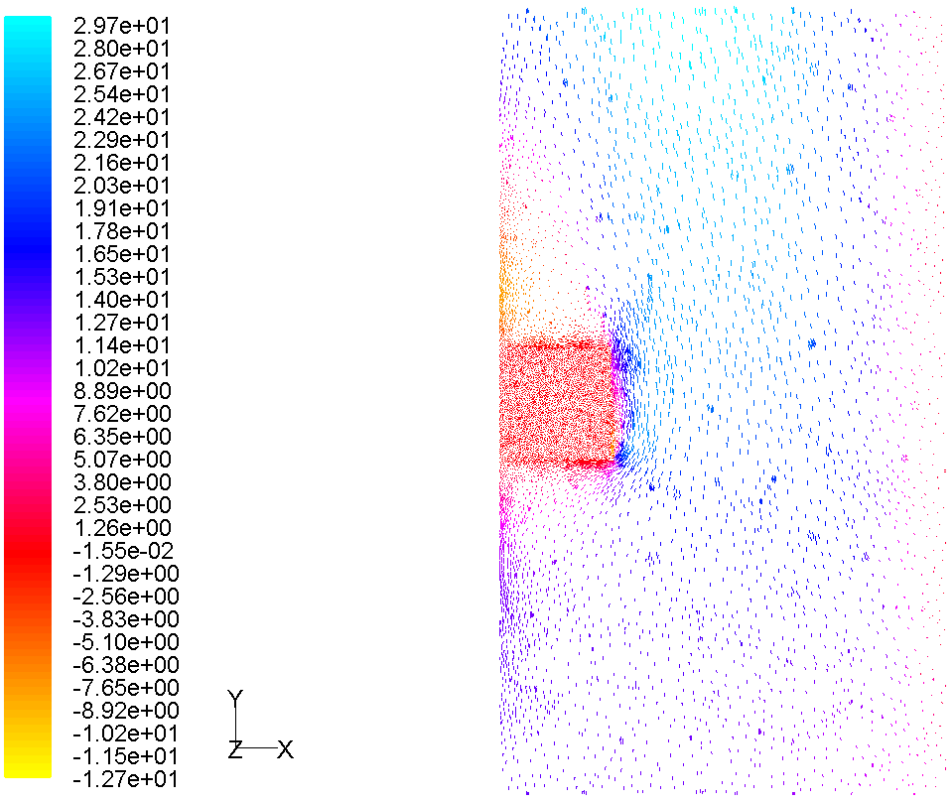

Figure 6.4 Side view of fluid velocity distribution

Figure 6.4 illustrates the fluid flow pattern and distribution in air zone. Most of air is heated up and flow up by buoyancy force. As shown in Figure 6.4, air near tank sidewall has maximum velocity because of less resistance. The velocity of air under tank is the smallest one because of blocking effect of tank bottom surface. A vertex forms above the tank and create some turbulence there. Heat transfer coefficients on tank sidewall, top, and bottom are different because of intensity of turbulence. Heat transfer coefficient of sidewall is the biggest.

6.3.2 System critical behavior and the influence of system scale

Figure 6.5 illustrates the evolution profile for the temperature at the tank center and the tank average temperature when the initial reactant temperature is set to be 460 K, which is a sub-critical temperature for small-scale system. It can be observed that the temperature at the tank center is slightly higher than the tank average temperature and exponentially increases with time. The system enters the thermal runaway regime whereas the small-scale system does not.

Generated energy from the decomposition reaction is proportional to reactant quantity, which is proportional to reactant volume. Because the available heat transfer area is proportional to the square of equivalent radius, the increase of heat transfer area may lag behind the increase of reactant volume given a large enough radius. Therefore, a chemical that is not hazardous in small quantity may become hazardous when stored in bulk quantity. Scaling up of storage and handling condition obtained from small-scale test must be carefully examined. CFD simulation may need to be conducted to safely scale up the storage process.

It is worth noting that the average heat transfer coefficients obtained from CFD simulation for the top, side, and bottom wall of the tank are 61.8, 96.3, and 39.6 $W/(m^2 \bullet K)$, respectively, which are around the heat transfer coefficient upper limit of heat exchanger with liquid inside and atmospheric gas outside, 75 $W/(m^2 \bullet K)$ [65]. The system for heat transfer coefficient of air-film, which typically is between 10 and 100 $W/(m^2 \bullet K)$ [46], does dominate the overall heat transfer coefficient.

The applicability of Semenov Theory for a large-scale system is also examined. The temperature changing profile for the tank is calculated by substituting heat transfer coefficients obtained from CFD simulation into equations (5.1) and (5.2). The result is also illustrated in Figure 6.5, which demonstrates that the predictive quality of Semenov Theory is fairly good and conservative. This demonstrates the Semenov Theory with appropriate reaction kinetics can be used to conduct preliminary critical behavior analysis for large quantity reactive chemicals given that appropriate heat transfer coefficient is used and system size is considered.

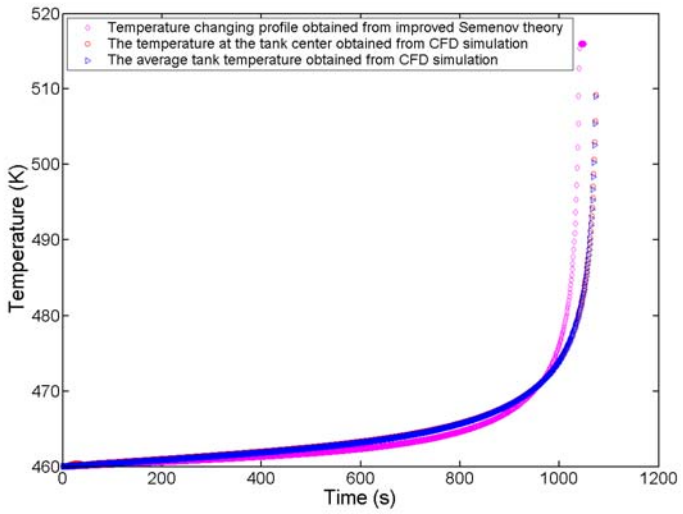

Figure 6.5 Comparison temperature-changing profiles obtained from improved Semenov Theory and CFD simulation

6.3.3 Fluid flow field

In the previous work [43, 44], because the initial reactant temperature is the same as the boundary temperature, the fluid at the center will first be heated up and will rise upward due to density decrease. Once the fluid hits the cold top surface, the fluid will cool and flow downward along the sidewall. In order to study the critical behavior of a reactive chemical, the initial reactant temperature is set higher than that of the surrounding air in this present work. Therefore, the fluid flow pattern obtained from analysis could be different from that of referenced works.

The evolution of an average thermal Grashof number and a diffusional Grashof number are calculated, respectively, and illustrated in Figure 6.6, which indicates that the thermal Grashof number is much larger than the diffusional Grashof number throughout the simulation. The average Prandtl and Schmidt number are 0.96 and 83.2, respectively. The comparison of these dimensionless numbers demonstrates that the thermal buoyant force dominates the convective flow development and drives heat and mass transfer in this present problem[75].

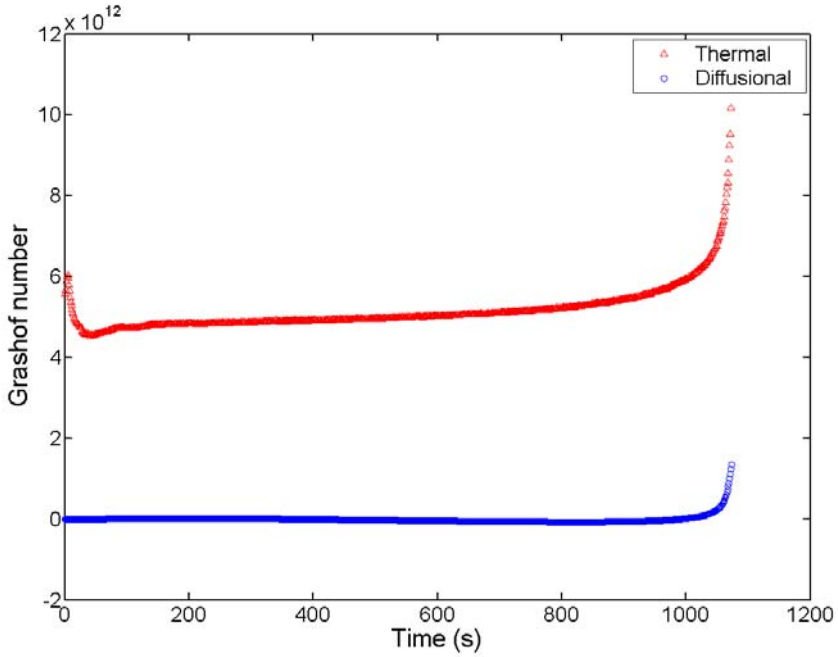

Figure 6.6 Evolution of average thermal and diffusional Grashof number

The evolution of an average Nusselt number at the tank sidewall and tank center velocity is illustrated in Figure 6.7 and a fluid flow-developing pattern is shown in Figure 6.8, respectively. Fluid development can be divided into three stages on the basis of Nusselt number.

In the first stage, $0 \le t \le 200$ second, the fluid flow develops because of the self-heating of the decomposition reaction and the cooling of the cold vessel wall. The fluid near the sidewall is cooled down first and flows downward. The fluid near the tank center begins to rise due to self-heating and the nearly incompressible characteristics of liquid. So a convective cell is formed near the tank sidewall as illustrated in Figure 6.8 (a). With reaction continuing, this single convective cell becomes larger and extends to

the tank center as shown in Figure 6.8 (b, c). Meanwhile, the fluid velocity at the tank center also increases and reaches a maximum velocity at about 40 seconds as shown in Figure 6.7. Thereafter, the fluid experiences an oscillation process, which is illustrated in the velocity changing profile at the tank center (Figure 6.7) and this oscillation process continues until the average Nusselt number reaches its equilibrium value at about 200 second. The period of oscillation is about 50 second as shown in Figure 6.7, which is the similar order of magnitude to the time of fluid circulation along the axial direction.

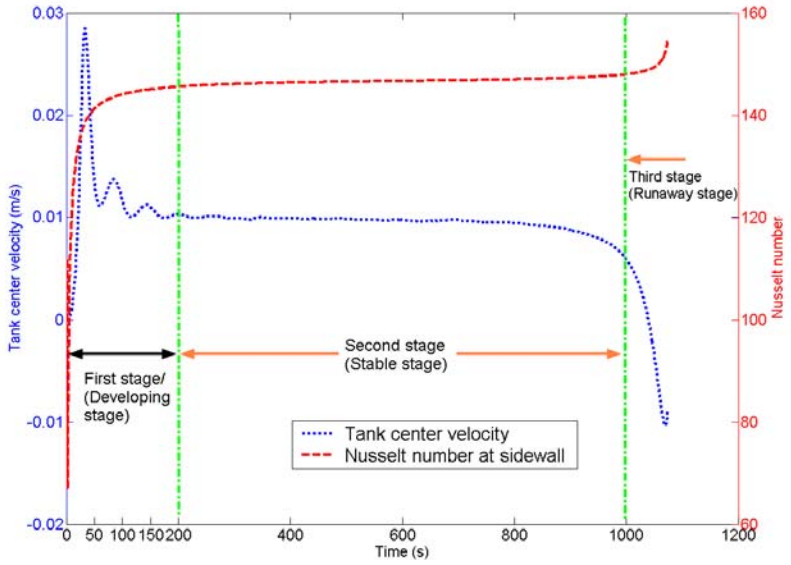

Figure 6.7 Evolution of the tank sidewall average Nusselt number

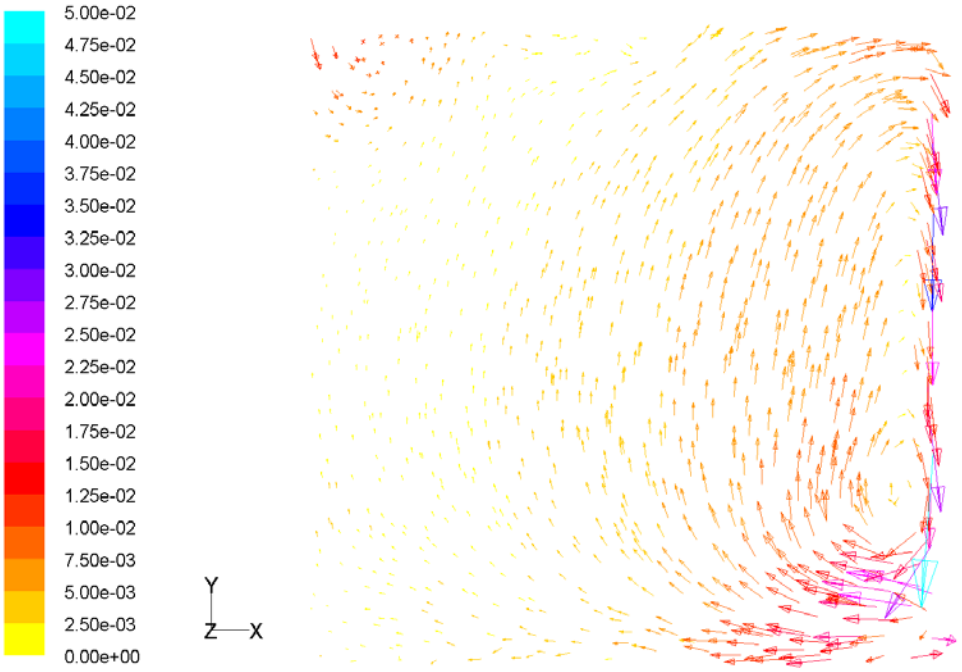

(a) t = 10 s

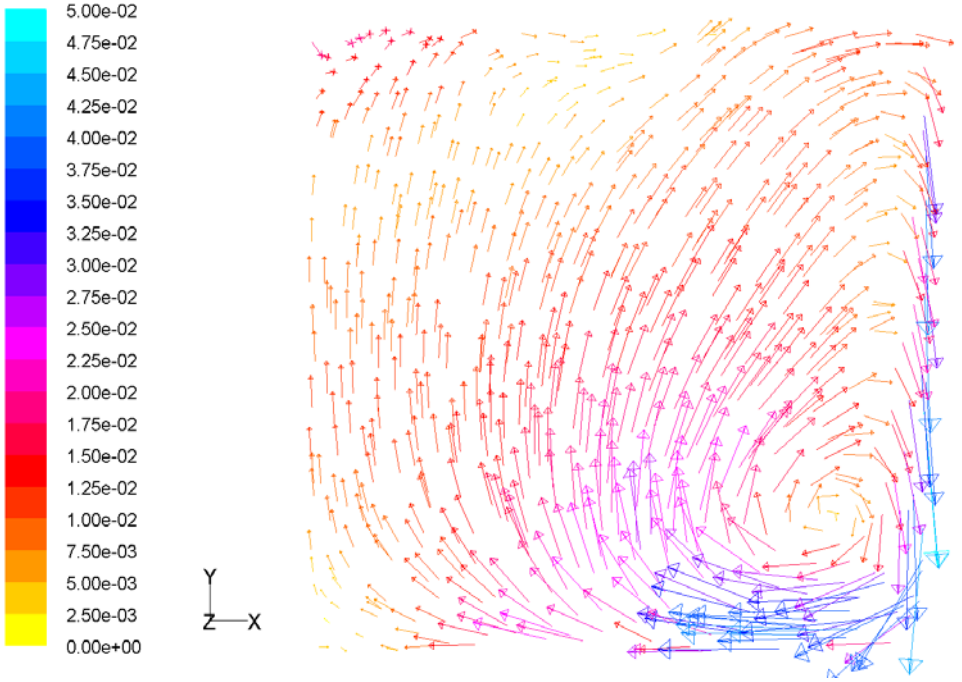

(b) t = 20 s

Figure 6.8 Fluid flow pattern development with time

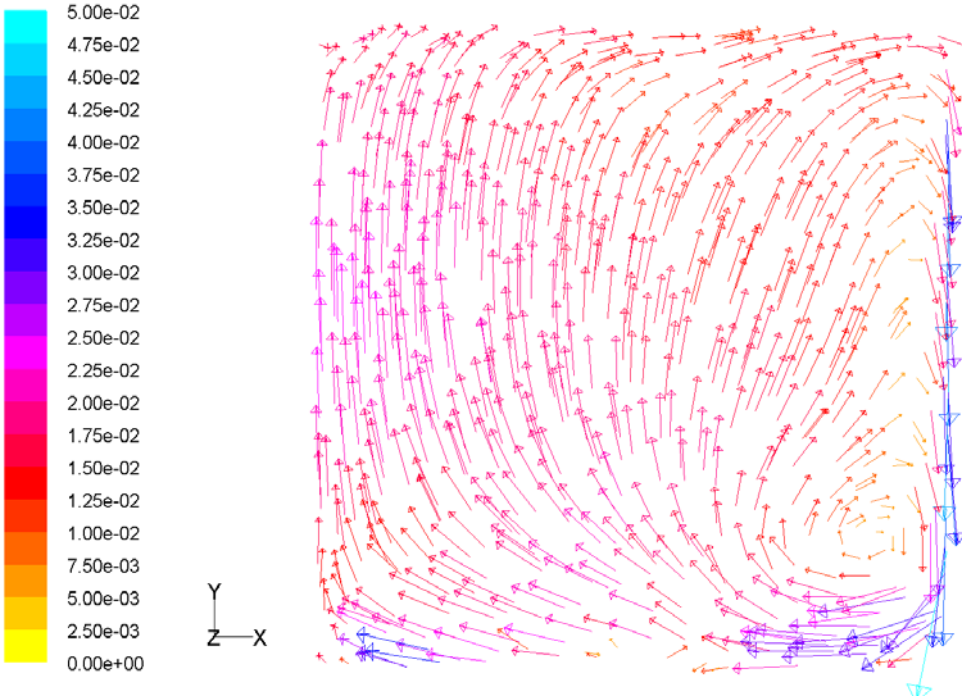

(c) t = 40 s

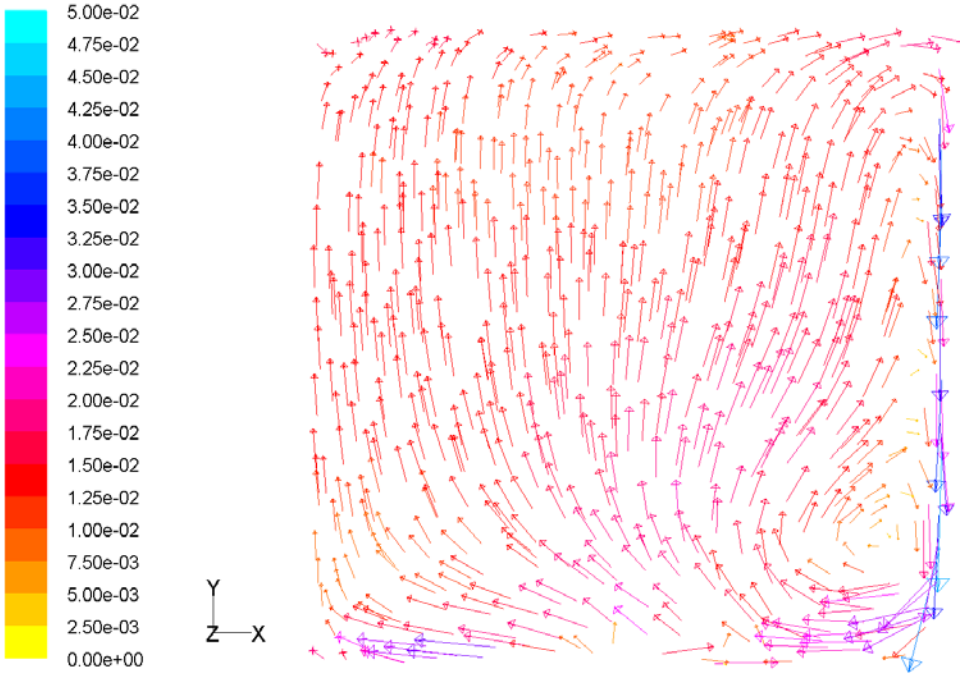

(d) t = 50 s

Figure 6.8 continued

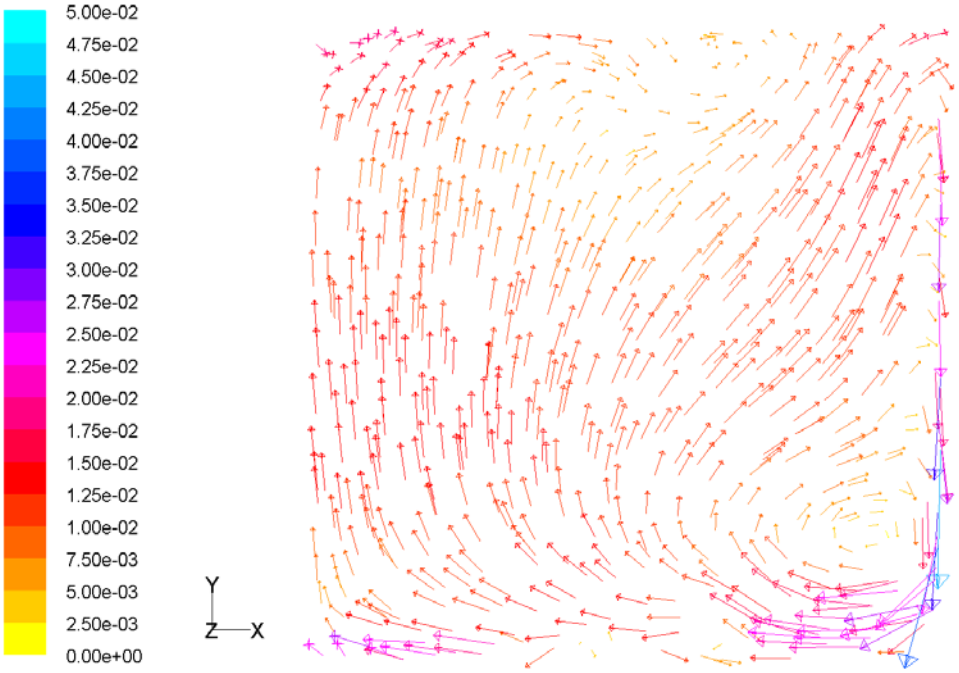

(e) t = 100 s

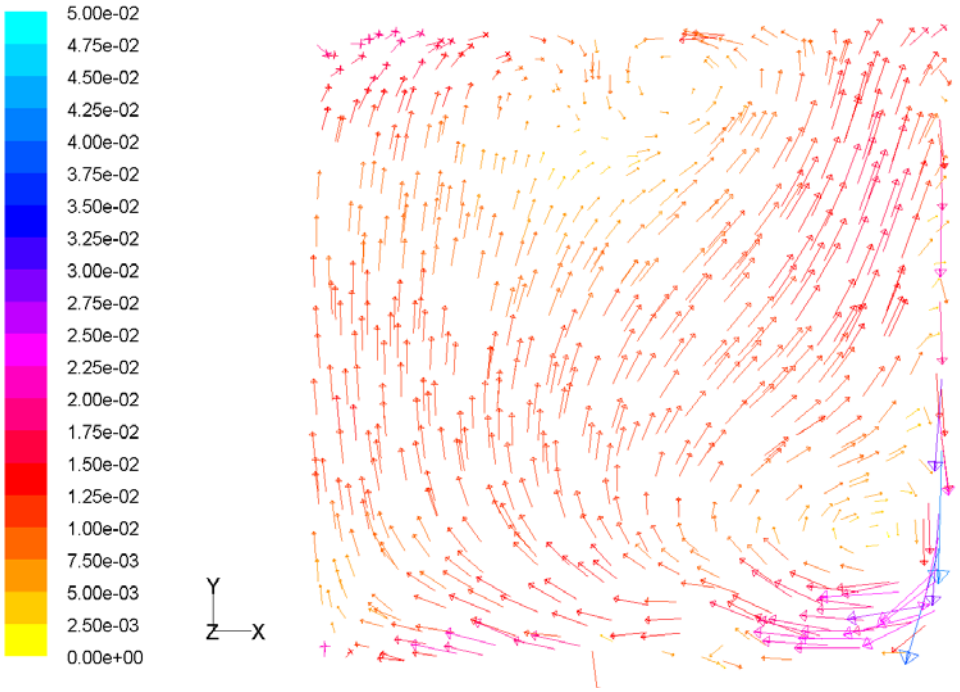

(f) t = 200 s

Figure 6.8 continued

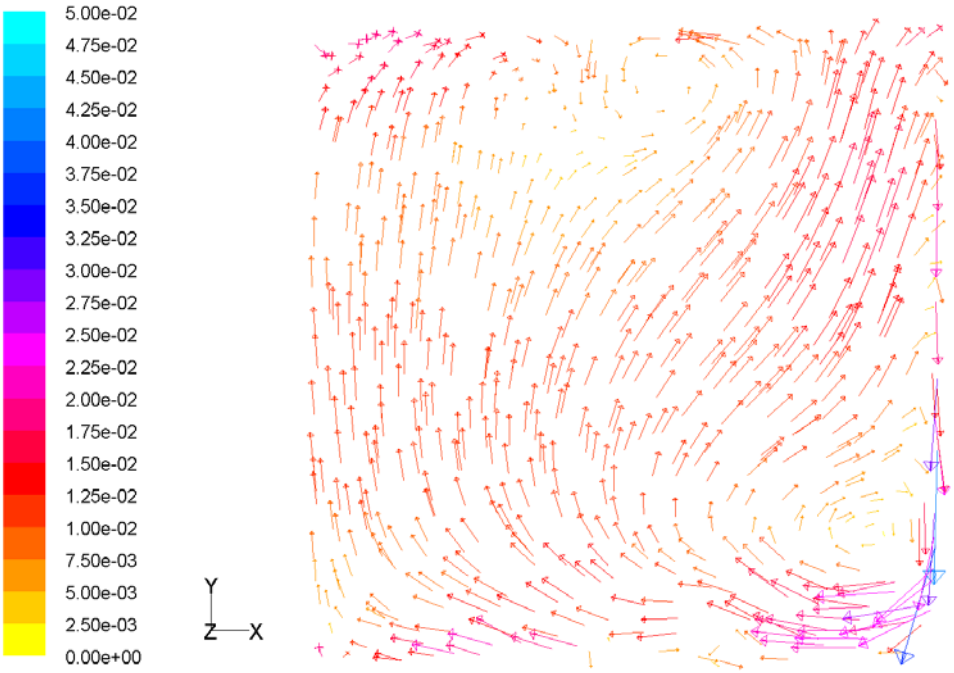

(g) t = 300 s

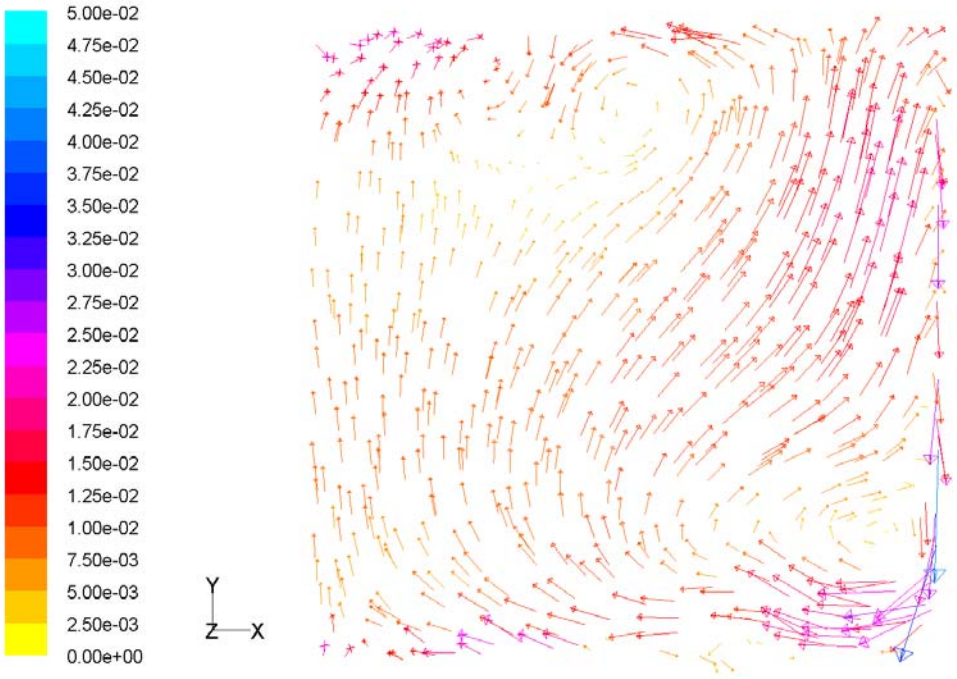

(h) t = 1000 s

Figure 6.8 continued

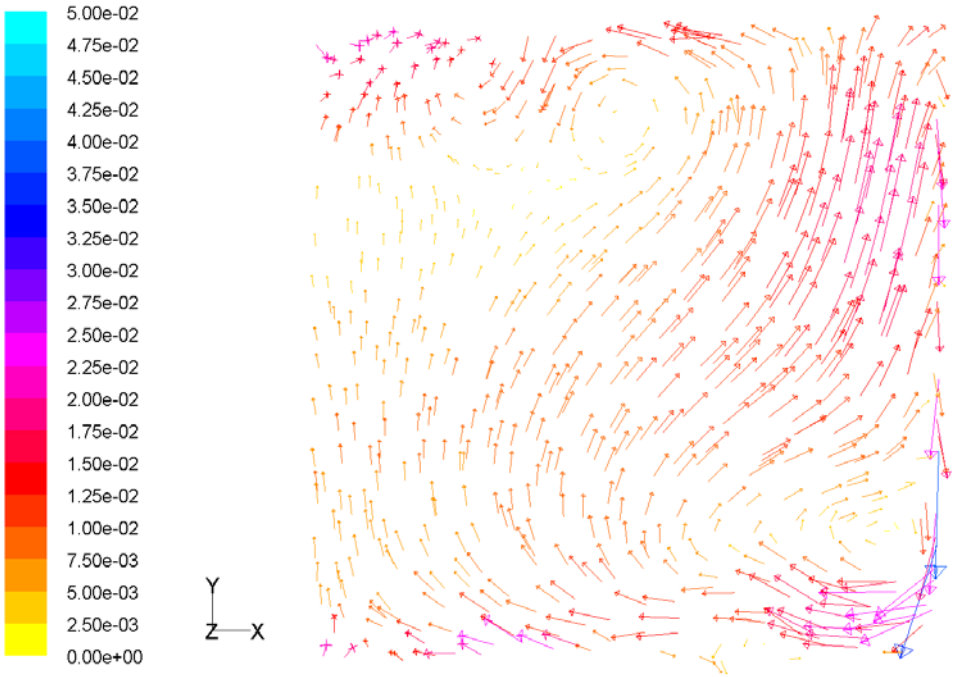

(i) t = 1020 s

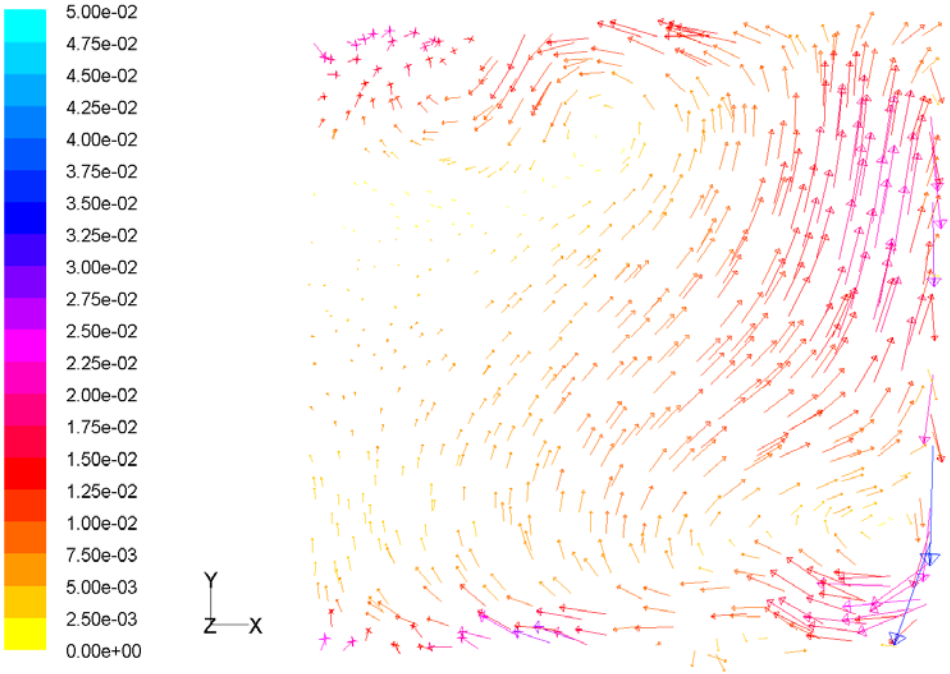

(j) t = 1040 s

Figure 6.8 continued

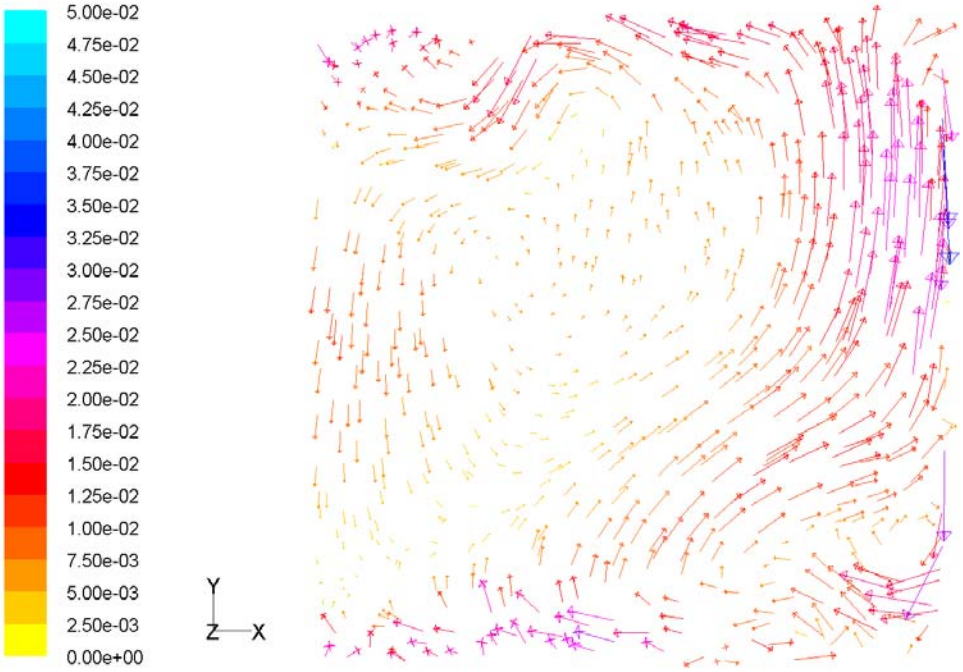

(k) t = 1060 s

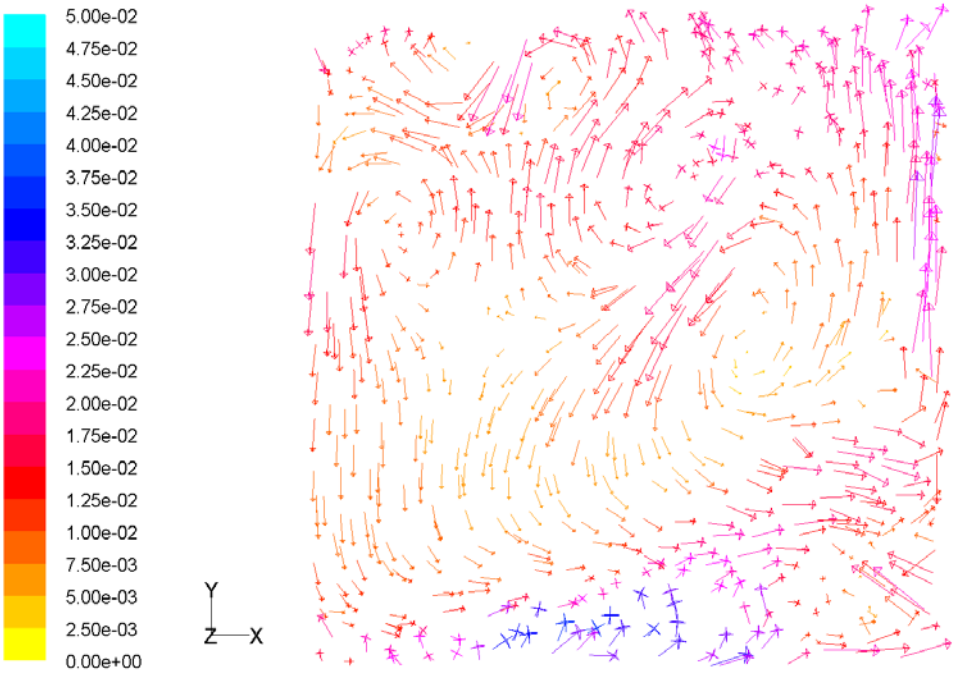

(l) t = 1070 s

Figure 6.8 continued

In the second stage, $200 \le t \le 1000$ seconds, the average Nusselt number reaches its quasi-equilibrium value and the fluid demonstrates a quasi steady state flow even though it is an unsteady process. Although the Nusselt number still increases slowly at this stage, the change of its magnitude is so small that fluid flow pattern is not significantly affected as shown in Figure 6.8 (f-h). At this stage, there are two convective cells existing inside the tank. One is the cell formed in the first stage, and the other is a heart shaped cell formed near the tank top wall as shown in Figure 6.8 (f-h). Velocity near the heart center is almost zero due to the two opposite flows from the left and right shoulder of the heart. The fluid velocity at the tank center maintains around 0.01 m/s as shown in Figure 6.7.

In the third stage, $t > 1000$ second, the system is in the thermal runaway regime and its fluid flow pattern is illustrated in Figure 6.8 (i-l). At this stage, the heart shape convective cell formed in the second stage begins to relocate and separate. In the previous two stages, the fluid rises in tank center part and flow back to the tank bottom near the tank sidewall as shown in Figure 6.8 (a-h). However at this stage, fluid velocity near the center first drops to zero and then flows downward, which is illustrated in Figure 6.7. This is due to the rapid temperature increase at thermal runaway stage, which drives more fluid rise, and the fluid has to find a new path to go back. Furthermore, several circulation cells develop in the tank and fluid flow becomes more violent as shown in Figure 6.8 (l).

Overall oscillating flow is only observed in the fluid flow developing stage and there is no significant oscillating flow observed in the later stages. Furthermore, natural

convection induced by concentration gradient does not play a significant role in the reacting flow in aqueous solution.

6.3.4 Temperature field

Figure 6.9 illustrates the isotherms of HAN in the tank for fluid flow development process. Although there is no obvious oscillating flow observed in fluid flow field, reactant temperature distribution shows a periodical developing pattern as shown in Figure 6.9. At 540 second, a new isotherm, 463.51 K, is formed near the upper-left corner of Figure 6.9 (a). Then another one appears near the up-right corner of Figure 6.9 (b) at 550 second. Thereafter, these two isotherms grow inside the tank as illustrated in Figure 6.9 (c-e). At 590 second, these two isotherms merge together as shown in Figure 6.9 (f). After they merge, this isotherm continues to grow and a new isotherm with higher temperature forms at 610 second as shown in Figure 6.9 (h) and repeats the same cycle described above. The period of this cycle decreases with the temperature increase. The birth locations of new isotherms are corresponding to the top part of the two convective cells existing in the second stage respectively, which are shown in Figure 6.8 (f-h). Since temperature difference between the isotherms is fairly small (normally less than 2 K except in the thermal runaway stage), a pseudo-uniform temperature distribution may be a reasonable approximation for tank of HAN stored in air.

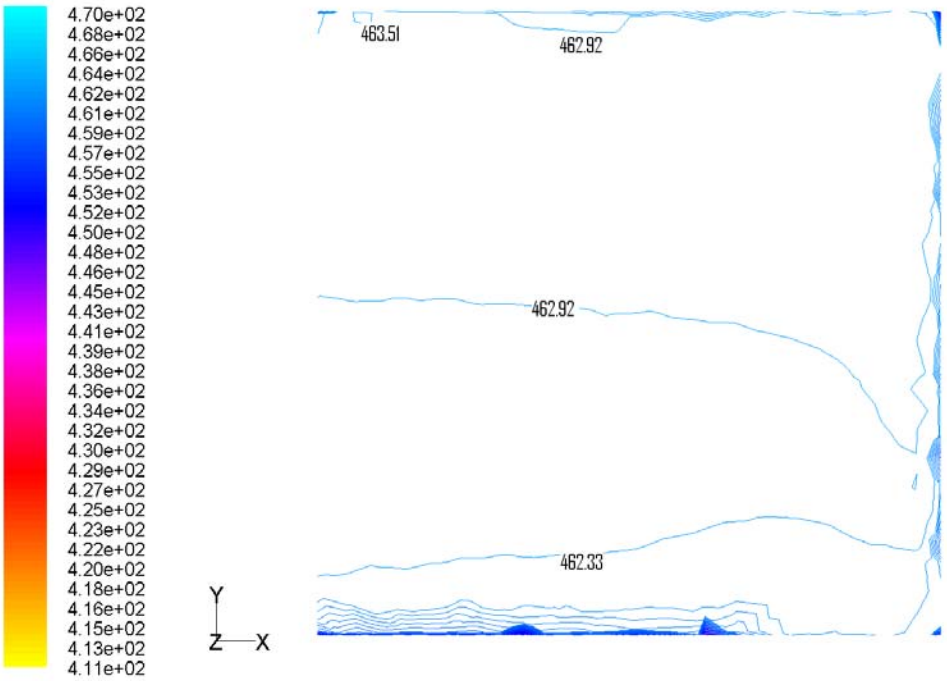

(a) t = 540 s

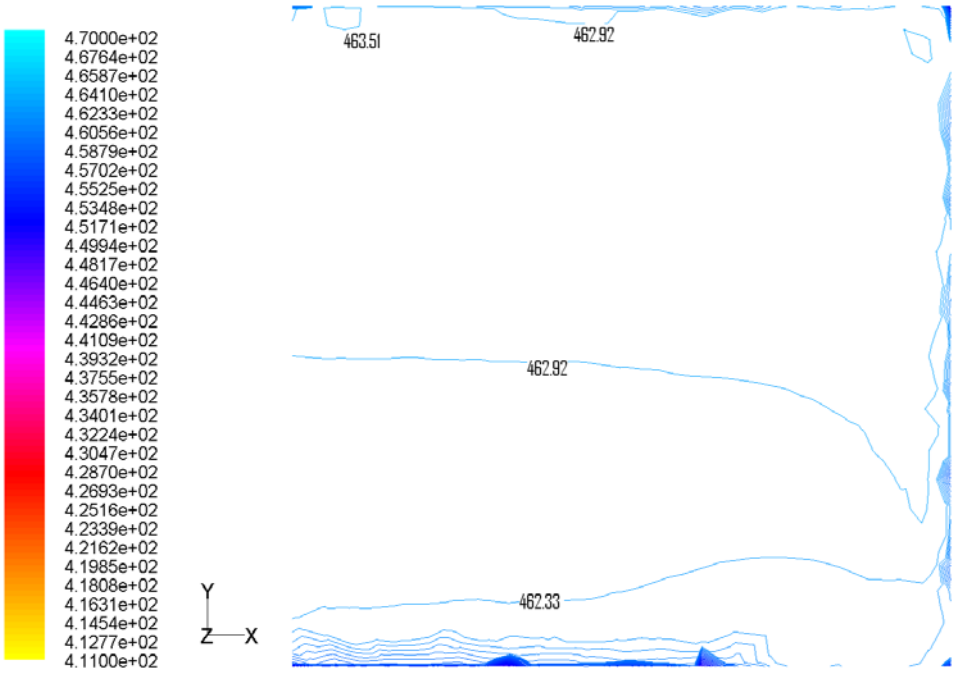

(b) t = 550 s

Figure 6.9 Illustration of isotherms in HAN storage tank

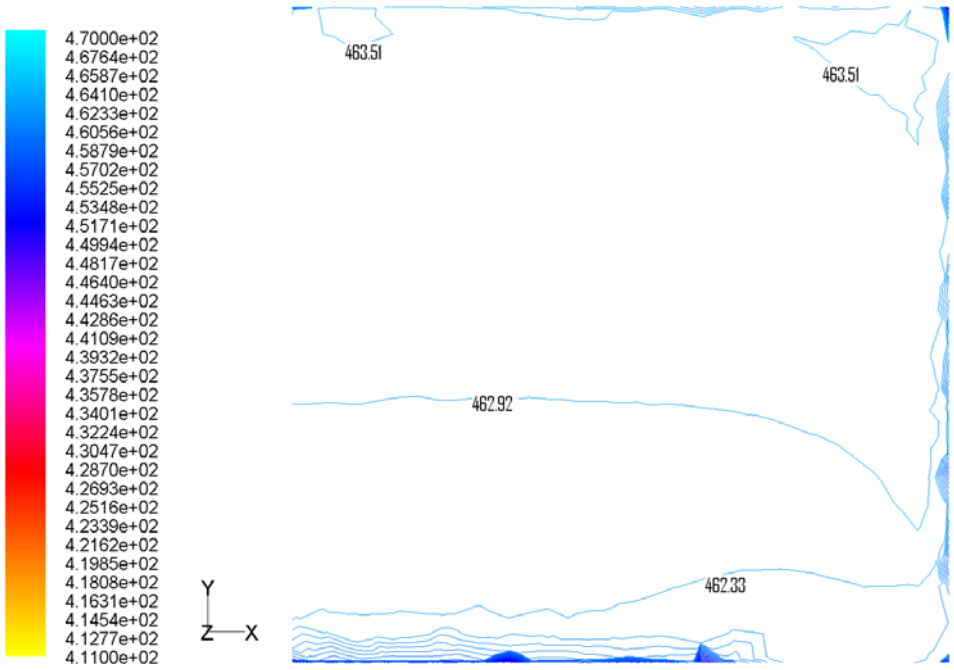

(c) t=560s

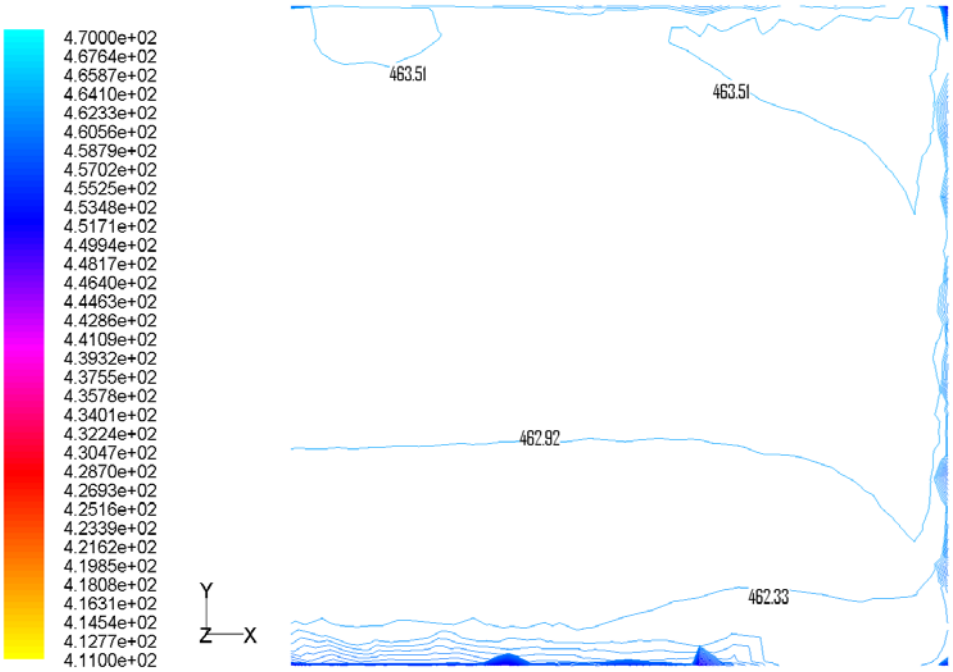

(d) t = 570s

Figure 6.9 continued

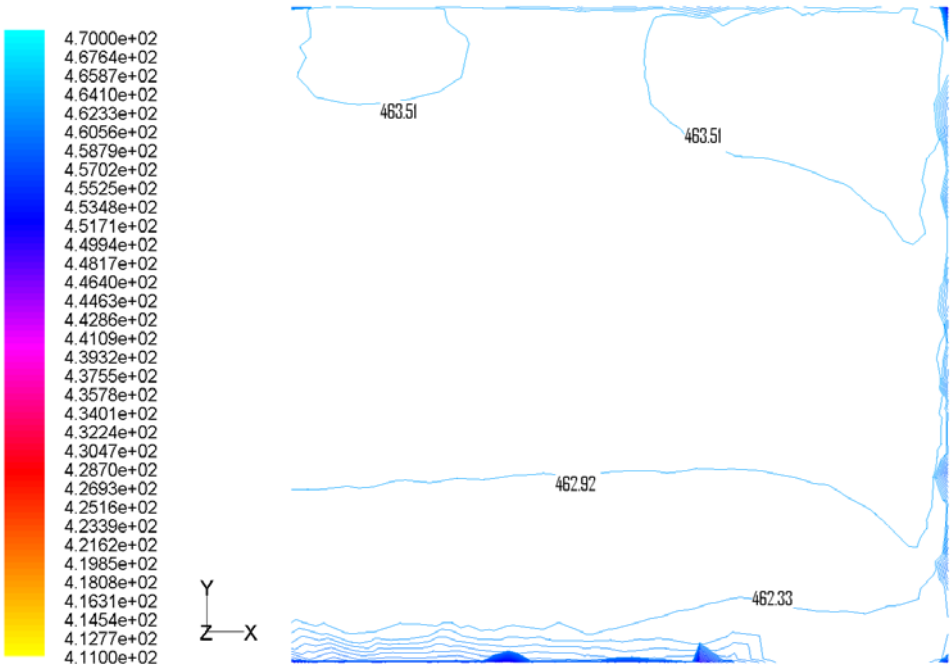

(e) t = 580 s

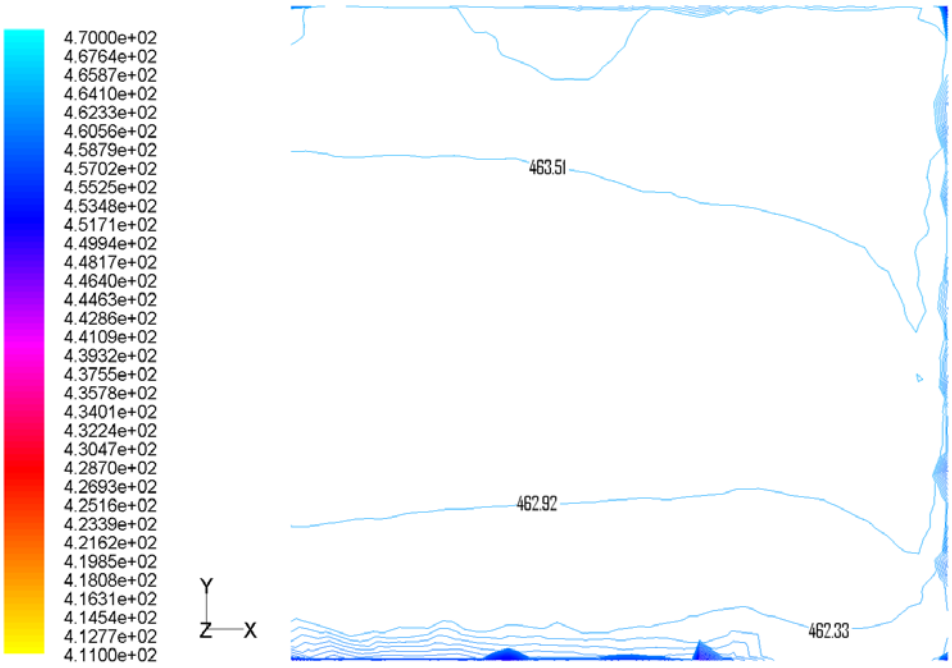

(f) t = 590 s

Figure 6.9 continued

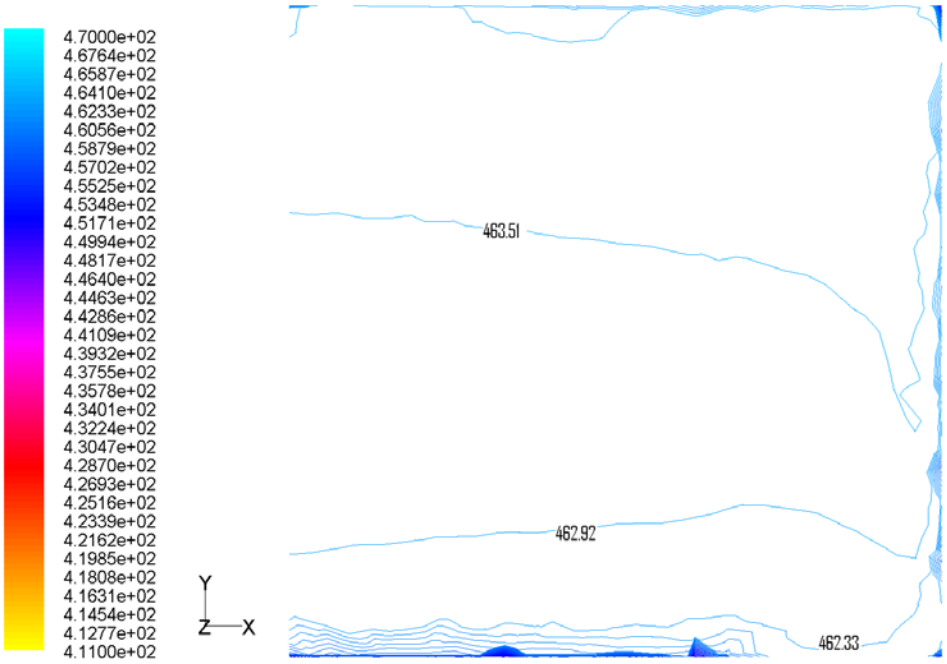

(g) t = 600 s

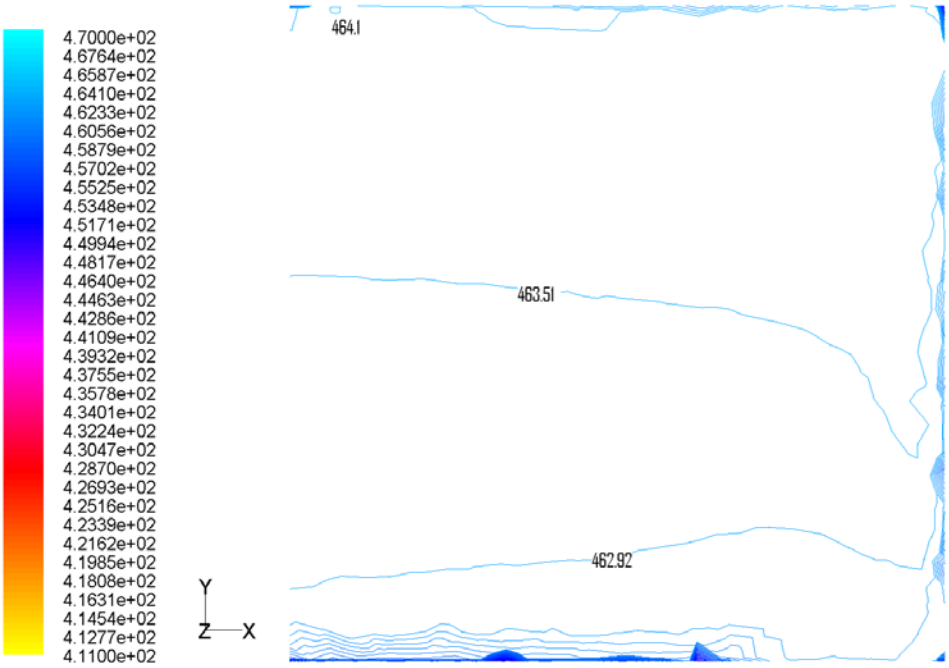

(h) t = 610 s

Figure 6.9 continued

Temperature distribution evolution along radial direction at different heights, 0.1m, 0.5m, and 0.9m, and axial direction, are also examined and shown in Figure 6.10. Comparison of Figure 6.10, a, b, and c, indicates there is no significant temperature difference at different heights of the tank, especially in the first two stages of fluid flow developing process (t < 200 second). Figure 6.10 (d) illustrates the temperature distribution along the tank axial direction and there is no significant temperature difference other than near the top and bottom tank wall or in the thermal runaway stage.

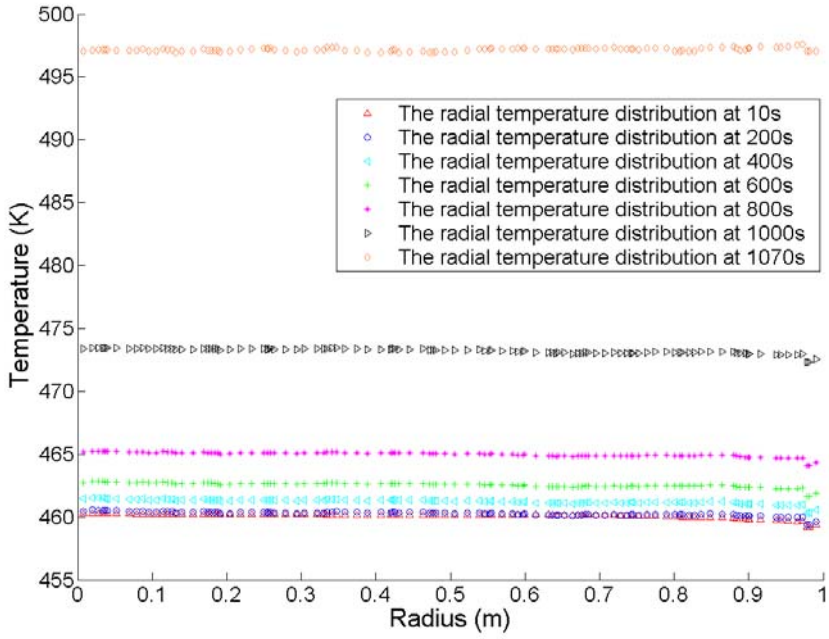

(a) y = 0.1 m

Figure 6.10 Temperature distributions along the radial directions and axial direction

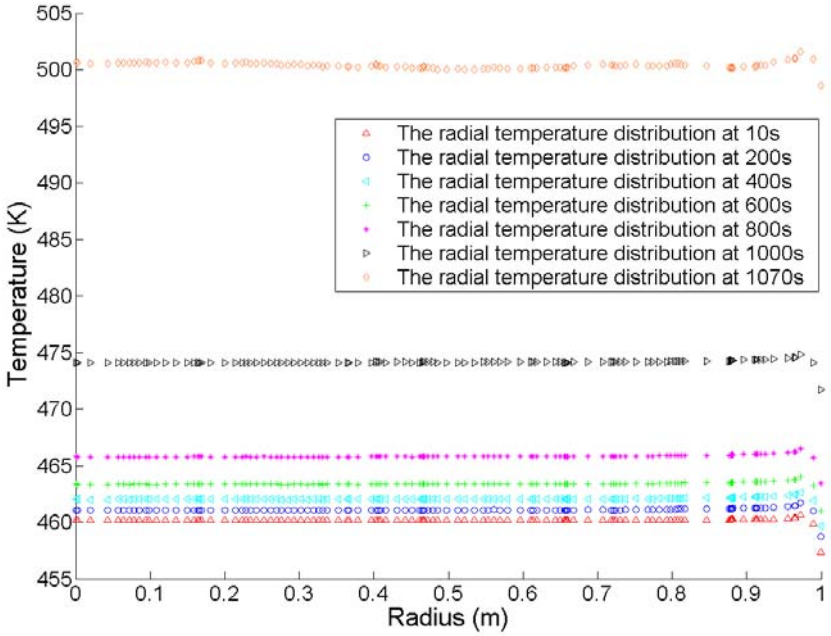

(b) y = 0.5 m

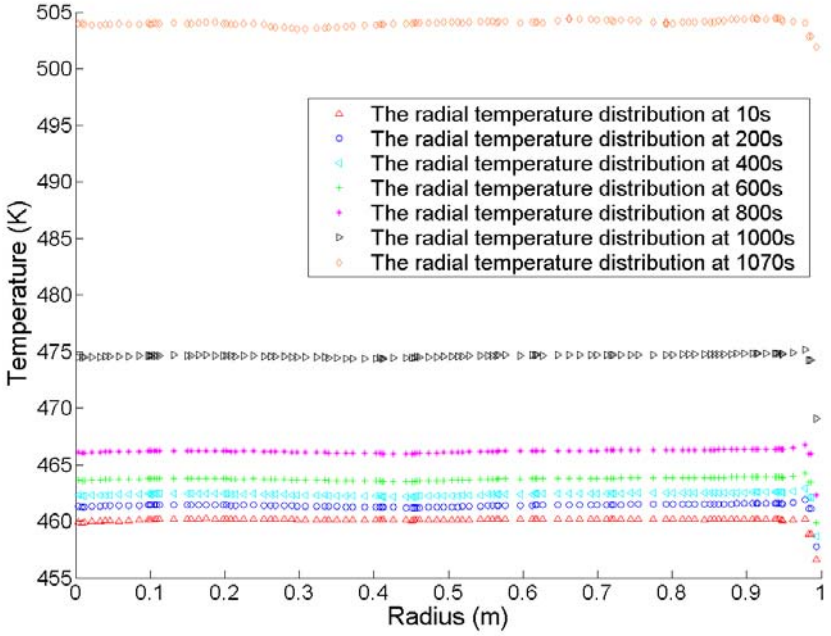

(c) y = 0.9 m

Figure 6.10 continued

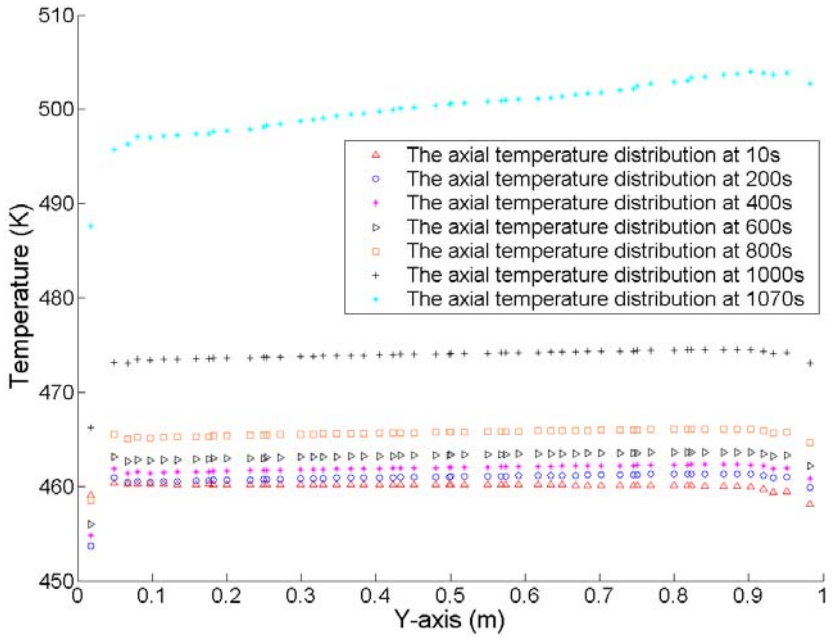

(d) x = 0, z = 0
Fig 6.10 Continued

Previous research reported the hot spot distribution for two cases, stable steady state and stable oscillatory state [43]. In the first case, the hot spot has a flat disk shape and is near the upper wall of the storage tank. In the second case, the hot spot has a donut shape and has a cycling life pattern, which includes growing, breaking-up, and merging. According to **Figure 6.9** and Figure 6.10, the temperature distribution of a tank stored in air is almost uniform and significant hot spot formation is not observed.

6.4 Conclusions

This present work presents a theoretical study on the influence of natural convection on the critical behavior of a reactive chemical in a vertical cylinder tank installed in air.

Simulation results in the air zone demonstrate constant tank boundary temperature, which actually assumes an existence of an infinite heat sink surrounding storage tank, is not realistic. In addition, simulation conducted to study heat transfer of storage tank should specify cooling fluid used and consider heat transfer resistance of that specific fluid. Otherwise heat removal rate will be overestimated and the conclusion obtained may mislead engineering practices.

For the reason of the large thermal resistance of air, there is no significant hot spot formation inside the tank and the feasible storage region of the large-scale system is smaller than that of small-scale system, where reactant temperature is assumed to be uniform. Although natural convection induced by temperature and concentration gradients do enhance both heat and mass transfer, the increase of heat generation with increasing quantity overwhelms the heat transfer enhancement due to natural convection and heat transfer area increase

Traditional Semenov Theory is proved to be able to provide screening analysis on critical behavior of large-scale system by using appropriate overall heat transfer coefficient and taking account of the system size. The results show that the critical condition obtained from non-convective system cannot be directly applied to the practical reactive chemical storage. System size issue and overall heat transfer coefficient must be carefully examined to obtain the appropriate storage and handling conditions.

7. CONCLUSIONS AND RECOMMENDATIONS

7.1 Conclusions

Reactivity hazard and critical behavior analysis was conducted for hydroxylamine nitrate. This reactivity hazard evaluation procedure includes adiabatic calorimeter measures, small-scale system critical behavior analysis with thermal explosion theory, and bulk chemical critical behavior analysis with computational fluid dynamics. The obtained results not only are applicable to safe usage of small quantity hydroxylamine nitrate, such as in academic unit and research laboratory, but also applicable to bulk quantity practices, such as manufacture, storage, and transportation.

The first overall autocatalytic decomposition model of hydroxylamine nitrate was proposed and validated by adiabatic calorimeter measurements. The contamination effects of nitric acid and/or iron ions were studied for diluted hydroxylamine nitrate solution. The results demonstrate that thermal stability of hydroxylamine significantly decreases with the presence of metal ions and acids. The results also demonstrate hydroxylamine nitrate must be periodically inspected to ensure it is not near it critical conditions. The obtained data fills some empty area for current hydroxylamine nitrate thermal stability database and can be used to improve related process safety.

Highest storage temperature for small quantity diluted hydroxylamine nitrate is determined for the first time by using thermal explosion theory. The result is consistent with adiabatic calorimeter measurements and can be used to provide guidance for safe handling of hydroxylamine nitrate. Computational fluid dynamics demonstrates thermal

stability data obtained from small-scale system cannot be directly applied to large quantity chemical system because increase of volume to surface ratio can easily overwhelm the associated heat transfer enhancement. This indicates fluid system also has a critical volume as solid system does.

7.2 Recommendations

All experiments and theoretical analysis are conducted on the commercially available hydroxylamine nitrate, the highest concentration of which is only 24 mass%. Experimental data are urgently needed for higher concentrations of hydroxylamine nitrate, which is mainly used in gun propellant or rocket industries. Vacuum distillation or laboratory synthesis may need to be conducted to achieve this objective.

Currently proposed hydroxylamine nitrate decomposition mechanism still cannot accurately describe decomposition behavior under adiabatic conditions, which represent the worst-case scenario for pressure relief design. In-situ measurements, including GC and HPLC should be integrated to explore decomposition mechanism and its parameters. In addition, current commercial adiabatic calorimeter introduces some uncertainty due to thermal inertia issue. Flow-cell calorimeter should be built to eliminate the influence of thermal inertia and provide more accurate data.

Large-eddy turbulence and thermal radiation model should be included in CFD simulation, which requires more computer resource to conduct more accurate large-scale system critical behavior analysis.

REFERENCES

1. *Improving Reactive Hazard Management*; U.S. Chemical Safety and Hazard Investigation Board: Washington, DC, 2002.

2. Chang, R. H.; Shu, C. M.; Duh, Y. S.; Jehng, J. M., Calorimetric Studies on the Thermal Hazard of Methyl Ethyl Ketone Peroxide with Incompatible Substances. *J Hazard. Mater.* **2007,** *141* (3), 762-768.

3. *Technical Report on Hydroxylamine Nitrate*; US Department of Energy: Washington, DC, 1998.

4. Zhang, C. Thermal Decomposition Study of Hydroxylamine Nitrate During Storage and Handling. M.S. Thesis, Texas A&M University, College Station, TX, 2006.

5. Schoppelrei, J. W.; Kieke, M. L.; Brill, T. B., Spectroscopy of Hydrothermal Reactions. 2. Reactions and Kinetic Parameters of $[NH_3OH]NO_3$ and Equilibria of $(NH_4)_2CO_3$ Determined with a Flow Cell and FT Raman Spectroscopy. *J. Phys. Chem.* **1996,** *100* (18), 7463-7470.

6. Lee, H.; Litzinger, T. A., Chemical Kinetic Study of HAN Decomposition. *Combust. Flame* **2003,** *135* (1-2), 151-169.

7. Mannan, S. *Lees' Loss Prevention in the Process Industries*. 3rd ed.; Elsevier: Burlington, MA, 2005.

8. Urben, P., *Bretherick's Handbook of Reactive Chemical Hazards*; Academic Press: New York, 2007.

9. Pedley, J. B.; Naylor, R. D.; Kirby, S. P., *Thermochemical Data of Organic Compounds* 2nd ed.; Chapman & Hall: New York, 1986.

10. NIST Chemistry WebBook. http://webbook.nist.gov/chemistry/, Oct 2008.

11. Sanderson, R. T., *Chemical Bond and Bond Energy* 2nd ed.; Academic Press: New York, 1976.

12. Benson, S. W., *Thermochemical Kinetics: Methods for the Estimation of Thermochemical Data and Rate Parameters*. 2nd ed.; John Wiley & Sons: New York, 1976.

13. A.Watson, O.; Ragatz, K. M.; Hougen, R. A., *Chemical Process Principles: Part II - Thermodynamics* 2nd ed.; John Wiley & Sons: New York, 1959.

14. Frisch, M. J.; Trucks, G. W.; Schlegel, H. B.; Scuseria, G. E.; Robb, M. A.; Cheeseman, J. R.; Montgomery, J. A.; Jr., T. V.; Kudin, K. N.; Burant, J. C.; Millam, J. M.; Iyengar, S. S.; Tomasi, J.; Barone, V.; Mennucci, B.; Cossi, M.; Scalmani, G.; Rega, N.; Petersson, G. A.; Nakatsuji, H.; Hada, M.; Ehara, M.; Toyota, K.; Fukuda, R.; Hasegawa, J.; Ishida, M.; Nakajima, T.; Honda, Y.; Kitao, O.; Nakai, H.; Klene, M.; Li, X.; Knox, J. E.; Hratchian, H. P.; Cross, J. B.; Bakken, V.; Adamo, C.; Jaramillo, J.; Gomperts, R.; Stratmann, R. E.; Yazyev, O.; Austin, A. J.; Cammi, R.; Pomelli, C.; Ochterski, J. W.; Ayala, P. Y.; Morokuma, K.; Voth, G. A.; Salvador, P.; Dannenberg, J. J.; Zakrzewski, V. G.; Dapprich, S.; Daniels, A. D.; Strain, M. C.; Farkas, O.; Malick, D. K.; Rabuck, A. D.; Raghavachari, K.; Foresman, J. B.; Ortiz, J. V.; Cui, Q.; Baboul, A. G.; Clifford, S.; Cioslowski, J.; Stefanov, B. B.; Liu, G.; Liashenko, A.; Piskorz, P.; Komaromi, I.; Martin, R. L.; Fox, D. J.; Keith, T.; Al-Laham, M. A.; Peng, C. Y.; Nanayakkara, A.; Challacombe, M.; Gill, P. M. W.; Johnson, B.; Chen, W.; Wong, M. W.; Gonzalez, C.; Pople, J. A., *Gaussian 03*, Revision C.02; Gaussian, Inc.: Wallingford CT, 2004.

15. ASTM Subcommittee. *The ASTM CHETAH* Version 7.0; The Computer Program For Chemical Thermodynamic and Energy Release Evaluation; ASTM Data Series DS51B: Philadelphia, 1994.

16. SENSYS evo DSC. http://www.setaram.com/SENSYS-evo-DSC.htm, Oct 2008

17. Burelbach, J. P. In Advanced Reactive System Screening Tool (ARSST), 2nd Annual Mary Kay O'Connor Process Safety Center Symposiums—Beyond Regulatory Compliance: Making Safety Second Nature, College Station, Texas, Oct 26-27, 1999.

18. Bohn, M. A., Thermal Aging of Rocket Propellant Formulations Containing ε-HNIW (ε-CL20) Investigated by Heat Generation Rate and Mass Loss. *Thermochim. Acta* **2003,** *401* (1), 27-41.

19. Wei, C.; Rogers, W. J.; Mannan, M. S., Detection of Autocatalytic Decomposition Behavior of Energetic Materials Using APTAC. *J Therm. Anal. Calorim.* **2006,** *83* (1), 125-130.

20. Smith, D. W., Runaway Reactions and Thermal Explosion. *Chem. Eng.* **1982,** *89* (25), 79-84.

21. Massot, M.; Genieys, S.; Dumont, T.; Volpert, V. A., Interaction of Thermal Explosion and Natural Convection: Critical Conditions and New Oscillating Regimes. *SIAM J. Appl. Math.* **2002,** *63* (1), 351-372.

22. Frank-Kamenetskii, D. A., *The Theory of Thermal Explosion. In Diffusion and Heat Exchange in Chemical Kinetics* 2nd ed.; Plenum Press: New York, 1969.

23. Morbidelli, M.; Varma, A., A Generalized Criterion for Parametric Sensitivity: Application to Thermal Explosion Theory. *Chem. Eng. Sci.* **1988,** *43* (1), 91-102.

24. Miguel A. Alos; Zaldivar, J. M.; Strozzi, F.; Nomen, R.; Sempere, J., Application of Parametric Sensitivity to Batch Process Safety: Theoretical and Experimental Studies. *Chem. Eng. Technol.* **1996,** *19* (3), 222-232.

25. Lacey, A. A., Critical Behavior of Homogeneous Reacting Systems with Large Activation Energy. *Int. J. Eng. Sci.* **1983,** *21* (5), 501-515.

26. Bilous, O.; Amundson, N. R., Chemical Reactor Stability and Sensitivity: II. Effect of Parameters on Sensitivity of Empty Tubular Reactors. *AIChE J.* **1956,** *2* (1), 117-126.

27. Kotoyori, T., Critical Temperatures for the Thermal Explosion of Liquid Organic Peroxides. *Process Saf. Prog.* **1995,** *14* (1), 37-44.

28. Gray, B. F., Critical Behavior in Chemically Reacting Systems--III. An Analytical Criterion for Insensitivity. *Combust. Flame* **1975,** *24*, 43-52.

29. Wu, H.; Morbidelli, M.; Varma, A., Approximate Criterion for Reactor Thermal Runaway. *Chem. Eng. Sci.* **1998,** *53* (18), 3341-3344.

30. Rice, O. K.; Allen, A. O.; Campbell, H. C., Induction Period in Gaseous Thermal Explosions. *J. Am. Chem. Soc.* **1935,** *57* (11), 2212-2222.

31. Shouman, A. R.; El-Sayed, S., Accounting for Reactant Consumption in the Thermal Explosion Problem. Part I. Mathematical Foundation. *Combust. Flame* **1992,** *88* (3-4), 321-344.

32. Shouman, A. R.; El-Sayed, S. A., Accounting for Reactant Consumption in the Thermal Explosion Problem. Part II. A Direct Solution with Application to the Frank-Kamenetskii Problem. *Combust. Flame* **1997,** 1*08* (4), 361-386.

33. Shouman, A. R.; El-Sayed, S. A., Accounting for Reactant Consumption in the Thermal Explosion Problem III. Criticality Conditions for the Arrhenius Problem. *Combust. Flame* **1998,** *113* (1-2), 212-223.

34. Shouman, A. R.; El-Sayed, S. A., Accounting for Reactant Consumption in the Thermal Explosion Problem. Part IV. Numerical Solution of the Arrhenius Problem. *Combust. Flame* **1999,** *117* (1/2), 422-428.

35. El-Sayed, S. A., Explosion Characteristics of Autocatalytic Reaction. *Combust. Flame* **2003,** *133* (3), 375-378.

36. Shouman, A. R., A Review of One Aspect of the Thermal-Explosion Theory. *J. Eng. Math.* **2006,** *56* (2), 179-84.

37. Bronshtein, I. N.; Semendyayev, K. A.; Musiol, G.; Muehlig, H., *Handbook of Mathematics*. 4th ed.; Springer: New York, 2007.

38. Shadid, J. N.; Salinger, A. G.; Pawlowski, R. P.; Lin, P. T.; Hennigan, G. L.; Tuminaro, R. S.; Lehoucq, R. B., Large-Scale Stabilized FE Computational Analysis of Nonlinear Steady-State Transport/Reaction Systems. *Comput. Method Appl. M.* **2006,** *195* (13-16), 1846-1871.

39. Wells, G. J.; Ray, W. H., Methodology for Modeling Detailed Imperfect Mixing Effects in Complex Reactors. *AIChE J.* **2005,** *51* (5), 1508-1520.

40. Dakhel, A. A.; Rahimi, M., CFD Simulation of Homogenization in Large-Scale Crude Oil Storage Tanks. *J. Petrol. Sci. Eng.* **2004,** *43* (3-4), 151-161.

41. Consul, R.; Rodriguez, I.; Perez-Segarra, C. D.; Soria, M., Virtual Prototyping of Storage Tanks by Means of Three-Dimensional CFD and Heat Transfer Numerical Simulations. *Sol. Energy* **2004,** *77* (2), 179-191.

42. Schuster, A.; Lakshmanan, R.; Ponton, J.; Sefiane, K., Simulation and Design of a Non-Adiabatic Multiphase Microreactor. *Int. J. Chem. React. Eng.* **2003,** 1, A45.

43. Sheu, L.-J.; Lin, J.-D.; Chen, J.-R., Numerical Analysis on the Hot Spot in Reactive Chemical Storage. *J. Loss Prevent. Proc.* **1999,** *12* (2), 125-136.

44. Campbell, A. N.; Cardoso, S. S. S.; Hayhurst, A. N., A Comparison of Measured Temperatures with those Calculated Numerically and Analytically for an Exothermic Chemical Reaction inside a Spherical Batch Reactor with Natural Convection. *Chem. Eng. Sci.* **2007,** *62* (11), 3068-3082.

45. *FLUENT 6.3 User's Guide*. Fluent Inc.: Lebanon, 2006.

46. Throne, J. L., *Technology of Thermoforming*. Hanser Publishers: Hinckley, OH 1996.

47. Wei, C.; Rogers, W. J.; Mannan, M. S., Thermal Decomposition Hazard Evaluation of Hydroxylamine Nitrate. *J Hazard. Mater.* **2006,** *130* (1-2), 163-168.

48. Wei, C.; Rogers, W.; Mannan, M. S., Detection of Autocatalytic Decomposition Behavior of Energetic Materials Using APTAC. *J Therm. Anal. Calorim.* **2006,** *83* (1), 125-130.

49. Amariei, D.; Courtheoux, L.; Rossignol, S.; Kappenstein, C., Catalytic and Thermal Decomposition of Ionic Liquid Monopropellants Using a Dynamic Reactor. Comparison of Powder and Sphere-Shaped Catalysts. *Chem. Eng. Process.* **2007,** *46* (2), 165-174.

50. Wei, J. B.; Shaw, B. D., Influences of Pressure on Reduced-Gravity Combustion of HAN-Methanol-Water Droplets in Air. *Combust. Flame* **2006,** *146* (3), 484-492.

51. Schoppelrei, J. W.; Brill, T. B., Spectroscopy of Hydrothermal Reactions. 7. Kinetics of Aqueous $[NH_3OH]NO_3$ at 463-523 K and 27.5 MPa by Infrared Spectroscopy. *J. Phys. Chem. A* **1997,** *101* (46), 8593-8596.

52. Cisneros, L. O.; Rogers, W. J.; Mannan, M. S., Effect of Air in the Thermal Decomposition of 50 mass% Hydroxylamine/Water. *J Hazard. Mater.* **2002,** *95* (1-2), 13-25.

53. Chippett, S.; Ralbovsky, P.; Granville, R., The APTAC: A High Pressure, Low Thermal Inertia, Adiabatic Calorimeter. International Symposium on Runaway Reactions, Pressure Relief Design, and Effluent Handling, New Orleans, LA, Mar 11-13 1998.

54. Townsend, D. I.; Tou, J. C., Thermal Hazard Evaluation by an Accelerating Rate Calorimeter. *Thermochim. Acta* **1980,** *37* (1), 1-30.

55. Wilcock, E.; Rogers, R. L., A Review of the Phi Factor During Runaway Conditions. *J. Loss Prevent. Proc.* **1997,** *10* (5-6), 289-302.

56. Wei, C. Thermal Runaway Reaction Hazard and Decomposition Mechanism of the Hydroxylamine System. Ph.D. Dissertation, Texas A&M University, College Station, TX, 2005.

57. Oxley, J. C.; Brower, K. R., Thermal Decomposition of Hydroxylamine Nitrate. Proceedings of SPIE-The International Society for Optical Engineering 872, Los Angeles, CA, Jan 13-15, 1988.

58. Sugikawa, S.; Umeda, M.; Sekino, J.; Matsuda, T.; Kodama, T., Evaluation of Safety Limit for Handling of Hydroxylamine Nitrate/Nitric Acid Solution as a Plutonium Reductant. International Symposium on Scientific Bases for Criticality Safety, Separation Process and Waste Disposal (JAERI-Conf 2002-004), Tokai, Ibaraki, Japan, Oct 31-Nov 2, 2001.

59. Gowland, R. J.; Stedman, G., Kinetic and Product Studies on the Decomposition of Hydroxylamine in Nitric Acid. *J. Inorg. Nucl. Chem.* **1981,** *43* (11), 2859-2862.

60. Gowland, R. J.; Stedman, G., A Novel Moving Boundary Reaction Involving Hydroxylamine and Nitric Acid. *J. Chem. Soc., Chem. Commun.* **1983**, (18), 1038-1039.

61. Bohn, M. A., Determination of the Kinetic Data of the Thermal Decomposition of Energetic Plasticizers and Binders by Adiabatic Self-Heating. Proceedings of the Workshop on the Microcalorimetry of Energetic Materials, 2nd, Leeds, UK, May 17-19 1999.

62. Steinbach, J.; Klais, O., Prediction of Self-reactive Properties from DTA-Measurements. *Inst.Chem. E.* **1997,** 141, 261-272.

63. Pembridge, J. R.; Stedman, G., Kinetics, Mechanism, and Stoichiometry of the Oxidation of Hydroxylamine by Nitric Acid. *J. Chem. Soc., Dalton Trans.* **1979**, (11), 1657-1663.

64. Shaw, B. D.; Williams, F. A., A Model for the Deflagration of Aqueous Solutions of Hydroxylammonium Nitrate. Proceedings of the Combustion Institute, 24th, Sydney, Australia, July 5-10 1992.

65. Schlünder, E. U., *VDI Heat Atlas*. Woodhead Publishing Limited: Duesseldorf, 1993.

66. Campbell, A. N.; Cardoso, S. S. S.; Hayhurst, A. N., The Influence of Natural Convection on the Temporal Development of the Temperature and Concentration Fields for Sal'nikov's Reaction, P $\rightarrow$ A $\rightarrow$ B, Occurring Batchwise in the Gas Phase in a Closed Vessel. *Chem. Eng. Sci.* **2005,** *60* (21), 5705-5717.

67. Campbell, A. N.; Cardoso, S. S. S.; Hayhurst, A. N., A Scaling Analysis of the Effects of Natural Convection, when Sal'nikov's Reaction: P $\rightarrow$ A $\rightarrow$ B Occurs, Together with Diffusion Heat Transfer in a Batch Reactor. *Chem. Eng. Res. Des.* **2006,** *84* (A7), 553-561.

68. Campbell, A. N.; Cardoso, S. S. S.; Hayhurst, A. N., Oscillatory and Nonoscillatory Behavior of a Simple Model for Cool Flames, Sal'nikov's reaction, P $\rightarrow$ A $\rightarrow$ B, Occurring in a Spherical Batch Reactor with Varying Intensities of Natural Convection. *Combust. Flame* **2008,** *154* (1-2), 122-142.

69. Vyn, W. T., Effect of Natural Convection on the Criteria for Thermal Explosion. Chemical and Physical Processes in Combustion, The Combustion Institute, Pittsburgh, 1990.

70. Benin, A.; Kossoy, A.; Sheinman, I.; Grinberg, P., Evaluating Thermal Explosion Hazard of Self-Reactive Substances by using Kinetics-Based Simulation Approach. *Int. J. Self Propag. High Temp. Synth.* **2006,** *15* (4), 297-307.

71. Merzhanov, A. G.; Abramov, V. G., Thermal Explosion of Explosives and Propellants. A review. *Propell. Explos. Pyrot.* **1981,** *6* (5), 130-148.

72. Liu, L.; Wei, C.; Guo, Y.; Rogers, W. J.; Sam Mannan, M., Hydroxylamine Nitrate Self-Catalytic Kinetics Study with Adiabatic Calorimetry. *J Hazard. Mater.* **2009,** *162* (2-3), 1217-1222.

73. Dobre, T. G.; Marcano, J. G. S., *Chemical Engineering: Modelling, Simulation and Similitude*; John Wiley & Son: New York, 2007.

74. Yaws, C. L., *Chemical Properties Handbook: Physical, Thermodynamics, Engironmental Transport, Safety & Health Related Properties for Organic & Inorganic Chemical* 1st ed.; McGraw-Hill: New York, 1998.

75. Bird, R. B.; Stewart, W. E.; Lightfoot, E. N., *Transport Phenomena*. 2nd ed.; John Wiley & Sons: New York, 2006.

VITA

Name: Lijun Liu

Address: Artie McFerrin Department of Chemical Engineering
c/o Dr. M. Sam Mannan
TAMU 3122
College Station, TX, 77843-3122

Email Address: lijun.liu@chemail.tamu.edu

Education: Ph.D., Chemical Engineering, Texas A&M University, USA, 2009
M.S., Chemical Engineering, Tianjin University, Tianjin, China, 2003
B.E., Chemical Engineering, Tianjin University, Tianjin, China, 2000